DEPARTMENT OF LIFE SCIENCES

PhD IN LIFE SCIENCES

CYCLE XXXIV

COORDINATOR Prof. Massimo Valoti

Identification of novel readouts to assess anti-fibrotic efficacy of new compounds in a bleomycin-induced pulmonary fibrosis mouse model

SCIENTIFIC DISCIPLINARY SECTOR: MED/04

University Tutor: **Prof.ssa Monica Lucattelli**

Company Tutor: **Dr.ssa Daniela Miglietta**
Chiesi Farmaceutici S.p.A

PhD Student: **Dr.ssa Debora Fragni**

ABSTRACT

Idiopathic pulmonary fibrosis (IPF) is a fatal interstitial lung disease with a poor prognosis and very limited therapeutic options. To date, Pirfenidone and Nintedanib are the only two therapies approved for IPF worldwide. However, these drugs can slow-down lung function decline without really stopping or reverting the fibrotic process, and in addition their use is associated with a series of side effects. The incomplete understanding of the disease and the limitations of current treatments make IPF a disease with a high medical need requiring novel treatment approaches. For these reasons, the new drugs coming from the research and development pipelines will be crucial to get new treatments for patients.

Despite widely used, the current animal models of IPF need to be improved in order to be as much predictive as possible in identifying new promising treatments for pulmonary fibrosis. One of the most challenging aspects of drug discovery for IPF is the identification of new therapies that can be translated effectively to the clinic, implying that very few compounds that have shown efficacy in animal models have been successful in human clinical trials and concluding that most of the preclinical models are poorly predictive and scarcely resembling the human disease. Currently the majority of new drugs investigated in preclinical models of IPF are dosed using a prophylactic dosing regimen, whereas patients are almost always treated after the fibrosis is well established. Moreover, the most popular endpoints examined in preclinical models of IPF are histological scoring and lung collagen content; however, lung function tests are more commonly used as primary endpoints in IPF patients.

In this scenario, considering the high unmet medical need and some limits that the preclinical research has to face, the main goal of this PhD project was to generate a robust and reliable preclinical model of pulmonary fibrosis, introducing novel readouts, suitable to select and to identify new pharmacological treatments for IPF with an higher translational potential. The approach pursued by this study could be very impactful to identify new potential treatments for IPF. To achieve the goal of this PhD project, performed in collaboration with Chiesi Farmaceutici, we (1) reproduced the most described preclinical model for IPF, the bleomycin (BLM)-induced pulmonary fibrosis mouse model by intratracheal (IT) administration, and we analyzed its main limitations; (2) looking at the clinic, we optimized the BLM model with the introduction of clinically more relevant parameters (i.e., lung function tests, lung imaging, oximetry (Sp02), and fibrotic biomarkers) through a new BLM oropharyngeal (OA) protocol and finally, (3) we explored the added value of these more relevant readouts by investigating the efficacy of Nintedanib, which was tested under therapeutic regimen.

The characterization of the BLM IT model proved to be useful in better understanding the development of BLM-induced lung fibrosis and allowed to define the therapeutic protocol to test the anti-fibrotic efficacy of Nintedanib in the model; however, it highlighted several limitations such as a patchy distribution of fibrotic lesions and poor sensitivity to pharmacological treatment using the two traditional preclinical readouts, histology and hydoxyproline (Hyp) lung content.

Those limitations were overcome by the use of the OA administration of BLM which led to a more homogeneous fibrosis throughout the lung lobes and by the introduction of more clinically relevant endpoints such as micro-computer tomography (CT) imaging and lung function measurements that are the same tests used to diagnose and monitor patients with IPF, as well as of emerging biomarkers currently under evaluation in the clinical setting, with the final aim to create a link between the preclinical model and the clinical practice. All these new readouts showed the same profile over time observed with histology in terms of development of fibrotic disease, and Nintedanib was able to significantly modulate them, confirming their relevance for monitoring lung fibrosis as well as the efficacy of new treatments. Among them, the measurement of lung function, in particular the forced vital capacity (FVC), demonstrated to be the most sensitive readout to assess the compounds efficacy and was selected also in our preclinical studies as the primary endpoint as for clinical trials, thus creating an important link between the preclinical model and the clinical setting.

In addition, we also worked to refine the histological analysis which still remains an important complementary evaluation to be coupled to the functional readouts. Currently the common histological analysis utilized in preclinical models of lung fibrosis is represented by the Ashcroft scoring system, which revealed some disadvantages such as a time-consuming process, operator-dependent results, limited sensitivity and, most critical, inability to get a direct link to clinics. Therefore, we introduced an automated image analysis by using an artificial intelligence (AI) approach, which improved this analysis recognizing histological features with more accuracy and consistency, reducing significantly the time of the analysis and making the evaluation independent from the operator.

In summary, this project demonstrated that in the mouse BLM-induced lung fibrosis model it has been possible to explore the same clinically relevant parameters used in IPF patients; in particular lung function tests such as FVC, that for its high translational value together with the high sensitivity to assess the efficacy of the compounds has been chosen as the primary endpoint to support the selection of novel treatments within our internal drug

discovery IPF projects. Furthermore, the introduction of these different readouts, that all go to the same direction, has from one side increased the robustness of the model and from the other side has allowed to bring this preclinical model to a level of complexity that mirrors the one observed in human IPF.

Overall, this PhD work has enhanced the translational value of the data obtained with the mouse BLM model increasing the chance of selecting promising compounds to advance to clinical trials and has concretely led to significant benefits to drug discovery process in the IPF research, improving the quality and the reliability of the search of novel anti-fibrotic drugs.

TABLE OF CONTENTS

1. INTRODUCTION

1.1 The Interstitial Lung Diseases

Interstitial lung disease (ILD) is an umbrella term, synonymous with diffuse parenchymal lung disease, which includes more than 200 different lung disorders characterized by variable degrees of inflammation and fibrosis of the pulmonary interstitium. Progression of all these disordes results in excessive deposition of fibrotic tissue, impaired oxygen transfer and scarring within the lung (*Morgenthau and Padilla, 2009*). Lung damage from ILDs is often irreversible and gets worse over time.

Although many of the ILDs share similar clinical, radiographic and sometimes even pathological features, the mechanisms of disease, treatment, prognosis and outcome are often very different making them independent from one another. Some forms of the ILDs have known etiologies including environmental exposures (e.g. asbestosis or silicosis), drug toxicity, radiation, and systemic fibrotic conditions (e.g. systemic sclerosis, rheumatoid arthritis, and collagen vascular disease). These can therefore be grouped into similar clinical characteristics. Despite this, the etiology of the most common form of ILDs, defined as Idiopathic Interstitial Pneumonias (IIPs), is still unknown. The diagnostic interpretation of the IIPs is often challenging because may show similar morphologic features, and therefore, this makes the classification of this group of diseases very problematic. In 2002, the American Thoracic Society (ATS) and European Respiratory Society (ERS) guideline, which has recently been updated in 2013, introduced a criterion for the characterization and diagnosis of major IIPs based on clinical, radiological and histological characteristics (*Travis et al. 2013*). In the updated classification of the IIPs, the major entities have been preserved and grouped into five distinct category of diseases: "chronic fibrosing IIPs" (idiopathic pulmonary fibrosis and idiopathic nonspecific interstitial pneumonia), "smoking-related IIPs" (respiratory bronchiolitis–associated interstitial lung disease and desquamative interstitial pneumonia), "acute or subacute IIPs" (cryptogenic organizing pneumonia and acute interstitial pneumonia), and "rare IIPs" (lymphoid interstitial pneumonia and idiopathic pleuroparenchymal fibroelastosis). Furthermore, it has been acknowledged that a final diagnosis is not always achievable, and the category "unclassifiable IIP" has been proposed. This may be the case when there are non-specific or conflicting clinical, radiological or histopathological findings, or when patients are unable or unwilling to undergo diagnostic procedures. The latest classification of the ILDs is schematized in **Figure 1.1.**
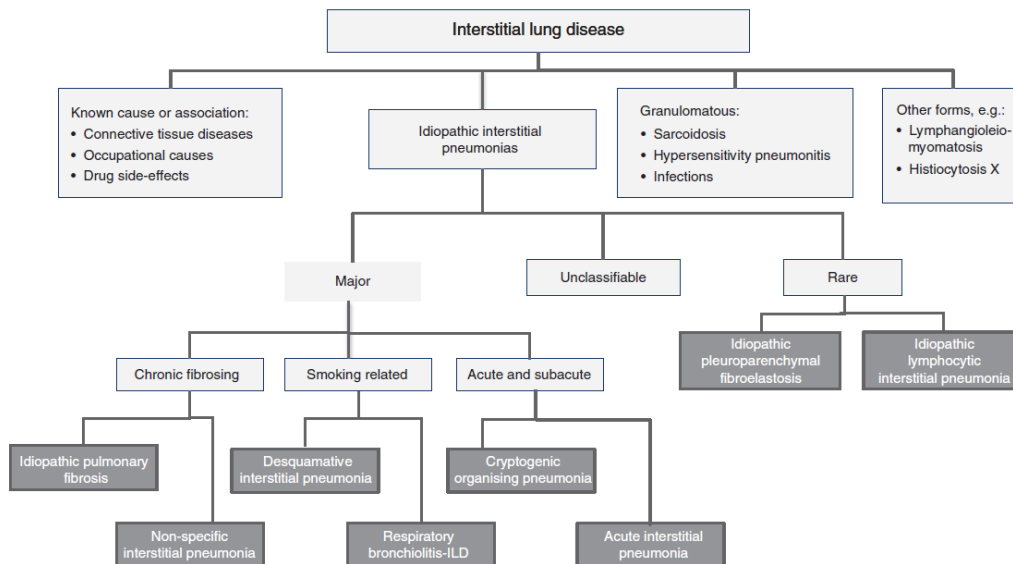
Figure 1.1 Classification of ILDs (*Zibrak and Price, 2014*).

1.2 Idiopathic Pulmonary Fibrosis

Idiopathic Pulmonary Fibrosis (IPF) is defined by the ATS/ERS/JRS/ALAT guidelines as a specific form of chronic, fibrosing interstitial pneumonia, of unknown cause, included in the heterogeneous group of ILDs (*ATS International Consensus Statement, 2000*). In particular, IPF is the most common and severe form of IIPs, characterized by progressive decline of lung function, respiratory failure and high mortality rate.

The disease, which occurs mainly in elderly males (typically in the sixth and seventh decades), is limited to the lungs, and associated with the histopathologic and/or radiologic pattern of Usual Interstitial Pneumonia (UIP) (*Raghu et al. 2011*). The histopathologic hallmark of UIP is a heterogeneous appearance in which areas severely affected by fibrosis alternate with areas of less affected or normal parenchyma. These histopathologic changes often affect the subpleural and paraseptal parenchyma most severely. Specifically, these regions are characterized by mild inflammation, usually consisting of a patchy interstitial infiltrate of lymphocytes, and fibrotic areas composed mainly of dense collagen and proliferating fibroblasts and myofibroblasts (so-called fibroblast foci). Indeed, lung parenchyma of IPF patients is characterized by repetitive local micro-injuries and ageing of alveolar epithelium. These micro-injuries result in aberrant epithelial-fibroblast communication with proliferation of myofibroblasts and a considerable extracellular matrix (ECM) accumulation with the consequent remodelling of lung interstitium. The fibrosis progression leads to a final step in which lung architecture is completely shuttered and the alveoli are replaced by large air spaces with thick fibrotic walls lined by bronchiolar

13

epithelium and often filled with mucin and inflammatory cells, defined as honeycomb lung. These morphological alterations of lung tissue, in turn, lead to decreased lung compliance, disrupted gas exchange, and ultimately respiratory failure and death (*Myers et al. 2014/ Chapter 3*).

1.2.1 Epidemiology

Determining the epidemiology of IPF is a difficult task. Precise estimates for the incidence and prevalence of IPF are not fully established, mainly due to the lack of uniform definition and diagnostic criteria in older reports, and differences in study methodology and populations (*Olson and Swigris, 2012*). Therefore, identifying the true incidence and prevalence of IPF remain a challenge and epidemiologic data should be considered as estimates only.

Although IPF is still regarded as a rare disease, it has been described that epidemiological rates of IPF are steadily increasing. A recent study conducted in UK reported that the incidence increased by 78% between 2000 and 2012, and the prevalence was doubling (*Strongman et al. 2018*). Recently, a systematic review of the global incidence of IPF estimated a rate of 2.8-9.3 cases per 100.000 people per year in Europe and North America, with significantly lower rates in Asia and South America (fewer than 4 cases per 100,000 person-years) (*Hutchinson et al. 2015*). Data from US Medicare beneficiaries show that the annual cumulative prevalence of IPF amongst individuals aged 65 years or older increased steadily from 202.2 cases per 100,000 people in 2001 to 494.5 cases per 100,000 people in 2011 (*Raghu et al. 2014*).

Commonly, IPF is more prevalent in men, who account for approximately 70% of all cases worldwide, than women. Moreover, as IPF is most commonly diagnosed in the elderly, population studies have demonstrated an increased incidence and prevalence of IPF with age progression, with the majority of cases diagnosed in the fifth through seventh decades of life (median age at diagnosis of 66 years) (*Zaman et al. 2018*). Recent mortality data from the US show an increase in IPF-related mortality. Specifically, the age-adjusted mortality rate increased by 28.4% in men (from 40.2 deaths per 1,000,000 in 1992 to 61.9 deaths per 1,000,000 in 2003) and 41.3% in women (from 39.0 deaths per 1,000,000 in 1992 to 55.1 deaths per 1,000,000 in 2003) (*Olson et al. 2007*). Similar trends have been reported in the UK (*Navaratnam et al. 2011*). With 5-year survival rate approaching 20%-30%, IPF is more lethal than several type of cancers (e.g. breast, ovarian, colorectal) (**Figure 1.2**) and represents an important public health problem, particularly in elderly

people (*Vancheri et al. 2010*). Thus, a more and better epidemiology might help us to better determine the burden and unmet needs of IPF, now and in the near future.
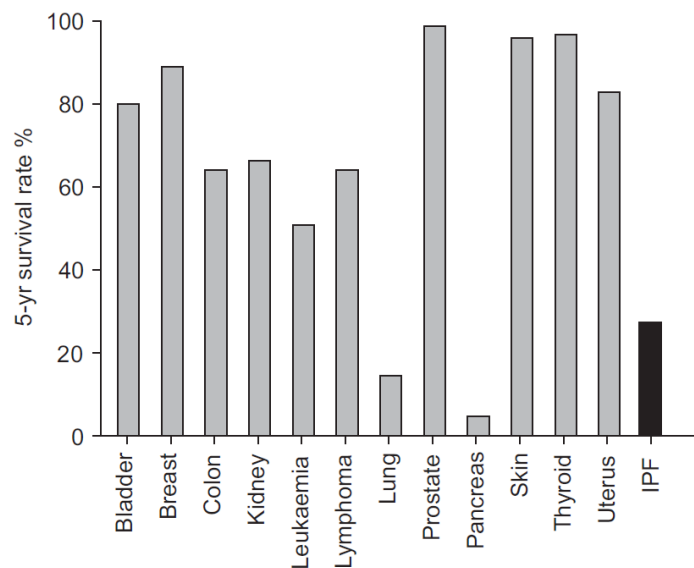
Figure 1.2 Comparison of the 5-year survival rate between IPF and different forms of cancer (*Vancheri et al. 2010*). Statistics for cancer are from the US National Cancer Institute.

1.2.2   Potential risk factors and comorbidities

Although IPF is, by definition, a disease of unknown causes, multiple factors have been shown to increase the risk of developing the disease. It is currently believed that IPF results from a complex interplay of genetic predisposition and environmental risk factors, which results in profound changes to epithelial cells and fibroblasts (*Selman and Pardo, 2014*).

Genetic factors

A genetic predisposition for IPF is suggested by several lines of evidence, the most persuasive one comes from studies of familial clustering of familial interstitial pneumonia (FIP), which occurs when two or more members of the same family have the disease. FIP, which accounts for <5% of all cases of IPF, is clinically and histologically indistinguishable from sporadic IPF, although familial forms tend to present at an earlier age and may display some differences in radiological pattern (*Lee et al. 2005*).

Large-scale genome-wide association studies have identified several specific genetic variants, both rare and common (**Figure 1.3**), associated with sporadic and familial forms of pulmonary fibrosis that confer risk for development of IPF (*Fingerlin et al. 2013; Noth et al. 2013*). Recently, Kaur and colleagues (*Kaur et al. 2017*), grouped these genetic

15

variants associated with predisposition to IPF into three major categories based on their suspected role in the pathogenesis of the disease:

- <u>Genes related to alveolar stability</u>: surfactant proteins are alveolar epithelial cells (AECs) type II specific proteins considered to be essential for normal lung function and homeostasis. Rare variants identified in the genes encoding surfactant protein C (SFTPC) and A (SFTPA2) have been associated with pulmonary fibrosis (*Lawson et al. 2004*). Specifically, studies suggest that mutations in the genes encoding these proteins lead to accumulation of misfolded protein resulting in increased endoplasmic reticulum (ER) stress and activation of the unfolded protein response, a cascade of events that, although designed to protect the cell, may lead to cellular apoptosis, and in the case of the aforementioned mutations, AEC apoptosis ensues which leads to a fibrotic response (*Tanjore et al. 2012*).

- <u>Genes linked to telomere biology and associated with accelerated cell senescence</u>: telomeres are specialized loop structures of repetitive nucleotide units at the ends of chromosomes that protect them from progressive shortening during the normal cell replication process. Recent studies have reported an association between numerous genes in the telomerase maintenance pathway and FIP, most importantly those related to catalytic activity, telomerase reverse transcriptase (TERT) and telomerase RNA component (TERC), but also linked to telomere stabilization, such as dyskerin pseudouridine synthase 1 (DKC1), poly(A)-specific ribonuclease (PARN), and regulator of telomere elongation helicase 1 (RTEL1). Among these mutations, TERT variants are the most frequently identified rare variants associated with IPF, occurring in approximately 15% of FIP and in 1–3% of sporadic cases (*Kaur et al. 2017*). Variations within these genes cause dysfunction of telomerase activity leading to accelerated telomere shortening. The exact mechanisms by which telomere defects cause lung disease are not fully understood, but they have been linked to epithelial cell senescence and an impaired response to epithelial injury (*Armanios and Blackburn, 2012*). Moreover, the observation that telomere shortening is not exclusively related to telomerase rare variant mutations (*Cronkhite et al. 2008*) and that telomere dysfunction correlates with worse survival in IPF (*Stuart et al. 2014*) lends further support to the hypothesis that telomere abnormalities contribute to disease pathogenesis, progression and outcome.

- <u>Genes affecting host defense</u>: genome-wide association studies indicated that the common variant polymorphism in the promoter region of mucin 5B oligomeric mucus/gel-forming (MUC5B), rs35705950, shows strongly association with development of both familial and sporadic IPF (*Seibold et al. 2011*). MUC5B, expressed by airway epithelial cells, encodes mucin 5B, which is a major gel-forming mucin in mucus with pulmonary anti-infectious

activities. Specifically, overexpression of MUC5B in IPF is localized in distal airways and honeycomb cysts, which are a histopathological finding in IPF, and the bronchiolar epithelium (*Yang et al. 2015*). The mechanism by which variants in MUC5B confer risk of lung fibrosis has not been fully elucidated, but, as mucins play a role in innate immunity, immune dysregulation could be a possible mechanism by which increased of MUC5B expression contributes to the pathophysiology of IPF. Alternatively, as IPF may be a disease of mucociliary clearance, overexpression of MUC5B, driven by the promoter polymorphism, may leads to impaired ciliary function, thereby allowing retention of particles and, consequently, recurrent lung injury. Interestingly, the mutant MUC5B not only appears to be predictive of pulmonary fibrosis but has also shown promise as prognostic indicator. In control subjects, the minor allele was associated with higher expression of the MUC5B in lung tissue, whereas in established IPF, MUC5B levels were uniformly elevated regardless of genotype. Moreover, the minor allele of MUC5B has been postulated to account for approximately 30% of the risk for developing IPF (*Evans et al. 2016*), and it is also associated with improved survival and better lung function than the wild-type genotype in established IPF (*Peljto et al. 2013*).

Common genetic variants, particularly three polymorphisms, within toll interacting protein (TOLLIP), an important regulator of innate immune responses, have also been associated with IPF susceptibility and prognosis (*Noth et al. 2013; Oldham et al. 2015*).
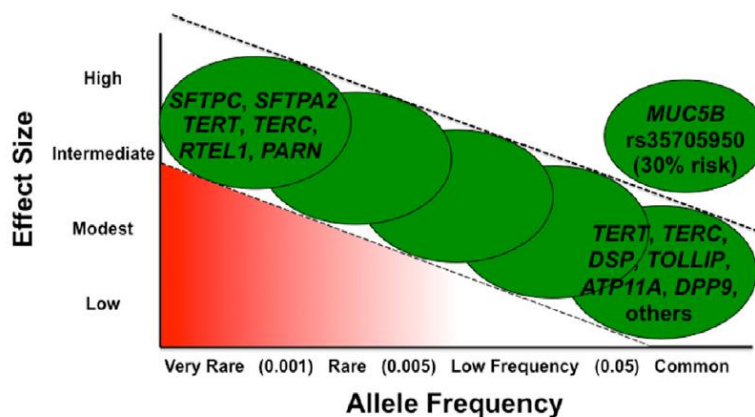
Figure 1.3 Relationship between allele frequency and penetrance of the risk allele and examples of genes with risk alleles for IPF. (*Kaur et al. 2017*). Rare variants (those with minor allele frequency of <0.1%) are thought to be highly penetrant and to have a greater effect size, but given their low frequency, they account for a smaller proportion of overall disease risk in the population. Conversely, common variants (those with minor allele frequency of >5%) have a smaller effect size but are present at higher frequency and, in aggregate, may contribute to a larger proportion of disease risk.

17

Environmental factors

Epidemiological studies have highlighted environmental and occupational exposures to wood and metal dust, pollution, gastric aspiration, smoking, and infections as factors that may confer an increased risk of developing IPF (*Taskar and Coultas, 2006*).

Cigarette smoking is probably the most common environmental exposure linked with the development of IPF, with prevalence ranging from 41–83%, and the risk is higher for smokers with a history of 21-40 pack-years (*Baumgartner et al. 1997*). The effects that this agent has on lung health are well known, and many of them are associated with some key points of the development of the disease. For example, cigarette smoke exposure can overexpress genes associate with epithelial-to-mesenchymal transition (EMT) and act negatively on important biological processes, like acceleration of telomere shortening and stress of the ER. Nicotine itself is able to induce the production of transforming growth factor-β (TGF-β), an important mediator of fibrosis in IPF. Moreover, the act of smoking involves repetitive mechanical stretch, which has been linked to micro-injury to the lung by increasing epithelial permeability, promoting the production of reactive oxidative species and impairing tissue regeneration (*Zaman and Lee, 2018*).

Some environmental and occupational exposures, particularly metal and wood dust, have also been linked with an increased risk for IPF (*Miyake et al. 2005*). Farming, stone cutting/polishing and exposure to livestock and to vegetable/animal dust have also been associated with IPF (*Baumgartner et al. 2000; Gustafson et al. 2007*). However, since epidemiologic studies of environmental risk factors are subject to a number of biases and limitations, these associations should be interpreted with caution.

The putative role of infectious agents in the etiology of IPF has been also investigated in several studies. Positive associations include Epstein Barr virus, cytomegalovirus, hepatitis C virus and human herpes viruses, although these findings have not been consistently replicated (*Molyneaux and Maher, 2013*). Moreover, recent data suggest that IPF is characterized by an increased bacterial burden in bronchoalveolar lavage (BAL) that also predicts disease progression and death (*Han et al. 2014; Molyneaux et al. 2014*); treatment with the antibacterial co-trimoxazole (added to standard treatment), has been shown to reduce mortality in patients with fibrotic IIPs including IPF, an effect possibly related to a reduction of respiratory infections (*Shulgina et al. 2013*).

Comorbidities

Emerging data support a role of gastroesophageal reflux (GER) with subsequent secondary and chronic micro-aspiration as the initial AECs insult driving aberrant tissue remodelling

in IPF (*Fahim et al. 2011*). In pre-clinical studies, aspiration of gastric fluid was shown to activate fibrotic cascades in the pulmonary parenchyma (*Appel et al. 2007*). Moreover, in a prospective study, Raghu and colleagues found that 80% of patients with well-characterized IPF had GER as determined by esophageal pH monitoring, a predictor of acid reflux (*Raghu et al. 2006*). The precise relationship between GER and IPF has yet to be established, but some groups suggest that increased reflux of gastric contents may represent the consequence of reduced lung compliance, distorted mediastinal anatomy and weakening of the lower esophageal sphincter (*Lee et al. 2010*). A recent meta-analysis suggested that pharmacological management of GER with anti-acid therapy was associated with a significant reduction in IPF-related mortality (*Fidler et al. 2018*). In addition, the results of a randomized controlled trial of laparoscopic anti-reflux surgery in IPF suggested also a possible benefit on lung function (*Raghu et al. 2018*).

Obstructive sleep apnea (OSA), an upset characterized by periodic apneas and/or hypopneas caused by partial or complete collapse of the upper airway, is also reported to be common in IPF, with prevalence estimates from 59-88% (*Zaman and Lee, 2018*). The hypothesis that OSA may be related to IPF is supported by the association between OSA and biomarkers that are associated with both lung injury and survival in IPF (*Kim et al. 2017; Lederer et al. 2009*). However, while these findings lend plausibility to a link between OSA and IPF, further research is needed to understand if OSA precedes IPF or vice versa, and to determine whether therapy for OSA can be of benefit in the management of IPF.

Several case-control studies have also suggested a link between IPF and diabetes mellitus (DM) (*Wang et al. 2020*). The main theory regarding the mechanism by which DM may be a risk factor for IPF relates to hyperglycemia-mediated overproduction of advanced glycosylation end products leading to oxidative injury and subsequent overexpression of pro-fibrotic cytokines, fibroblast proliferation and ECM deposition (*Yang et al 2011*). Metformin, the most commonly prescribed drug for DM, has been demonstrated *in-vitro* to attenuate EMT mediated by TGF-β. *In-vivo* studies of metformin have demonstrated attenuation in the bleomycin-induced pulmonary fibrosis mouse model (*Sato et al. 2016*) and more recently, reversal of lung fibrosis (*Rangarajan et al. 2018*).

1.3 Clinical Presentation of IPF

The onset of IPF symptoms is usually progressive and insidious, and the main symptoms find in anamnesis are unexplained chronic dyspnea, reported initially as exertional, and cough, that is often dry. Symptoms are reported to lung specialists after several months from their beginning, because often they are overlooked in the context of ageing in general and sometimes in the history of smoking or other associated comorbidity, such as emphysema, heart disease or a respiratory tract infection. Because of the symptoms overlap, diagnosis of IPF can be delayed for months after its symptomatic onset; generally, the median duration of symptoms before diagnosis is 24 months (*Lancaster et al. 2021*).

About physical examination, bibasal end-inspiratory crepitations, known as velcro-like crackles (rales), are the most common features during chest auscultation. It is very important to recognize them, because through their identification a physician can suspect an ILD and address a patient to specialists for appropriate investigations and an early diagnosis. Digital clubbing, present in 25% to 50% patients, is another clinical finding which can be observed in patients with IPF. Symptoms such as weight loss, fever, fatigue, malaise and joint pain or swelling are uncommon in IPF and should suggest an alternative diagnosis of other forms of ILDs (e.g. pulmonary fibrosis associated with connective tissue disease). Cyanosis, signs of right ventricular failure and peripheral edema may occur in more advanced stages of the disease, together with respiratory failure (*ATS International Consensus Statement, 2000*).

Pulmonary function tests typically demonstrate a restrictive pattern, characterized by reduction in forced vital capacity (FVC) and total lung capacity (TLC), reflecting the increased lung stiffness (and reduced lung compliance) caused by the accumulation of scar tissue and the subsequent architectural distortion of the lung parenchyma. Diffusing capacity of the lung for carbon monoxide (DLCO) is almost invariably reduced due to both a contraction of the pulmonary capillary volume and ventilation and perfusion mismatching. The decline in DLCO may represent the only functional abnormality in early or mild disease. In addition to its diagnostic role, pulmonary function tests are useful in quantifying disease severity and predicting outcome (*Alhamad et al. 2001*). Resting arterial oxygen saturation is usually normal, but with exercise widening of the alveolar-arterial oxygen gradient (P(A-a) O_2), oxygen desaturation, and hypoxemia are commonly observed.
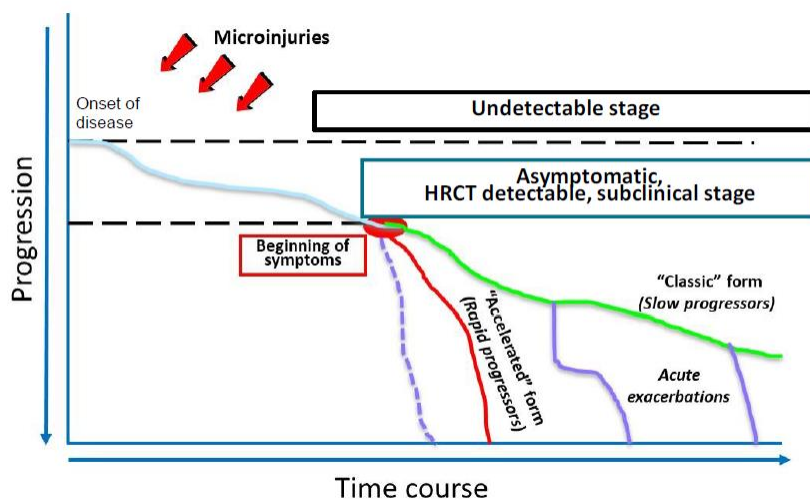
1.4   Natural history of IPF

The natural history of IPF has been described as a progressive decline in subjective and objective pulmonary function until death from respiratory failure or complicating comorbidities (*Gross and Hunninghake, 2001*). The rate of functional decline and disease progression in IPF is highly heterogeneous and unpredictable. Data from the placebo arms of large clinical trials show that the mean annual rate of decline in FVC ranges from 0.13 to 0.21 litres (*Ley et al. 2011*). Moreover, available longitudinal studies do not allow a clear assessment of median survival in IPF. Several retrospective longitudinal studies suggest a median survival time from 2 to 3 years from the time of diagnosis (*King et al. 2001*). However, recent data from clinical trials of patient with preserved pulmonary function suggest this may be an underestimate (*Raghu et al. 2004*).

There appear to be several possible clinical phenotypes of IPF, and for a given patient, the natural history is unpredictable at the time of the diagnosis. It is well recognized that symptoms precede diagnosis by a median of 1 to 2 years and radiographic evidence of disease may even precede symptoms, suggesting the existence of a relatively long period of subclinical disease. Progression of asymptomatic to symptomatic IPF and clinical phenotypes of IPF are represented in **Figure 1.4**. The classic clinical course of IPF is one of *slowly progressive* disease, with patients reporting a history of worsening dyspnea and/or dry cough lasting for months to years. A subgroup of patients, mainly male heavy smokers, experience a rapidly progressive disease course (referred to as *accelerated* IPF) characterized by a poor short-term prognosis. A study, conducted by Selman and coworkers, describes a series of features in patients with rapid decline comparing with slow progressors (*Selman et al. 2007*). Notably, accelerated IPF differs from the typical slowly progressive form in terms of outcome and gene expression profile, despite having similar age, lung function, chest imaging and histology findings at the time of the diagnosis. In this work, rapid progressors show a median survival from the time of diagnosis of 25 months, while slow progressors had a median survival of 93 months. Interestingly, patients with a slower decline experienced symptom from more time before diagnosis (45.9 versus 3.6 months) than patients with a more rapid deterioration did. This would mean that rapid progressors consult physicians shortly after the beginning of symptoms, probably because they deteriorate faster, as opposed to slow progressors in which symptoms are overlooked, and so later reported to a physician.

Patients with IPF may also suffer sudden deterioration of their condition during a relatively stable disease course, defined as *acute exacerbation*. It remains uncertain whether acute exacerbations of IPF (AE-IPF) represent an acceleration of the underlying fibroproliferative

lung process or the sequelae of clinically unrecognized triggers (e.g. infection). There is no established consensus approach to the diagnosis of acute exacerbation of IPF, however it generally requires a combination of the following symptoms: worsening of dyspnea within days to weeks (generally < 30 d); evidence of abnormal gas exchange or a decrease in PaO2; new bilateral ground-glass opacities and/or consolidation superimposed on a UIP radiological pattern; and absence of infection, heart failure, pulmonary embolism, or other identifiable causes (*Collard et al. 2007*). Studies evaluating the clinical significance of AE-IPF have provided discordant incidence rates, likely due to differences in study design, patient populations and definition of AE. Indeed, while in a large retrospective study the 1-year and 3-year incidences of AE-IPF were as high as 14.2% and 20.7%, respectively (*Song et al. 2011*), data from the placebo arms of most large clinical trials suggest that AE-IPF are infrequent events in patients with mild-to-moderate disease (*Kim et al. 2012*). Importantly, the risk of an exacerbation does not appear to be linked to the level of lung function impairment, age, or smoking history (*Kim et al. 2006*). The significance of AE-IPF rests on its poor prognosis, with mortality exceeding 60% during hospital stay and 90% within 6 months after discharge (*Collard et al. 2013*).

Figure 1.4 Heterogeneity of the natural history and clinical phenotypes of IPF patients (Image modified and adapted from *Selman et al. 2007*)**.**

1.5   Diagnosis of IPF

The diagnosis of IPF is based on the recognition of a specific radiological and histological presentation in an appropriate clinical context. According to the official evidence-based guideline for the diagnosis of IPF (*Raghu et al. 2011*), this disease is associated with a histopathological and/or radiological pattern of UIP. However, the diagnosis of IPF is very difficult because the UIP pattern seen in IPF is often indistinguishable from the UIP pattern of other forms of ILD. Recently, in 2018, two guidance documents for the diagnosis of IPF have been published by international experts representing major respiratory and radiological societies, providing a new updated revision of diagnostic criteria (*Raghu et al. 2018; Lynch et al. 2018*). According to these guidelines, a diagnosis of IPF require the following criteria:

- Exclusion of other known causes of fibrosing ILD [e.g. domestic and occupational environmental exposures, connective tissue disease (CTD), drug toxicity].
- The presence of the High-Resolution Computer Tomography (HRCT) pattern of UIP.
- Specific combinations of HRCT patterns and histopathology patterns in patients subjected to surgical lung biopsy (SLB), when possible.

The clinical assessment requires an inquiring mind, a clear understanding of the differential diagnosis for IPF and a comprehensive and structured approach to confirm and exclude known causes and associations of other ILDs, such as hypersensitivity pneumonitis, CTD, pneumoconiosis, and iatrogenic causes (e.g. drug toxicity, irradiation). A clear focus of a patient's clinical examination should be performed to establish the clinical probability of IPF, which is particularly increased when the patient is older than 60 years, male, and has a history of cigarette smoking (*Brownell et al. 2017*).

If a specific diagnosis is not made or no potential cause for ILD is identified, further evaluation is influenced by the patterns of HRCT images of the chest to ascertain or exclude the diagnosis of IPF. Therefore, HRCT plays a pivotal role in the initial assessment of suspected IPF, considerably influencing subsequent management decision. The diagnostic approach is highly reliant on images generated from volumetric acquisition, as it improves detection of all abnormalities even if subtle and focal. High-quality images are essential, and the technical requirements include thin section (<2 mm) and high spatial resolution reconstruction algorithms (*Kusmirek et al. 2016*). Moreover, images should be obtained at full inspiration to total lung capacity with patient position in decubitus supine.

The most recent 2018 guidelines for diagnosis of IPF suggested four diagnostic categories based on HRCT findings: "UIP pattern", "probable UIP pattern", "indeterminate for UIP pattern" and "alternative diagnosis" (*Raghu et al. 2018*) (**Table 1.1**).

Table 1.1 HRCT criteria for the UIP pattern (Table adapted from *Raghu et al. 2018*).

UIP	Probable UIP	Indeterminate for UIP	Alternative diagnosis
o Predominantly subpleural and basal distribution; distribution is often heterogeneous* o Reticular pattern with peripheral traction bronchiectasis or bronchiolectasis+ o Honeycombing	o Predominantly subpleural and basal distribution; distribution is often heterogeneous o Reticular pattern with peripheral traction bronchiectasis or bronchiolectasis	o Subpleural and basal predominant o HRCT features and/or distribution of lung fibrosis that do not suggest any specific etiology	o Upper-lung or mid-lung predominant fibrosis o Peribronchovascular predominance with subpleural sparing o Any of the following: predominant consolidation, extensive pure ground glass opacity (without acute exacerbation), extensive mosaic attenuation with extensive sharply defined lobular air trapping on expiration, diffuse nodules or cysts

* Variants of distribution: occasionally diffuse, may be asymmetrical.
+ Reticular pattern is superimposed on ground glass opacity, and in these cases, it is usually fibrotic. Pure ground glass opacity, however, would be against the diagnosis of UIP or IPF and would suggest AE, hypersensitivity pneumonitis, or other conditions.

UIP is the hallmark radiological pattern of IPF. The typical HRCT features seen in UIP include reticular opacities with obligatory honeycombing, often associated with traction bronchiectasis/bronchiolectasis (**Figure 1.5**). Ground glass opacities may also be present, but they are not the predominant abnormalities and, if present, are usually admixed with reticular abnormality and honeycombing. All these features are characteristically peripheral/subpleural with basal predominance, although they are often patchy; some degree of upper lung involvement is also common, and in some cases the craniocaudal distribution of UIP may be relatively uniform (*Gruden et al. 2013*). Up to 25% of patients with IPF have an asymmetric distribution of fibrosis (*Tcherakian et al. 2011*).
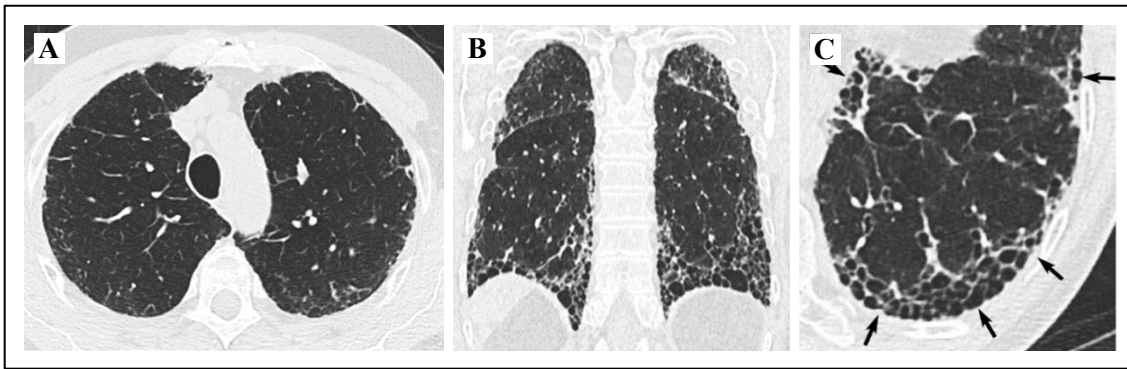
Figure 1.5. Typical UIP HRCT pattern (Image adapted *Raghu et. al 2018*). Axial and coronal HRCT images (**A-C**) for a patient with typical UIP showing the presence of subpleural and basal predominance of reticular abnormality with traction bronchiectasis and honeycombing, with a clear craniocaudal gradient on coronal images (**B**). (**C**) Magnified view of the left lower lobe illustrating typical characteristics of honeycombing, consisting of clustered cystic airspaces with well-defined walls and variable diameters (arrows).

The predictive positive value of radiological diagnosis of UIP pattern on HRCT has been reported to be between 90-100% in several studies (*Raghu et al. 2018*). Therefore, in the appropriate clinical context, a typical UIP pattern by HRCT provides a secure diagnosis of IPF without the need to perform a SLB or other invasive tests *(Lynch et al. 2018)*. Conversely, SLB should be considered when the CT pattern is "probable" or "indeterminate" with UIP, or when the clinical features suggest an alternative diagnosis. Despite histopathology is no longer the diagnostic gold standard in IPF, SLB remains in the 2018 guidelines an important method for the histological confirmation of the UIP pattern and consequently for the final diagnosis of IPF. Therefore, an appropriate combination of HRCT imaging patterns and histological patterns is essential to establish a final diagnosis (*Raghu et al. 2018)*. Video-assisted thoracoscopic surgery is the preferred approach to SLB for patients who can tolerate single lung ventilation, rather than open thoracotomy. In patients with severe physiologic impairment or substantial comorbidity, the risks associated with SLB may outweigh the benefits of establishing a secure diagnosis of IPF: therefore, the final decision regarding whether to pursue a biopsy must be tailored to the clinical situation of the individual patient. Ideally, the biopsy samples should be taken from multiple lobes, due to the high variability in the distribution and morphology of abnormalities and should measure at least 2-3 cm along the pleural margin and be 1-2 cm deep (*Cavazza et al. 2010*).

The histopathologic hallmark and chief diagnostic criterion of UIP is a low magnification appearance of patchy dense fibrosis that is causing remodeling of lung architecture, often

resulting in honeycomb changes, and alternates with areas of less affected parenchyma (**Figure 1.6**). These histopathologic changes typically affect the subpleural and paraseptal parenchyma most severely. Inflammation is usually mild and consists of a patchy interstitial infiltrate of lymphocytes and plasma cells associated with hyperplasia of type II pneumocytes and bronchiolar epithelium. The fibrotic areas are composed mainly of dense collagen, although scattered subepithelial foci of proliferating fibroblasts and myofibroblasts (fibroblast foci) are often present. Microscopic honeycombing is characterized by cystic fibrotic airspaces that are commonly lined by bronchiolar epithelium and filled with mucus and inflammatory cells. Smooth muscle metaplasia in the interstitium is commonly seen in areas of fibrosis and honeycombing.
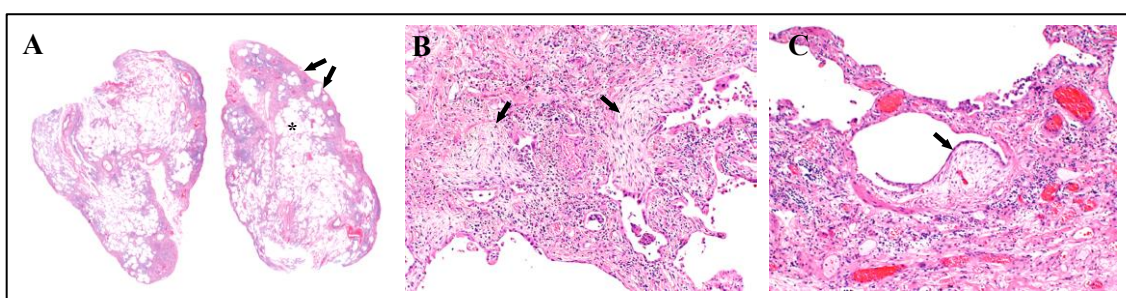
Figure 1.6 Typical histological UIP-IPF pattern (Image adapted from *Lynch et al. 2018*). (**A**) Scanning power microscopy showing classical UIP-IPF pattern characterized by dense fibrosis with a predilection for subpleural and paraseptal parenchyma with associated architectural distortion in the form of microscopic honeycomb change (arrows) and relatively unaffected lung parenchyma (*). (**B-C**) Higher-magnification photomicrograph shows readily identifiable fibroblast foci (arrows). The fibroblast foci are pale and oedematous and somewhat convex or rounded in appearance and adjacent to scarring.

A definitive pathologic diagnosis of the UIP pattern can be made when all these features are present, particularly when honeycombing is present. However, even in the absence of honeycombing, a definite diagnosis of a UIP pattern can still be made if all of the other typical features are present. Complete histopathological criteria for the diagnosis and exclusion of UIP pattern are reported in **Table 1.2**.

Table 1.2 Histopathological criteria for the UIP pattern (Table adapted from *Raghu et al. 2018*).

UIP	Probable UIP	Indeterminate for UIP	Alternative diagnosis
o Dense fibrosis causing architecture remodelling with frequent honeycombing	o Some histologic features from column 1 are present but to an extent that precludes a definite diagnosis of UIP-IPF *And*	o Fibrosis with or without architectural distortion, with features favoring either a pattern other than UIP or features favoring UIP secondary to another cause[*]	o Features of other histologic patterns of IIPs (e.g., absence of fibroblast foci or loose fibrosis) in all biopsies
o Patchy lung parenchyma involvement by fibrosis	o Absence of features to suggest an alternative diagnosis *Or*	o Some histologic features from column 1, but with other features suggesting an alternative diagnosis[+]	o Histologic findings indicative of other fibrotic disease (e.g., fibrotic hypersensitivity pneumonitis, Langerhans cell histiocytosis, sarcoidosis, or smoking-related interstitial fibrosis
o Predominant subpleural and/or paraseptal distribution of fibrosis	o Honeycombing only		
o Fibroblast foci at the edge of dense scars			

[*]Granulomas, hyaline membranes, prominent airway-centered changes, areas of interstitial inflammation lacking associated fibrosis, marked chronic fibrous pleuritis, organizing pneumonia.
[+]Features of an alternative diagnosis should include a cellular inflammatory infiltrate away from areas of honeycombing, prominent lymphoid hyperplasia including secondary germinal centers, and a distinctly bronchiolocentric distribution that could include extensive peribronchiolar metaplasia.

1.6   Pathogenesis of IPF

Despite the comprehensive understanding of IPF pathogenesis remains elusive, research efforts in the last few years have reached important milestones, making the concept "idiopathic" less compelling. The old concept of pulmonary fibrosis being a direct consequence of chronic inflammation has been replaced by the idea of an aberrant wound-healing process involving interstitial and alveolar spaces of the lung (*Pardo and Selman, 2002*). The current paradigm suggests that IPF is an epithelial-fibroblastic disorder whereby continuous micro-repetitive injury to the epithelial cells within the lung causes abnormal wound healing responses including epithelial apoptosis and senescence, aberrant proliferation and differentiation of fibroblasts and myofibroblast, formation of fibrotic foci, excessive deposition of ECM components, and fibrotic-related immune reaction. All these aberrant signals ultimately resulting in an irreversible accumulation of scar tissue, characterized by collagen deposition, which dramatically remodel the lung architecture by stiffening the distal airspaces and parenchyma, leading progressive loss of function (*Wolters et al. 2014; Nathan Sandbo 2013/ Chapter 8*).

The pathogenic cascade, following the injury to the lung epithelium, involves a multitude of cellular types and complex cell-matrix interactions, through various biochemical

mediators and specific signalling pathways. The proposed abnormal wound healing model of IPF is schematized in **Figure 1.7**.

Alveolar epithelial injury

Repeated injury to the alveolar epithelium is believed to be the initiating trigger for the development and sustainment of the fibrotic process. However, the exact cause of mechanism of these multiple injuries are still unknown. AECs, in a form of monolayer, cover the alveolar wall and communicate with the endothelial cells through the epithelial basal lamina. This architecture represents the primary gas-exchanging interface of the lung that allows the rapid diffusion of oxygen and carbon dioxide between the alveolar airspace and blood. The normal alveolar epithelial lining is composed by AECs, type I and type II. The AECs type I are the most represented cells in the alveolar-capillary interface, covering more than 96% of the total alveolar surface area. They are highly specialized and have a flat morphology, which provides a thin membrane for gaseous exchange. Type II AECs are cuboidal in nature and they are usually localized in the corners of the alveoli, lying adjacent to the mesenchymal cells. playing a crucial role in lung homeostasis. Specifically, they are involved in the secretion of surfactant proteins (SPs), retain proliferative capacity, and are responsible for the regeneration of epithelium after injury, including trans-differentiation to type I cells (*Sandbo, 2013/ Chapter 8*).

Under normal circumstances, when damage of the alveolar surface occurs, injured type I AECs are replaced by type II AECs. This results in hyperplastic proliferation of the type II AECs in order to cover the exposed alveolar surface. After the interruption of the injuring stimulus, the exceeding cells undergo regulated apoptosis, while the remaining AECs type II differentiate into type I pneumocytes, thus repairing the alveolar injury and re-establish epithelium integrity and functionality (*Selman and Pardo, 2006*). This requires coordinated, spatially and temporally regulated responses, including inflammatory responses as well as the activation of local coagulation pathways and the formation of a provisional matrix along which activated fibroblast and myofibroblasts migrate promoting wound contraction. In the final remodeling stage, the wound area is resolved, and normal tissue structure and structural integrity is restored (*Strieter, 2008*).

In IPF, lung epithelium is markedly abnormal showing evidence of hyperplastic type II AECs, transitional epithelial cells with areas of bronchiolization and squamous metaplasia (*Cavazza et al. 2010*). Specifically, the integrity of the basement membrane remains disrupted with hyperplastic type II AECs proliferation on an inappropriate ECM without restoration of normal alveolar structures. An aberrant wound repair response can then be

initiated during which the residual epithelial cells, predominantly type II AECs, together with inflammatory cells are thought to release several pro-fibrotic cytokines, growth factors, especially TGF-β, and other chemokines at the site of injury promoting a fibrotic tissue-repair response. The epithelial injury ultimately promotes the activation and proliferation of fibroblasts and myofibroblasts and the formation of a stiffened ECM (*Camelo et al. 2014; Kasper and Bath, 2017*). Because of this event, the AECs undergo the EMT, a process in which the cells lose the characteristic of a full differentiated epithelial cells, such as cuboidal shape, and they become cells of the mesenchymal lineages, showing reduced cell adhesion and increased motility. At the same time, they lose most epithelial markers in favour of mesenchymal markers (*Sandbo, 2014. Chapter 8*). The failure of AECs type II to repopulate the epithelium and restore the normal condition leads to the activation of fibroblasts (*Knudsten et al. 2016*).

Role of fibroblast and origin of myofibroblast

Fibroblasts are elongated, spindle-shaped, not terminally differentiated mesenchymal cells, committed to re-establish a normal and well-structured ECM in wound healing repair process. Specifically, they have a fundamental role in producing proteins that compose the ECM, such as collagen and fibronectin, in addition to glycosaminoglycans and proteoglycans that constitute the space-filling substances of the connective tissue (*Kendall and Feghali-Bostwick, 2014*). Moreover, fibroblasts modulate ECM turnover through the expression of matrix metalloproteinases (MMPs), which degrade ECM, and their inhibitors, tissue inhibitors of metalloproteinases (TIMPs). This cell type can respond to a broad series of stimuli, such as cytokines and growth factors. During IPF pathogenesis, both lung and fibrocytes-derived fibroblasts are persistently exposed to profibrotic mediators secreted by activated fibroblast, leading to excessive deposition of ECM and trans-differentiation to myofibroblasts. Myofibroblasts are thought to play a vital role in the development of IPF and are probably responsible for the enhanced synthesis of abnormal matrix observed in pulmonary fibrosis. Myofibroblasts express α-smooth muscle actin (α- SMA) and represent an intermediary phenotype between fibroblasts and smooth muscle cells (*Darby et al. 1990; Roy et al. 2001*). The main function of this mesenchymal cell is synthesis and secretion of ECM proteins, wound contraction ability, ECM remodeling and resistance to apoptosis. In myofibroblasts, α-SMA microfilaments organize in bundles and associate with contractile proteins, such as non-muscle myosin, creating a cellular apparatus defined as stress fibers. The transient appearance and disappearance of myofibroblasts are observed during normal healing and repair process; their number dramatically increases after an injury, during

which they contribute to the formation of the granulation tissue and they produce the contractile force needed to close the wound (*Gabbiani, 2003*). When the tissue healing is completed, the majority of cells undergoes apoptosis and a poorly cellularized scar substitutes the granulation tissue. On the other hand, in IPF, the persistent presence of myofibroblasts is a constant feature (*Pardo and Selman 2002*). During activation and proliferation, fibroblasts/myofibroblasts release pro-fibrotic factors, first of all TGF-β, which can cause AEC damage. These cells also secret MMPs which may disrupt the basement membrane, alter the tissue architecture and inhibit alveolar re-epithelialisation (*Selman and Pardo, 2002*). Failure of alveolar re-epithelialisation can cause a continuous fibrotic response through activation of myofibroblasts that further inhibit re-epithelialisation. In IPF, apoptosis-resistant myofibroblasts are organized as pools called "fibroblastic foci", the histological hallmarks of the pathology, which are mainly located in alveolar regions of hyperplastic or apoptotic epithelial cells. Activated fibroblasts inside the fibroblastic foci produce huge quantities of proteins that compose the extracellular matrix and some of them (in particular elastin, collagen type V, and tenascin C) stimulate an additional cellular differentiation into myofibroblasts, establishing a positive feedback mechanism (*Blaauboer et al. 2014*). Although the presence of myofibroblasts within the fibrotic lesion is apparent, their origin and the reasons why they organize in morphologically distinct foci in IPF remains elusive. There is ample evidence showing that myofibroblasts can be transformed from tissue fibroblasts in presence of TGF- β (*Desmoulière et al. 1993*) and interleukin-4 (IL-4) (*Mattey et al. 1997*) *in-vitro*, but *in-vivo*, how myofibroblasts are acquired in the site of fibrotic lesion of IPF is largely unknown. Based on their similar cellular kinetics, it is assumed that myofibroblasts are transformed cells from pre-existing resident tissue fibroblasts with the influence of stimulatory cytokines, such as TGF-β (*Phan, 2002*). Some studies suggested that circulating fibrocytes derived from bone marrow stem cells could be an extra-pulmonary source of fibroblasts and myofibroblasts in IPF (*Lama and Phan, 2006; Hashimoto et al. 2004; Ishii et al, 2005*). Another possible source of myofibroblasts in fibroblastic foci is AECs by EMT. Strong evidence indicates that AECs are the primary source of mediators that functions chemotactic factors or mitogens for mesenchymal cells, including platelet-derived growth factor (PDGF), TGF-β, tumor necrosis factor-α (TNF-α), and endothelin 1 (*Selman and Pardo. 2006*). These factors probably contribute mostly to the migration, proliferation, and differentiation of resident mesenchymal cells.

ECM remodeling phase

The ultimate result of IPF is abnormal tissue remodelling, characterized by extensive deposition of connective tissue followed by constant destruction of the lung parenchyma to form fibrotic lesions. In a normal lung, architecture and ECM environment are maintained by the constant and tightly regulated control between matrix production and proteolysis. During IPF, matrix organization is severely altered with increased accumulation of different matrix components, including fibronectin, hyaluronic acid, and various isoforms of collagen. Excessive collagen deposition is one of the principal hallmarks of a fibrotic process and its complex and disorganized structure in IPF is responsible of the stickiness and rigidity of the lung. The fibrotic role of collagen is not due only to its accumulation, but also to its uncorrected processing and organization. Studies of the collagen content of IPF lungs have demonstrated that collagen III is the primary component in areas of alveolar septal fibrosis while collagen I is more represented in areas of mature fibrosis. The exact molecular mechanisms responsible for abnormal matrix remodelling are poorly understood, although dysregulation in tissue turnover involves mainly two families of proteinases, MMPs and TIMPs. An imperfection in the balance and in the spatial localization of these enzymes plays a role in the matrix accumulation typical of IPF (*Sandbo, 2013 / Chapter 8*). The MMPs role is not only related to degradation and modification of extracellular matrix component; they are also important for other cellular mechanisms, such as proliferation, differentiation and apoptosis, because they are able to cleave and activate a large number of mediators and cell surface receptors. Thus, a dysregulation in this class of enzymes has an important effect in the pathogenesis of IPF, irrespective of his involvement with ECM (*Pardo et al. 2016*).
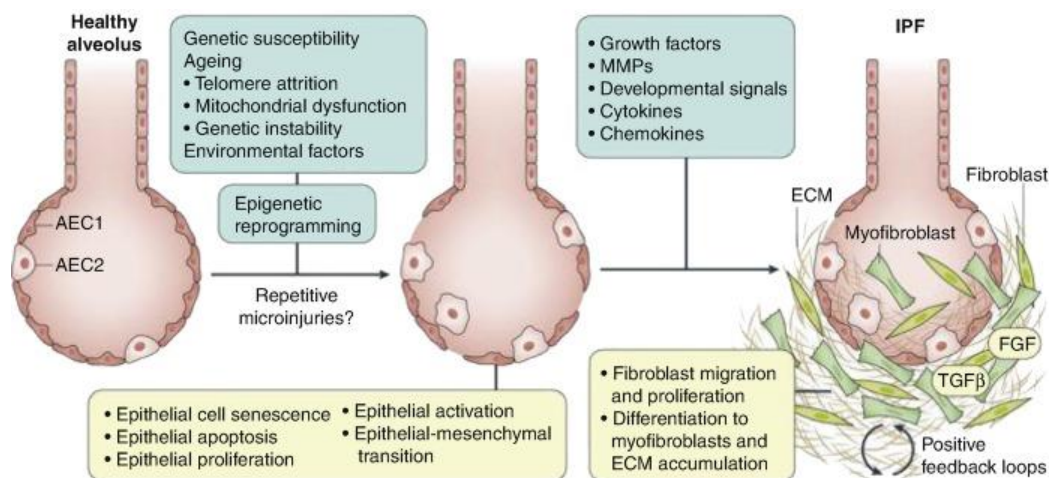
Figure 1.7. A proposed pathogenetic model of IPF *(Martinez et al. 2017)*.

1.7 Current treatment for IPF

The pharmacological approaches attempted in clinical trials for IPF have undergone a huge change during the past ten years, reflecting the new knowledge on the pathogenesis of the disease and the better definition of the diagnostic criteria. At the beginning of the history of IPF, scientists and physicians thought that pulmonary fibrosis was a direct consequence of a long process of inflammation triggered by alveolar injury. Based on these evidences, in the past, the typical regimen of care for patients with IPF was a therapy based on anti-inflammatory and immunosuppressive drugs, such as corticosteroids. Nevertheless, none of these therapies proved effective in treating the disease, and in a phase III clinical trial based on a triple combination therapy of anti-inflammatory and immunosuppressive (prednisone, azathioprine and N-acetylcysteine), the study was stopped due to increased risk of death besides the ineffectiveness in preserving lung function (*Datta et al. 2011; Izumi et al. 2012*). The failure of anti-inflammatory and immunosuppressive therapies together with the new paradigm that IPF could rise from an aberrant wound healing process with a disorganized remodelling of the EMC resulting in a scarred lung parenchyma, have shifted the focus to drugs with anti-fibrotic and anti-proliferative properties. On the wave of this new information and thanks to the optimization of the clinical studies design, with suitable endpoints, in the last few years two different anti-fibrotic molecules were approved and recommended for the treatment of IPF: Pirfenidone and Nintedanib, two compounds with pleiotropic mechanisms of action. Both drugs are able to slow down functional decline and disease progression in IPF, but neither drug improves or even stabilizes lung function, or improves quality of life (*Kreuter et al. 2015*); therefore, they do not offer a cure and are also associated with tolerability issues (*Galli et al. 2017*).

Pirfenidone (Esbriet®), an orally administered pyridine, is a small molecule with a pleiotropic effect developed by InterMune Inc. (now Roche), and approved for clinical use in the treatment of mild-to-moderate IPF by the two major drug agencies, the European Medicines Agency (EMA) and the American Food and Drug Administration (FDA) in 2011 and 2014 respectively. Although the exact mode of action for this molecule remains elusive, Pirfenidone has been shown to have anti-inflammatory, antioxidative and anti-proliferative properties in a number of cellular and animal models of inflammation and fibrosis (*Macias-Barragon et al. 2010*). Several *in-vitro* studies on human lung fibroblasts have shown that Pirfenidone reduces markers of oxidative stress (*Giri et al. 1999; Misra et al. 2000*), the proliferation of lung fibroblasts and their differentiation into myofibroblasts by attenuating key TGF-β-induced signalling pathways, the expression of TGF-β-induced

heat-shock protein 47, which is involved in processing/secretion of procollagen, and reduces expression of α-SMA and collagen type I (*Conte et al. 2014; Nakayama et al. 2008*). Moreover, in animal models of bleomycin-induced pulmonary fibrosis, Pirfenidone has also been shown to diminish TGF-β levels, the influx of fibrocytes, the number of myofibroblasts and the accumulation of inflammatory cells (*Oku et a. 2008; Kakugawa et al. 2004*). Pirfenidone also reduced the accumulation of hydroxyproline, a major component of collagen and marker of fibrosis, and levels of procollagen I and III in these models.

The conditional recommendation in international guidelines for the use of Pirfenidone in patients with IPF is essentially based on the outcomes of three phase III clinical trials: CAPACITY-004, CAPACITY-006 and ASCEND (*Noble et al. 2011; King et al. 2014*). Specifically, the two concurrent CAPACITY trials involved patients with mild-to-moderate IPF, and the primary endpoint was change in percentage predicted FVC from baseline to week 72. Although the study 004 met this primary endpoint showing mean decline in percentage FVC –8.0% in the high-dose Pirfenidone arm (2,403 mg/day) compared to –12.4% in the placebo arm at 72 weeks of treatment (p=0.001), in the study 006, the difference between groups in predicted FVC change at week 72 was not significant (–9.0% *versus* –9.6% in the treatment and placebo arms respectively, p=0.501) (**Figure 1.7 A**) (*Noble et al. 2011*). Due to discrepancies between the two CAPACITY trials in meeting their primary endpoints, the US FDA requested a subsequent double-blind, randomized, placebo-controlled phase III trial to confirm the efficacy and safety of Pirfenidone in IPF. In the ASCEND study, the inclusion criteria were modified to enroll patients at higher risk of disease progression and the primary endpoint was the change from baseline to week 52 in the percentage of predicted FVC. The mean decline from baseline in FVC was 235 mL in the Pirfenidone group and 428 mL in the placebo group (absolute difference 193 mL, relative difference 45.1%; p<0.001) (**Figure 1.7 B**) (*King et al. 2014*). Furthermore, a pooled analysis of the two CAPACITY and the ASCEND studies (a total of 1247 patients) revealed a positive outcome in terms of mortality. At 1 year, Pirfenidone at 2,403 mg/day reduced the proportion of patients with a ≥10% decline in percentage predicted FVC or death by 43.8% and increased the proportion of patients with no decline by 59.3% compared with placebo (*Noble et al. 2016*). Overall, Pirfenidone was generally well tolerated in practice, with the most common side effects being gastrointestinal discomfort and skin-related complications which, however, rarely led to treatment discontinuation.
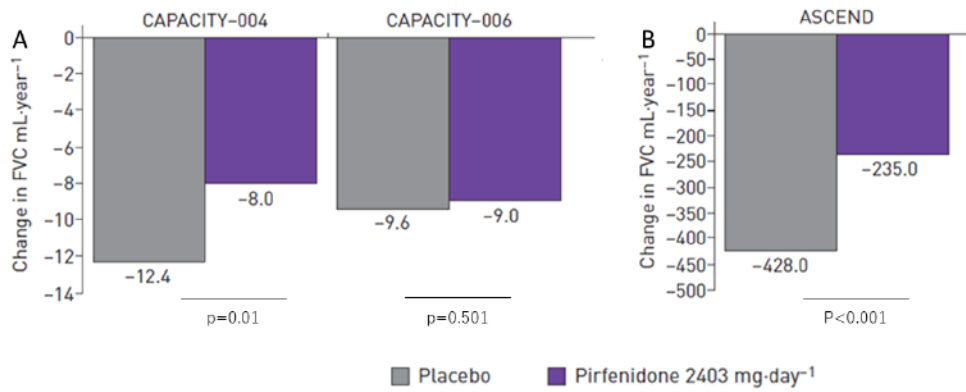
Figure 1.7 Mean change from baseline in percentage predicted FVC in the **A**) phase III CAPACITY-004, CAPACITY-006, and **B**) ASCEND studies (Image reproduced from *Richeldi et al. 2018*).

Nintedanib (Ofev®), an indolinone derivative, is an orally active small molecule developed by Boehringer Ingelheim and approved for the treatment of IPF by the EMA and FDA, in 2015 and 2014 respectively. Nintedanib, also known as BIBF 1120, is a potent intracellular tyrosine kinases inhibitor which acts on multiple downstream signalling pathways involved in fibrogenesis. Specifically, Nintedanib competitively binds to the adenosine triphosphate binding pocket of these receptors inhibiting the activation of the platelet-derived growth factor receptors (PDGFR), vascular endothelial growth factor receptors (VEGFR) and fibroblast growth factor receptors (FGFR) signalling cascades which are critically involved in the proliferation, migration and differentiation of lung fibroblasts/myofibroblasts, the hallmark cells in the pathology of IPF (*Hilberg et al. 2008*). Originally developed as a potent angiogenesis inhibitor for cancer treatment, Nintedanib also demonstrated to exert anti-fibrotic activities both *in-vitro* in human lung fibroblasts and *in-vivo* in bleomycin-induced pulmonary fibrosis in rodents. In human lung fibroblasts, Nintedanib has been shown to inhibit fibroblast proliferation, growth factor-stimulated fibroblast motility and contraction, and TGF-β-induced fibroblast to myofibroblast transformation (*Hostettler et al. 2014*). In animal models of pulmonary fibrosis, Nintedanib has demonstrated anti-fibrotic effects including reductions in lung collagen content and morphometric fibrosis scores and reduced expression of TGF-β and procollagen I. Anti-inflammatory effects of Nintedanib have been also demonstrated by reductions in lymphocytes and neutrophils counts in BALF, reduced inflammatory cytokines and reduced histological inflammation (*Wollin et al. 2014; Wollin et al. 2015*).

At a clinical level, the conditional recommendation for the use of Nintedanib in international guidelines is based on the outcomes from three clinical studies:

TOMORROW, INPULSIS-1 and INPULSIS-2 (*Richeldi et al. 2011; Richeldi et al. 2014*). The phase II TOMORROW trial showed that Nintedanib, 150 mg twice daily, effectively reduced the annual rate of decline in FVC by 68.4%, as compared to placebo group (60 mL *versus* 190 mL, respectively; p<0.06 with the closed testing procedure for multiplicity; p<0.01 with hierarchical testing) (**Figure 1.8 A**) (*Richeldi et al. 2011*). Subsequently, the phase III program INPULSIS, consisting of two 52-week parallel, identical placebo-controlled, multicentral trials was developed to further evaluate the efficacy and safety of Nintedanib in 1066 patients with IPF. Outcomes from both studies confirmed Nintedanib efficacy in reducing significantly the annual rate of decline in FVC, the primary endpoint, as compared with placebo group (INPULSIS-1: difference 125.3 mL (−114.7 mL and −239.9 mL, respectively; p<0.001); INPULSIS-2: difference 93.7 mL (−113.6 mL and −207.3 mL, respectively; p<0.001)) (**Figure 1.8 B**) (*Richeldi et al. 2014*). A pooled and meta-analyses of the TOMORROW and the two INPULSIS studies further supported the beneficial effect of Nintedanib versus placebo over 52 weeks both in terms of disease progression, time to first acute exacerbation, maintenance of health-related quality life and time to all-cause and on-treatment mortality (*Richeldi et al. 2016*). In similarity to Pirfenidone, post-hoc analysis has suggested that Nintedanib is equally efficacious in patients with mild or severe disease irrespective of baseline characteristics (*Costabel et al. 2016*) and appears to be equally effective in patients with a "possible UIP" pattern compared to those with "definite UIP" radiologically (*Raghu et al. 2017*). The most common adverse events related to the use of Nintedanib mainly affect the gastro-intestinal tract. Particularly, diarrhea is the most frequent adverse event, followed by nausea and vomiting; weight and appetite loss are also quite frequent (*Richeldi et al. 2016*).
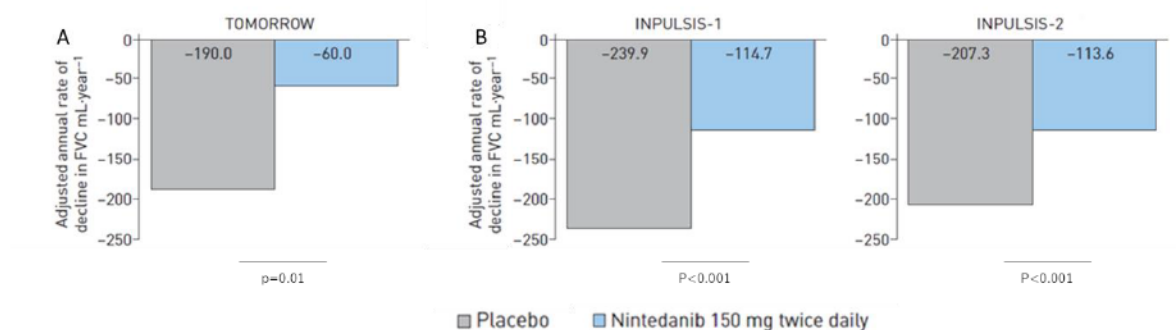
Figure 1.8 Annual rate of change from baseline over time in FVC in the **A**) phase II TOMORROW, **B**) phase III INPULSIS-1 and INPULSIS-2 studies (Image reproduced from *Richeldi et al. 2018*).

Since the two drugs have very similar beneficial effects in treating IPF (*Rochwerg et al. 2016*), there is no general answer about which drug could be better prescribe to a patient with IPF. Actually, there have been no head-to-head comparisons, and there are no any biomarkers to identify responders to either drug. Therefore, in the absence of clear evidence, treatment decision will depend on what is more appropriate for each single patient (e.g. patient preference, comorbidities and concurrent medications). For instance, photosensitivity and cutaneous rash limit the use of Pirfenidone in patients that possess dermatologic pathology or that cannot avoid sun exposure. Conversely, Nintedanib will be prescribed with caution in patient who receives concomitant anticoagulant therapy due to the anti-angiogenic properties of the drug. Moreover, no data are available to guide clinicians regarding the timing of initiation of therapy, how a response should be defined, and when the therapy should be discontinued (*Raghu and Selman, 2015*).

1.8 Future pharmacological approaches in IPF

IPF treatment remains one of the major challenges for the respiratory physicians and for the community of clinical and translational investigators. Although the use of two anti-fibrotic drugs, Pirfenidone and Nintedanib, has been approved for the treatment of IPF, many gaps are still to be filled. First, as mentioned in the previous paragraph, neither of the two drug stops the disease, but they only slow the pace of disease progression; moreover, both therapies have tolerability issues, and because side effects are relatively common, they lead to treatment discontinuation in a non-negligible proportion of patients. Second, neither drug improves quality of life or symptoms, such as dyspnea and cough. Third, there is no clear mortality benefit, and it remains to be determined to what extent a beneficial effect on functional decline translates to a significant survival effect. Fourth, the effect of either drug on major comorbidities of IPF patients, such as pulmonary hypertension, venous thromboembolism or lung cancer, has still to be evaluated. At present, there is no treatment that can cure IPF. The only possibility to improve the survival of patients with IPF is the lung transplantation, but, due to age and comorbidities, this represents a realistic therapeutic option only for a small portion of selected patients. For this reason, the remaining unmet medical needs continue to stimulate the research to the identification of new concepts or interventions aimed at treating IPF. These strategies may include biomarkers guiding therapy, novel drugs targeting different pro-fibrotic pathways in fibrosis, and the use of combination therapies.

1.8.1 Biomarkers

The IPF disease course and response to anti-fibrotic therapy demonstrates marked heterogeneity, making diagnosis and individual prognosis very difficult. Thus, a prerequisite for future personalized therapy for IPF could be the development of biomarkers that can guide diagnostic, prognostic and therapeutic approaches in managing the disease. Currently, several potential biomarkers categorized according to the different pathways involved in the pathogenesis of IPF in three groups, namely biomarkers associated with AEC dysfunction, biomarkers associated with ECM remodeling and fibroproliferation, as well as biomarkers related to immune dysfunction, are under study and some of the most promising candidates are summarized in **Table 1.3**.

Diagnostic biomarkers

Despite advances in imaging technology and disease classification systems, accurate diagnosis of IPF can remain elusive. Therefore, the identification of specific and non-invasive biomarkers that can guide the early diagnosis and differential diagnosis of IPF is of great interest. A number of peripheral blood biomarkers, including markers of AEC damage, immune dysfunction as well as ECM remodeling such as MMPs, have been studied with the aim to discriminate IPF patients from healthy individuals. However, their ability to distinguish IPF from other forms of ILDs is still conflicting (*Jee et al. 2019*). The PROFILE (Prospective Study of Fibrosis in Lung Endpoints) study, the first study performing a sequential evaluation of >100 serum protein biomarkers, demonstrated the importance of these markers in IPF, showing significantly elevated levels of MMP-1, MMP-7 and SP-D in IPF patients compared to healthy controls (*Saini et al. 2012*). Notably, in the pioneer work by Rosas et al., levels of MMP-1 and MMP-7 have been found to be elevated in the plasma, in BAL fluid (BALF), and in tissue of IPF patients as compared to healthy controls and their combination showed to distinguish IPF patients from those with either chronic respiratory disorders (*Rosas et. al 2008*) or other ILDs (*Morais et al. 2015*). The biomarkers of AEC damage and dysfunction, SP-D and Krebs von den Lungen (KL-6)/Mucin 1 (MUC1), have also been widely used in clinical practice in Japan as part of the diagnostic work-up for ILDs for more than 10-years, although evidence from clinical trials validating their clinical efficacy in IPF remains limited (*Ishikawa et al. 2012; Homma et al. 2018*). Further studies in broader prospective cohorts will be needed to establish the reliability of these markers in routine clinical settings and thus, currently none of these are recommended by guidelines for diagnostic purposes in IPF (*Raghu et al. 2018).

Prognostic biomarkers

Progression in IPF is challenging to predict due to the heterogeneity of the population. FVC decline has been shown to be a predictor of mortality in IPF (*du Bois et al. 2011*) and is the most robust parameter adopted in clinical trials. However, baseline FVC is not an early predictor of the disease. Therefore, prognostic biomarkers that reflect disease state, in term of severity or progression are urgently needed to guide patient management. Several biomarkers are currently under exploration, with promising significant association with prognosis of IPF. Threshold serum levels of KL-6, or sequential changes in KL-6 levels, have been shown to predict lung function decline or outcome in patients with IPF. Elevated baseline KL-6 levels have been also associated with increased risk of AE-IPF. High serum levels of SP-A and SP-D have been associated with decreases in DLCO and FVC as well as with early mortality. Among the biomarkers associated with immunity dysfunction, C-C motif chemokine ligand 18 (CCL-18) demonstrated to correlate with lung function and mortality in both IPF patients. Finally, among those associated with ECM remodeling, MMP7 is considered one of the most promising prognostic biomarkers in IPF, with circulating levels correlating with disease severity assessed by FVC and DLCO and with survival reported in several studies (*Inoue et al. 2020*). Furthermore, as extracellular collagen fragments generated by MMPs and released into circulation may provide an indirect measure of MMP activity, the role of these neoepitopes have been the focus of a recent work, the PROFILE (Prospective Observation of Fibrosis in the Lung Clinical Endpoints) study (*Jenkins et al. 2015*). In this study by Jenkins and coworkers, 6 of 11 collagen-derived neoepitopes showed increased serum levels in patients with IPF compared with those in healthy volunteers and higher levels in patients with progressive vs stable disease. Patients with IPF showing faster rates of increase in these biomarkers over 3 months showed more rapid disease progression and reduced survival. Other promising predictors of progression and survival in patients with IPF were found to be cancer antigen (CA)19-9 and CA-125, as recently reported in the multicenter PROFILE longitudinal cohort study (*Maher et al. 2017*).

Therapeutic biomarkers

Despite some diagnostic and prognostic biomarkers are showing some promise, there is still a lack of biomarkers that can help to identify those individuals that most likely benefit from treatment (stratification biomarkers) and biomarkers that can measure the individual's treatment response (pharmacodynamic biomarkers). In a recent study, some biomarkers were tested to interact with Pirfenidone treatment and whether it could serve as prognostic,

predictive or pharmacodynamic biomarker (*Neighbors et al. 2018*). There, Pirfenidone treatment effects were consistent regardless of baseline biomarker levels, and Pirfenidone treatment had no meaningful pharmacodynamic effect on the plasma levels of these biomarkers. In this regard, retrospective analysis in small studies reported that KL-6 levels decreased in stable IPF patients on Pirfenidone (*Kuwano et al. 2002; Okuda et al. 2013*). Similarly, reduced levels of SP-D have been reported after Pirfenidone treatment in IPF in a small Japanese study (*Okuda et al. 2013*). These data were in agreement with a Japanese retrospective analysis showing prognostic effects of SP-D in an IPF cohort receiving Pirfenidone (*Ikeda et al. 2017*). However, despite interesting these data are quite limited and confirmation and validation in prospective and larger cohorts is required. Finally, the INMARK trial also investigated the effect of Nintedanib on the two markers of epithelial damage, CA19-9 and CA-125, suggesting a potential role of this latter as a biomarker of response to Nintedanib in patients with IPF (*Jenkins et al. 2020*). Taken together, reliable predictive therapeutic biomarkers are still missing and the information available so far is very limited.

Despite the last decade saw great interest, motivation, and progress in biomarkers research, driven by significant advances in the understanding of IPF pathogenesis, the clinical use of the previously described biomarkers is strongly limited in "real life" IPF, indeed none of them has been validated yet and the current evidence are insufficient to support their routinely clinical use. The main reasons concern the fact that most of these biomarkers have been studied in an observational and retrospective manner, and the samples were generally limited; the lack of a longitudinal analysis in the majority of biomarkers investigated; the absence of a robust validation of the assays in independent validation cohorts; furthermore, the comparability of different studies is hindered due to the use of different collection protocols and biological materials for biomarker analysis. Other challenges that preclude pooling of results and accurate comparison of studies include the lack of a gold standard for measuring disease activity, standardized assays for biomarker testing, discrepancy in thresholds defining positive and negative results, and the highly heterogeneous nature of IPF itself.

The development of clinically validated biomarkers for IPF represents, therefore, the central challenge to translational research in the field over the next decade. In this context, an encouraging work is represented by the project PROLIFIC (PROgnostic Lung FIbrosis Consortium), that in collaboration with the Pulmonary Fibrosis Foundation and several pharmaceutical companies, is developing Multiplex well-qualified assays of a selected

group of 12 relevant biomarkers in IPF, to be used within the clinical setting; such platforms should contribute to an improved screening, prognosis, and care of IPF patients (*3rd Annual IPF Summit; August 27-29, 2019; San Diego, CA*).

Overall, future investigations, including longitudinal and high throughput biomarker analyses into prospective clinical trials with huge patient numbers, ideally in combination with clinical endpoints and with genotyping of these patients, will allow the identification of early predictors of disease progression and different subgroups of patients with heterogeneous disease courses, different prognosis and response to treatment. These studies should be the prerequisite for a more "personalized" medicine in patients affected by IPF.

Table 1.3 Candidate biomarkers for IPF and the strength of evidence supporting their clinical role. (Table adapted from *Inchingolo et al. 2018*)

Biomarkers	Mechanism of action	Significance in IPF
Alveolar epithelial cell damage and dysfunction		
KL-6/MUC1	High molecular-weight glycoprotein strongly expressed on bronchiolar and type II AECs, promoting migration, proliferation and survival of lung fibroblasts	Correlation with disease severity (imaging and lung function tests); increased levels suggest worse prognosis; higher levels in AE-IPF
SP-A and SP-D	Surfactant proteins produced by type II AECs and Clara cells, involved in the lung host innate immunity	Strong predictors of early mortality
CA-125 and CA19-9	Tumor markers, mucous associated carbohydrate antigens increasing in metaplastic epithelium in fibrotic lesions	Predictor of progression and increased mortality
Aberrant fibrogenesis and ECM remodelling		
MMP-1, MMP-3, MMP-7	Zinc-dependent proteases involved in the breakdown of ECM components	Correlation with disease severity; predictors of worse outcome
Neoepitopes	Circulating protein fragments generated as result of the ECM remodeling and released from the tissue into the circulation	Association with mortality; potential predictors of occurrence and outcome
Periostin	ECM protein promoting ECM deposition and mesenchymal cells proliferation	Correlation with physiological progression
Osteopontin	Glycoprotein involved in cell adhesion and migration	Support for differentiation with non-IPF ILD
Circulating fibrocytes	Bone-marrow-derived progenitor cells that circulate in the bloodstream and migrate to sites of tissue injury, differentiate into fibroblasts and are capable of producing ECM components	Correlation with lung function tests; increased level associated with worse survival
Lysyl oxidase-like 2 (LOXL2) protein	Enzyme secreted by activated fibroblasts that facilitates the cross-linking of type 1 collagen Molecules and plays a key role in ECM remodeling and fibrogenesis	Association with risk of progression and higher mortality
Immune dysregulation and inflammation		
CCL-18	Chemokine produced by alveolar macrophages involved in the stimulation of collagen production by lung fibroblasts	Predictor of progression and increased mortality
Intercellular adhesion molecule 1 (ICAM-1)	Adhesion molecule expressed on leukocytes and vascular endothelial cells; marker of oxidative stress in the lungs	Predictor of mortality
C-X-C motif chemokine 13 (CXCL-13)	Chemokine playing a role in autoimmune processes, mediating B-cell homing to inflammatory foci	Predictor of progression and mortality

Table 1.3 *(continued)*

Biomarkers	Mechanism of action	Significance in IPF
Immune dysregulation and inflammation		
Chitinase-3-like protein 1 (YKL-40)	Chitinase-like protein produced by alveolar macrophages and type II AECs involved in innate immunity and ECM remodeling	Predictor of worse outcome
Damaged endothelium		
VEGF	Growth factor regulating angiogenesis enhancing vascular permeability	Association with disease severity, and predictor of progression

1.8.2 Novel therapeutics targets

Growing understanding of the pathogenesis of IPF and the observation that both Pirfenidone and Nintedanib are pleiotropic in their action suggests that a variety of putative mediators and signalling pathways are likely to be involved in the pathogenesis of IPF and that, truly effective therapies will be needed in order to target pro-fibrotic signalling pathways at multiple levels. Numerous potential molecular targets of novel therapeutics agents have been identified, many of which are currently in early clinical trials. The **Figure 1.9** shows a schematic representation of the scenario of the most emerging drug candidates for IPF under development nowadays.

Anti-connective tissue growth (CTGF) factor antibodies

CTGF is a pleiotropic growth factor that acts as a key regulator of several cellular responses, including cell adhesion and migration, angiogenesis and vascular permeability, myofibroblast activation, extracellular matrix deposition, and tissue remodeling (*Lipson et al. 2012*). CTGF is normally expressed in low levels in healthy individuals, however, when expressed in excess it leads to upregulation of TGF-β, deposition of ECM and inhibition of ECM degradation through the inhibition of MMPs (*Wang et al. 2011*). In consideration of its important role in fibrosis development, CTGF has been suggested as a potential molecular target in IPF. In preclinical studies, rodents knocked out for Smad3 genes expressed lower production of CTGF and were found to be resistant to TGF-β-induced lung fibrosis (*Bonniaud et al. 2004*). Moreover, elevated CTGF levels has been measured in serum and BALF of IPF patients (*Kono et al. 2011*).

Pamrevlumab (FG-3019), is a fully humanised monoclonal antibody directed against CTGF, developed by FibroGen. In the PRAISE study (NCT01890265), a phase II, randomised, double-blind, placebo-controlled trial, Pamrevlumab, administered at two

doses (15 mg/kg and 30 mg/kg) by intravenous infusion every 3 weeks, demonstrated a good safety and tolerability profile and yielded promising outcomes with regard to changes from baseline in FVC percentage predicted at week 48, disease progression and extent of pulmonary fibrosis by quantitative HRCT imaging (*Gorina et al. 2017; Richeldi et al. 2020*). The initiation of two parallel phase III trials, ZEPHYRUS and ZEPHYRUS-2 (NCT03955146 and NCT04419558), that are currently recruiting, has been announced to further evaluate the efficacy and safety of Pamrevlumab (30 mg/kg intravenous administered every 3 weeks), in subjects with IPF who are not being treated with approved IPF therapies and in subjects with IPF who were previously treated with an approved therapy but who discontinued that therapy, respectively.

Pentraxin (PTX)-2

PTX-2, also known as serum amyloid P, is a circulating innate immune regulatory protein that binds to Fc-gamma receptors on monocytes and inhibits their differentiation into pro-fibrotic fibrocytes and TGF-β producing macrophages, thus promoting epithelial healing and resolution of fibrosis (*Pilling et al. 2007*). Low serum PTX-2 levels have been observed in patients with IPF (*Dillingh et al. 2013*), and in animals with bleomycin-induced fibrosis administration of recombinant PTX-2 has been shown to reduce collagen content and α-SMA levels (*Murray et al. 2010*).

PRM-151 is an intravenously administered recombinant form of human PTX-2 protein (*Getsy et al 2011*), which is developed by Promedior. A phase I trial (NCT01254409) assessing safety, tolerability and pharmacokinetics of PRM-151 in patients with IPF has shown a trend towards improvement on FVC percentage predicted and 6-min walk distance (6MWD) during the treatment period (*van den Blink et al. 2016*). A further phase II study (NCT02550873) demonstrated significant effects in reducing pulmonary function decline and stability in 6MWD over 24 weeks compared to placebo with an acceptable safety profile (*Raghu et al. 2018*). Recently, the launch of a phase III trial (NCT04552899) for PRM-151 in IPF has been announced, using change from baseline to week 52 in FVC as a primary endpoint and 6MWD as a key secondary endpoint.

Autotaxin (ATX)-lysophosphatidic acid (LPA) pathway inhibitors

ATX is an enzyme that plays a central role in epithelial cell apoptosis and endothelial cell damage through the release of bioactive LPA (*Aoki et al. 2008*). Specifically, ATX converts lysophosphatidylcholine into LPA, and represents the main source of extracellular LPA. LPA, which acts through at least six G protein-coupled receptors, called LPARs, is the

origin of the signalling cascade of various fibrogenic pathways. LPA1R has been implicated in the development of IPF given its role in mediation of fibroblast recruitment, vascular leak, and endothelial barrier dysfunction in animal models. In the bleomycin mouse model of pulmonary fibrosis, for example, LPA1R-deficient mice showed reduced levels of fibroblast recruitment and decreased vascular permeability, indicating a protective role for decreased LPA signaling (*Tager et al. 2008*). Furthermore, levels of LPA and ATX have been found to be elevated in BALF and exhaled breath condensate in patients with IPF, thus suggesting a role of the ATX-LPA pathway in fibrogenesis (*Tager et al. 2012; Oikonomou et al. 2012; Montesi et al. 2014*).

GLPG1690 is an oral selective ATX inhibitor, developed by Galapagos, targeting the LPA signaling. GLPG1690 has been shown to be effective as anti-fibrotic in several animal models. In mice with bleomycin-induced pulmonary fibrosis, GLPG1690 reduced collagen content and lung fibrosis (*Tager et al. 2008*) and was superior to Pirfenidone on both of these measures (*Ongenaert et al. 2016*). Moreover, in GLPG1690-treated mice, there is an inverse relationship between LPA and GLPG1690 plasma levels (*van der Aaar et al. 2016*). The safety, tolerability, pharmacokinetic and pharmacodynamic profile of GLPG1690 was analyzed over a 12-week period, in the phase IIa FLORA trial recently published (NCT02738801). GLPG1690 was well tolerated by IPF patients with a similar safety profile, as placebo and preliminary efficacy analyses demonstrated encouraging results towards halting FVC decline (*Maher et al. 2018*). The two parallel phase III multicenter studies (ISABELA 1 and 2) started in November 2018 to further evaluate the efficacy of GLPG1690 for the treatment of IPF (NCT03733444 and NCT03711162) (*Maher et al. 2019*). Unfortunately, in February 2021, the ISABELA phase III trials were discontinued, following a regular review of unblinded data, that concluded that GLPG1690 benefit-risk profile no longer supported continuing these studies.

BMS986020 is an oral, selective small-molecule antagonist of LPA1R, developed by Bristol-Myers Squibb. In a phase II, multiple-dose, placebo-controlled trial (NCT01766817), that assessed the efficacy and safety of BMS-986020 in patients with IPF (who were not on Pirfenidone or Nintedanib), treatment with BMS986020 600 mg twice a day exhibited significantly slower rates of decline in FVC from baseline to 26 weeks versus placebo. Although dose regimens of BMS-986020 were well tolerated in most patients, they were associated with presumed hepatobiliary toxicity as manifested by dose-related elevations in hepatic transaminases and blood alkaline phosphatase in some patients, and treatment-related serious adverse events of cholecystitis, which led to early termination of the study (*Palmer et al. 2018*). Preclinical research indicated that these hepatobiliary effects

observed with BMS-986020 were likely off-target effects specific to this molecule and not mediated via antagonism of LPA, based on comparing BMS-986020 with a structurally distinct LPA1R (*Rosen et al. 2017*). These results suggest that structural variations in LPA1R antagonists may result in different safety profiles in patients with IPF. Currently, a phase II study (NCT04308681) of a novel promising LPA1R antagonist with oral bioavailability and antifibrotic activity, BMS-986278, is planned with the purpose to provide the effectiveness, safety, and tolerability in participants with pulmonary fibrosis.

G protein-coupled receptor (GPR) agonists/antagonists

GPRs are integral membrane proteins that are used by cells to convert extracellular signals into intracellular responses. GPRs are considered as one of the largest families of validated drug targets, which involve in almost overall physiological functions and pathological processes. PBI-4050 is a medium-chain fatty acid synthetic analogue with agonist and antagonist ligand affinity towards two GPRs, GPR40 and GPR84 respectively, which targeting and inhibiting multiple pathways involved in pulmonary fibrosis including inhibition of ERS and reactive oxygen species production, EMT and fibrocyte/fibroblast recruitment, migration, proliferation and differentiation (*Gagnon et al. 2018*). PBI-4050 is an orally administered small-molecule compound developed by Liminal BioSciences with demonstrated anti-fibrotic and anti-inflammatory properties. In preclinical models, PBI-4050 significantly reduced pro-fibrotic and inflammatory cytokines, included TGF-β1, CTGF and interleukin-23 and 6, showed antioxidant properties and reduced α-SMA expression, collagen I deposition, fibronectin expression, plasminogen activator inhibitor-1 expression and fibrosis (*Gagnon et al. 2015; Gagnon et al.2016; Leduc et al. 2014*). PBI-4050 has just completed a phase II open-label, single-arm study (NCT02538536), showing positive results in terms of safety, tolerability, and efficacy as a monotherapy and in combination with Nintedanib or Pirfenidone (*Khalil et al. 2019*). Additional pivotal placebo-controlled phase II/III clinical trials of PBI-4050 alone or in combination with Nintedanib are currently being planned. However, recently Liminal BioSciences is stopping the clinical development of PBI-4050 for IPF, based on interim pharmacological data from a phase I clinical trial (NCT04695041) testing it at ascending doses in healthy volunteers.

Galactin-3 inhibitor

Galectin-3 is another circulating protein, which plays a key role in fibrosis development through the activation of macrophages and myofibroblasts. Specifically, galectin-3 is a β-galactoside binding lectin that regulates the expression of TGF-β receptors on the surface of AECs and is a mediator of TGF-β-induced lung fibrosis. Bleomycin-treated galectin-3

knockout mice show reduced lung fibrosis and lung collagen levels, while AECs and fibroblasts from galectin-3 knockout mice show reduced myofibroblast activation, EMT and collagen I production in response to TGF-β (*Mackinnon et al. 2012*). Galectin-3 levels are also elevated in the BALF and serum of patients with IPF (*Mackinnon et al. 2014*).

TD139 has been developed by Galecto Biotech as a specific inhibitor of the galactoside binding pocket of galactin-3. It is an inhaled drug, administered via dry-powder inhaler. In mice treated with bleomycin, TD139 reduced β-catenin activation, galectin-3 expression and total lung collagen. TD139 also reduced galactin-3 expression in macrophages from the BALF of patients with IPF (*Mackinnon et al. 2014*). A phase I/II randomized, placebo-controlled, multiple dose expansion clinical trial (NCT02257177), designed to assess TD139 safety, tolerability, pharmacodynamics and pharmacokinetics was recently completed and results demonstrated that the treatment was safe and well tolerated. Patients also showed improvements in several markers associated with IPF progression (*Hirani et al. 2017*). A phase IIb clinical trial (NCT03832946) is currently recruiting IPF patients, with the aim to test the efficacy and safety of TD139. Patients will receive one of the two doses of inhaled TD139 (either 3 or 10 mg once daily) or a placebo, and the primary outcome measure will be the change in FVC over 52 weeks.

C-Jun NH2-terminal Kinase (JNK) pathway

The stress-activated protein kinase, JNK is an important modulator of cell death and, in some settings, a major driver of apoptosis (*Dhanasekaran and Reddy, 2008*). Phosphorylated JNK has been associated with fibroblast activity in lung specimens from IPF patients and greatly activated JNK has been found in bleomycin- treated mice (*Wygrecka et al. 2012*). Moreover, data have shown that JNK signaling pathway is activated by TGFβ1 and downregulates VEGF D expression in human lung fibroblasts *in-vitro* (*Cui et al. 2014*).

CC-90001, developed by Celgene (now Bristol Myers Squibb), is a novel orally administered second-generation JNK inhibitor with bias for JNK1 over JNK2. In a preclinical model, CC-90001 attenuated lung collagen and α-SMA (*Bennett et al. 2017*). A current phase II trial (NCT03142191) is evaluating the efficacy and safety of CC-9000 after that a first-generation JNK inhibitor, CC-930, showed effects on reducing biomarker plasma levels and maintenance of stable FVC in patients with IPF (NCT01203943) (*van der Velden et al. 2016*).

Rho Kinase Pathway

Rho-associated coiled-coil protein kinases (ROCKs) are downstream effectors for Rho GTPases that mediate a number of cellular functions, including adhesion, migration, and phagocytosis, by regulating actin cytoskeleton dynamics (*Olson, 2008*). In lung fibrosis, ROCKs are activated by both biochemical (i.e. TGF-β, thrombin and LPA) and mechanical (i.e. increased matrix stiffness) stimuli (*Knipe et al. 2015*), and pharmacological inhibition of ROCK has been shown to protect mice from experimentally induced lung fibrosis (*Zhou et al. 2013*). Both ROCK1 and ROCK2 contribute to the development of experimental pulmonary fibrosis by inducing exaggerated AECs apoptosis, pulmonary vascular permeability, and fibroblast activation, suggesting that partial inhibition of either ROCK isoforms or both together has the potential to be an effective therapeutic strategy for pulmonary fibrosis (*Knipe et al. 2018*).

KD025 (SLX-2119) is an orally administered selective ROCK2 inhibitor, developed by the biopharmaceutical company Kadmon. Preclinical studies showed that KD025 inhibits ROCK2, reducing type I collagen secretion and scar tissue formation, and improving organ function in models of fibrosis. Data also showed that ROCK2 inhibition with KD025 significantly reduced established lung fibrosis and inflammation and improved pulmonary function in a dose-dependent manner (*S.D. Waksal, Kadmon. Jefferies healthcare conference, 2015*). An open-label phase II study (NCT02688647) assessed the safety, tolerability, and efficacy of KD025 400 mg once daily in patients with IPF, who were previously treated with Pirfenidone or Nintedanib, or both. The drug was safe and well tolerated and demonstrated clinical benefit, with a numerically lower decline in FVC compared to the control arm (absolute difference of 127 mL in median decline of FVC and a relative difference of 73%) (*Business Wire, 2018*).

Currently, another promising ROCK2 selective inhibitor, RXC007 developed by Redx Pharma, is starting a phase I trial. The primary objective of this first-in-human study is to evaluate the safety profile of single and multiple ascending doses of RXC007, administered as an oral capsule once a day, in healthy volunteers (*RXC007 (ROCK2 selective) - Redx*).

Anti-integrin antibody

Integrins as transmembrane receptors play a pivotal role in ECM adhesion, and integrin αvβ6, a key mediator of TGF-β activation, is known to be involved in the regulation of fibrogenesis and epithelial injury (*Tatler and Jenkins, 2012*). In a murine model of bleomycin-induced pulmonary fibrosis, partial inhibition of integrin αvβ6 was found to effectively inhibit TGF-β activation, epithelial injury, and pulmonary fibrosing processes

without aggravating inflammatory processes (*Horan et al. 2008*). Moreover, the elevated expression of αvβ6 integrin in lung tissue samples of patients with IPF suggests that αvβ6 monoclonal antibodies could represent a promising new therapeutic strategy for treating pulmonary fibrosis.

BG00011 (STX-100), is a humanised monoclonal antibody directed against this αvβ6-integrin, developed by BioGen. The safety and tolerability of subcutaneously administered multiple, escalating doses of BG00011 in patients with IPF was investigated in a phase IIa study (NCT01371305). The study has been completed recently, and data have not been published but were presented at ATS 2018 conference (*Raghu et al. 2018*). Subcutaneous weekly administration of BG00011 was safe and well tolerated, except for the highest dose (3 mg/kg subcutaneous weekly). The study also demonstrated a decrease in active TGF-β signaling as evidenced by dose dependent reductions in SMAD2 phosphorylation and TGF-β target gene expression in BAL cells in patients receiving BG00011. However, a second phase IIb (NCT03573505) study to evaluate the efficacy and safety of B00011, planned to start in 2018, was terminated early due to safety concerns. Despite this, two studies, a phase I and phase IIa respectively, are currently evaluating the safety and tolerability of the αvβ1, β3, and β6 selective inhibitor, IDL-2965 (Indalo Therapeutics), in healthy subjects and individuals with IPF (NCT03949530), and the αvβ6 receptor occupancy by the αvβ1 and β6 selective inhibitor, PLN-74809 (Pliant Therapeutics), in patients with IPF (NCT04072315); this latter is under examination in another phase IIa multicenter, 3-part, randomized, double-blind, dose-ranging, placebo-controlled study to evaluate the safety, tolerability, and pharmacokinetics in participants with IPF (NCT04396756).

Leukotriene (LT) antagonists

LTs are pro-inflammatory and pro-fibrogenic mediators derived from the 5-lipoxygenase (5-LO) pathway of arachidonic acid metabolism. A role for LTs in progression of IPF has been identified (*Peters-Golden and Henderson, 2007*), in particular for LTB4 (*Izumo et al.2009*). In lung biopsies from patients with IPF, the 5-LO metabolic pathway was observed to be constitutively activated, with strong correlations between tissue LT levels and the degree of inflammation and fibrosis (*Wilborn et al. 1996*).

The LTB4 antagonist, Tipelukast (MN-001), is a novel, orally bioavailable small molecule, developed by MediciNova, which exerts multiple anti-fibrotic and anti-inflammatory functions including LT receptor antagonism, inhibition of phosphodiesterases 3 and 4, and 5-LO. In mice with bleomycin-induced lung fibrosis, Tipelukast reduced fibrosis, assessed histologically, and reduced the tissue density and hydroxyproline content of the lungs

(*Mastuda, 2014*). A single-center, randomized, placebo-controlled, double-blind, 6-month phase IIa clinical trial followed by a 6-month open-label extension of Tipelukast (NCT02503657) to evaluate its efficacy, safety and tolerability in participants with moderate to severe IPF is now fully enrolled (*Bascom et al. 2020*). The primary endpoint is FVC change from baseline to week 26 and the estimated study completion date is the second-quarter of 2021 (*Bascom et al. 2021*). However, recently published data reported that six months of treatment with Tipelukast failed to significantly improve lung function in adults with IPF.

Activin receptor-like kinase 5 (ALK-5) inhibitor

TGF-β is one of the most player in driving lung fibrosis and in the pathogenesis of IPF. TGF-beta1 acts through the TGF-beta type I and type II receptors to activate intracellular mediators, such as Smad proteins, the p38 mitogen-activated protein kinase, and the extracellular signal-regulated kinase pathway. ALK-5 is a TGF-β type I receptor, and its inhibition has been reported to exhibit anti-fibrotic effects in models of lung fibrosis (*Higashiyama et al. 2007; Koh et al. 2015*). Since TGF-β signaling via the interaction with ALK-5 plays a fundamental role in mediating pro-fibrotic responses, pharmacologic inhibition of the receptor kinase may represent a novel targeted approach for the control of pulmonary fibrosis.

TD-1058 is an inhaled, selective inhibitor of ALK-5, developed by Theravance Biopharma. A phase I, 3-part, randomized, double-blinded, placebo-controlled study (NCT04589260) is currently planned with the aim to evaluate the safety, tolerability, pharmacokinetics, and pharmacodynamics of TD-1058 inhaled solution of single and multiple ascending doses in healthy subjects and subjects with IPF.

Chitinases Inhibitor

Chitotriosidase (CHIT1) and acidic mammalian chitinase (AMCase) are the enzymatically active chitinases that have been implicated in the pathology of chronic lung diseases, including IPF (*Bargagli et al. 2007*). The CHIT1 activity is highly elevated in BALF, induced sputum and serum from patients with sarcoidosis, scleroderma and IPF, and correlates with disease progression. Moreover, pharmacological inhibition of chitinase demonstrated strong therapeutic efficacy in murine model of chronic airway inflammation and pulmonary fibrosis. These data indicate that inhibition of chitinases might represent a novel therapeutic approach for pulmonary diseases as well as in IPF.

GLPG4617, formerly known as OATD-01, is a novel, potent and selective CHIT1/AMCase inhibitor, originally developed by OncoArendi Therapeutics (now Galapagos). Preclinical data demonstrated that GLPG4617 provides significant therapeutic efficacy, comparable to Nintedanib, in the bleomycin-induced pulmonary fibrosis model in mice (*Dymek et al. 2018*). In phase Ib clinical studies involving healthy volunteers, the therapy was found to be well-tolerated and to effectively suppress chitinase activity, supporting its proposed mechanisms of action (*Dyjas et al. 2019; Koralewski et al. 2020*). Now, Galapagos plans to launch a phase II trial to evaluate the safety and efficacy of GLPG4617 in IPF patients.
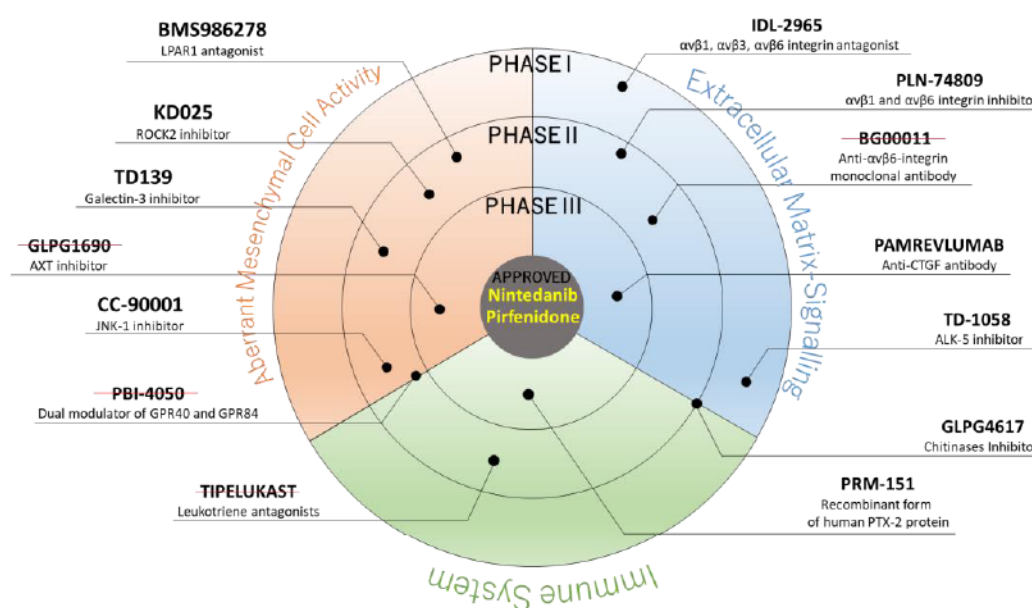
Figure 1.9 Promising drug candidates for IPF under development. Drugs are divided on the basis of the clinical phase in which they are actually located (information taken from https://www.clinicaltrials.gov/ct2/home) and of the target on which they interfere.

1.8.3 Combination therapy

The pathogenesis of IPF is a complex interplay of genetic and environmental factors activating numerous and coexistent pro-fibrotic pathways in multiple cell types. In this context, combination therapy could be an effective approach to IPF management.

So far, mainly three studies have explored the feasibility of combined treatment with Nintedanib and Pirfenidone in individuals with IPF. In 2015, the first randomized phase II trial in Japanese patients with IPF demonstrated that Nintedanib had an acceptable safety profile when added to ongoing Pirfenidone therapy (*Ogura et al. 2015*). Later in 2017, in the INJOURNEY trial, Vancheri and colleagues investigated the safety of combining Pirfenidone and Nintedanib in treating IPF. In this trial, IPF patients were randomized to

receive Nintedanib with add-on Pirfenidone or Nintedanib alone in an open-label study for 12 weeks. The total number of adverse effects were similar in the two groups and in keeping with the adverse event profiles of each drug; however, gastrointestinal adverse events occurred with greater frequency in the combination group. Despite this, adherence rates were similar in both groups, thus suggesting that Nintedanib plus Pirfenidone therapy had a feasible safety and tolerability profile in IPF. Moreover, although the study was not appropriately powered to assess efficacy, there were promising exploratory effects on lung function decline in the combination therapy compared to Nintedanib alone (12-week FVC decline of −13.3 mL versus −40.9 mL, respectively) (*Vancheri et al. 2018*). In a further study, the safety of Nintedanib added to pre-existing Pirfenidone treatment in 89 IPF patients showed no new safety signals to the known safety profile of either therapy alone (*Flaherty et al. 2018*). Another recent open-label trial also indicated that co-administration of these drugs had no relevant effect on their pharmacokinetic drug-drug interaction (*Richeldi et al. 2019*). However, other combination therapies in IPF have been less promising, such as in the phase II PANORAMA study, that investigated the tolerability and safety of pirfenidone with add-on N-acetylcysteine, based on its antioxidative effects, yielding negative results (*Behr et al. 2016*), and the INSTAGE study, which failed to meet its primary endpoint when compared Nintedanib with Sildenafil, a phosphodiesterase-5 inhibitor, versus Nintedanib alone (*Kolb et al. 2018*).

Overall, although the results of these trials provide evidence that the combination of Pirfenidone and Nintedanib are promising with regards to tolerance and safety, whether combination therapy adds benefit over single-agent therapy is still unknown. The next step in this regard should be to perform larger controlled studies to investigate the efficacy of these combination therapies. This may require the use of different endpoints, or the enrolment of subgroups of patients with IPF, for example patients with rapidly progressing disease, or disease that is refractory to monotherapy.

1.9 Preclinical models of pulmonary fibrosis

IPF as a whole is innately challenging to model due to its age-related, idiopathic nature and the highly complex underlying pathobiology. However, most of our understanding of this disease is based on experimental models that have improved over time, increasing in complexity and accuracy as quickly as the availability of new and emerging technologies. To date, several models of pulmonary fibrosis are available to be used in preclinical studies, both *in-vitro/ex-vivo* and *in-vivo* (**Figure 1.10**).
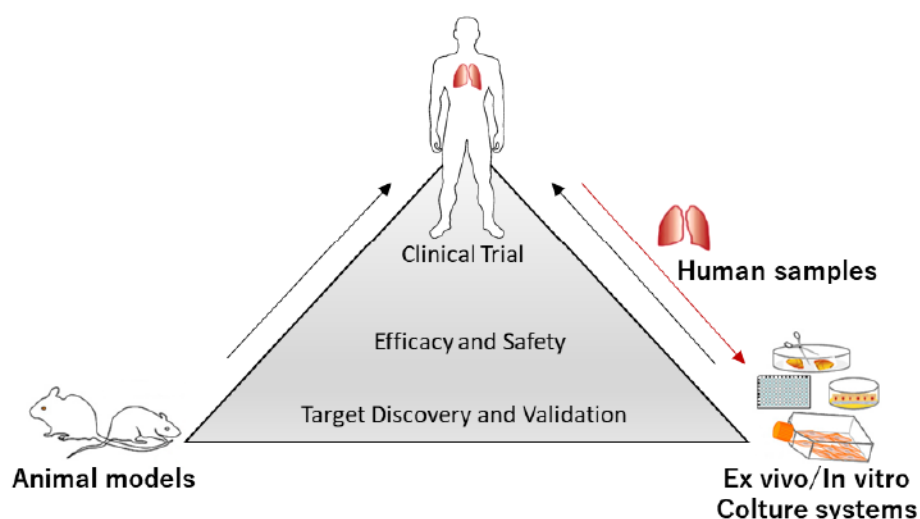
Figure 1.10 Overview of modeling for pulmonary fibrosis and integration with human disease (Image adapted and modified from *Yanagihara et al. 2020*). An integrated approach to drug development pipeline using both relevant animal models and appropriate *in-vitro/ex-vivo* approaches, should provide robust validation of pharmacological mechanisms of action and help to move promising targets to clinical trials.

1.9.1 *In-vitro* models of pulmonary fibrosis

Different lung cell types, including epithelial, endothelial, mesenchymal, and immune cells, contribute to IPF pathology. Immortalized human lung cells lines (e.g., non-small cell adenocarcinoma: A549; lung fibroblasts: IMR-90s; submucosal adenocarcinoma cell: Calu-3) have been used to model specific aspects of pulmonary fibrotic disease (*Sundarakrishnan et al. 2018*). Cell lines are feasible and easy to maintain as they are able to divide infinitely; however, immortalization induces permanent phenotypic changes in these cells and hence, results obtained using cell lines may not accurately replicate human lung physiology. Thus, recent research has focused on utilizing non-transformed primary lung cells from humans' donors. Among them, pulmonary fibroblasts are the key effector cells in lung fibrosis and the most widely used primary cell type *in-vitro* due to the ease of

isolation and culture techniques (*Balestrini et al. 2012*). AECs and microvascular endothelial cells, whereas, require sophisticated isolation techniques and special media with matrices. While primary cells are better at replicating *in-vivo* lung phenotype, they are limited by donor-based variabilities. On the other hand, even with phenotypic alterations, cell lines provide a relatively robust platform for conducting parallel studies with high throughput capacity. Therefore, choosing an appropriate cell type is important depending on the purpose of the experiment.

Most *in-vitro* models for pulmonary fibrosis have been based on two-dimensional (2D) cultures of cells. These models involve seeding cells suspended in media, composed of growth factors, onto a tissue culture treated plastic or glass substrate to determine cellular characteristics. These systems are relatively inexpensive, they offer rapid growth of cells and controlled conditions to study cellular changes and provide a standard platform to evaluate single cell responses to growth factors or drugs. The simplicity of 2D culture has aided in understanding individual cellular phenomena and has led to the identification of several fibrotic mediators. However, it remains an unsatisfactory approach due to a series of disadvantages. For instance, the primary limitation of 2D monolayer culture is their inability to mimic the three-dimensional (3D) nature of lung tissue, and so the fact that it investigates the response of cells that are completely isolated from their biological context. Moreover, the tissue culture plastic or glass are extremely stiff (106 kPa) substrates, completely different from that of the normal lung parenchyma (1–15 kPa) (*Engler et al. 2006*), and because matrix stiffness has been shown to affect cellular phenotype, standard tissue culture substrates do not permit studies evaluating cellular mechanics.

Scar-in-a-jar *in-vitro* assay has become increasingly popular in many research laboratories for screening compounds. This assay is similar to a 2D culture as it involves seeding a monolayer of fibroblasts into a tissue culture treated plastic substrate. However, the uniqueness of this model is that it involves the additional of Ficoll which is a non-interacting, natural hydrophilic polysaccharide capable of causing macromolecular crowding promoting collagen synthesis at a faster rate, thus reducing incubation time. Therefore, this assay allows in situ assessment of the area of collagen type I deposition per cell and it is also possible to detect collagen cross-linking. Furthermore, it is considered high-throughput assay for compound screening as the effect of compounds on TGF-β-induced collagen synthesis, α-SMA expression, proliferation, and cell toxicity can be measured simultaneously within a single well (*Chen and Raghunath, 2009*). Although this model is considered a good system to identify therapeutic targets compared to the standard 2D monolayer *in-vitro* culture, the Scar-in-a-jar assay also has several disadvantages. For

example, the assay only involves one cell type, cells are grown on a stiff substrate, the cells require exogenous TGF-β to promote collagen synthesis, and the model is unable to recapitulate fibroblast foci.

Based on these limitations, over the past few years, the development of more complex *in-vitro* models of lung fibrosis capable to mimic microenvironments observed in normal tissues have now become of great interest. Complex matrices of biological origin have therefore begun to be used to cultivate cells in an environment similar to the humans lung and the models gradually increased dimensionality, moving from 2D to 2.5D, until 3D. 3D *in-vitro* models, where cells are embedded in a complex environment with different polarity, exposing them to ECM interactions and soluble growth factor/cytokine gradients, mimic native lung tissue microenvironment with greater accuracy compared to 2D and 2.5D models. 3D systems can replicate cell-cell and cell-matrix interactions, matrix stiffness, and structure. Moreover, these models permit migration, chemotaxis, cellular traction and integrin adhesions, in all three planes. Due to these benefits, different 3D models have been developed such as the hydrogel systems, lung spheroids and organoids, lung-on-a-chip and precision-cut lung slides (PCLS).

Hydrogels are water-swollen cross-linked natural or synthetic polymers that are employed as scaffold for *in-vitro* models, specially fibroblast cultures, to mimic the native structure of the ECM (*Smithmyer et al. 2014*). Collagen type I-based hydrogels *in-vitro* models are very helpful in the study of fibroblast behavior when exposed to chemical and physical stimuli induced by the ECM.

Lung spheroids refers to adult lung cells or lung stem cell populations cultured in the form of aggregates utilizing low-adhesion plates, hanging drop cultures, suspension cultures or micropatterned plates (*Fang and Eglen, 2017*). Lung organoids are self-assembling structures of lung stem cells that follow sequential lung developmental paradigms, with discrete pseudo-glandular, canalicular and saccular stages (*Chen et al. 2017*). Both lung spheroids and organoids are superior to 2D cultures since they can replicate the typical cell-cell and cell-matrix interactions, similar to *in-vivo* conditions. Spheroids may enable high throughput drug testing. However, spheroids have a too simple of an architecture to mimic real organs, while organoids mimic some, but not all the structure and function of real organs and lack vasculature and air-liquid interface.

Organ-on-a-chip systems are a complex, 3D bioengineered devices which replicate organ/tissue level responses in miniature chips created using lithography techniques. Specifically, lung-on-a-chip are systems that replicate not only the lung structure with all the cell and matrix interactions but also they permit investigation under a much more

dynamic environment, biomechanical signals in the form of shear stress due to perfusion and strain, similar to human breathing and blood flow (*Yanagihara et al. 2020*).

Among the 3D approaches, the PCLS model has emerged as the most useful and promising *ex-vivo* tools for studying human lung fibrosis, and to support preclinical studies (*Alsafadi et al. 2017*). This model involves fresh human lung tissue from lung resections or explants or animal tissues, which are filled with low melting point agarose (to prevent organ collapse) and subsequently cut with precision into 250-1000 μm thick slices and cultured in vitro. In this way, the PCLS used as 3D lung tissue cultures retain native lung tissue architecture, ECM protein composition, and stiffness with viable multiple lung resident cells. Therefore, the generated lung tissue cultures can offer a large range of applications for biomechanical, physiological, toxicological and pharmacological studies. The most important advantage of using PCLS is that they can be used to assess the effects of drugs directly in situ on the lung structural cells. However, one of the most significant limiting factors using PCLS is the lack of fresh tissue availability. Additionally, PCLS are limited in that they can be used only in short-term studies of one week or less (*Uhl et al. 2015*), are difficult to standardize and they do not reproduce the lung functions. Nevertheless, this model represents the best combination of biological complexity, high-throughput capacity for pre-clinical testing of novel anti-fibrotic drugs and give mechanistic insights in modulating lung cell phenotypes.

Despite the development of innovative *in-vitro* models with the addition of an increasing level of biological complexity, these models do not yet possess the same physiological environment of the *in-vivo* models and all the intricate cellular and matrix connections and stimulus that are present in living tissues.

1.9.2 In-vivo models of pulmonary fibrosis

Attempts to elucidate disease pathogenesis, identify potential biomarkers and unravel novel therapeutic targets have relied on *in-vivo* models. Over the past few decades, several animal models of pulmonary fibrosis have become available to study the pathobiology of IPF (*Tashiro et al. 2017*), but no one seems to be able to fully recapitulates the histopathologic pattern of UIP or exhibit features of progressive and irreversible disease like human IPF (*Moore et al. 2013*). In addition, although several compounds have shown efficacy in reducing the progression of pulmonary fibrosis using animal models, only few of these compounds have confirmed their beneficial effects for IPF in clinical trials. This, however, should do not underestimate the fact that animal models are essential prerequisites for revealing molecular mechanisms involved in the pathogenesis of lung fibrotic processes

and the subsequent development and validation of prognostic tests and therapeutic interventions.

Pulmonary fibrosis like features can be induced in different species by a variety of agents, and these different agents can be administered via many different routes and using distinctive dosing regimens. Although cases of spontaneous lung fibrosis are known in some common mammalians (like dogs, horses, cats and donkeys), rodents remain the most used preclinical models for lung fibrosis, since in these species fibrotic lesions have a rapid onset and their duration enable drug testing. Moreover, rodents, being small animals, are easy to house and handle and the management costs are reduced compared to larger species (*Gelfand, 2002*). Regarding the study of IPF, as recently recommended by the "Official ATS Workshop Report about the Use of Animal Models for the Preclinical Assessment of Potential Therapies for Pulmonary Fibrosis", mice are the first-line animals for preclinical testing, especially due to the ease of handling, availability of reagents, their well characterized immune systems, and the possibility of utilizing transgenic models (*Jenkins et al. 2017*). However, murine models do not fully recapitulate classical IPF histopathology, likely explained by anatomic differences between murine and human lungs, temporal homogeneity of animal models and potentially distinctive pathobiological mechanisms involved in human disease. Since rats may have histopathology that is more reminiscent of IPF, in the same report, the rat is recommended as the second species, that can be used subsequently if the confirmation of the efficacy of a compound is required or in case of an impossibility to use the mouse (*Jenkins et al. 2017*). Moreover, considering that a single model does not resemble all the characteristic of the disease, the possibility to expand the model with two or more animal models of different species could be a good choice to improve the efficacy of preclinical studies (*Tashiro et al. 2017*).

Different approaches to model experimental models of pulmonary fibrosis exist, and most of them are characterized by the use of an agent, which is able to induce the first injury triggering the fibrotic process in the lung. Among the various experimental agents, bleomycin is the most widely used and best characterized agent to induce pulmonary fibrosis, due to its fast action leading to the early appearance of histopathological alterations that closely mimic the acute phase of the disease (*Jenkins et al. 2017*). As well as bleomycin several other fibrotic agents have been used with varying degrees of success.

Fluorescein isothiocyanate (FITC) has been shown to cause fibrosis like changes over a similar time scale to bleomycin. FITC is a fluorescent molecule with the advantage that molecular deposition in the lung can be easily visualized. The disadvantages of this model are that certain histopathological features, such as fibroblast foci, are not observed, and

there is a large amount of variation in the fibrotic response generated by different batches of FITC (*Degryse and Lawson, 2011*).

Administration of silica or asbestos to the lungs has also been shown to illicit persistent fibrosis (*Koli et al. 2016; Cheresh et al. 2015*). However, as with FITC, there are histopathological features that are missing with respect to the histopathological features seen in patients with IPF.

Systemic delivery of paraquat also produces fibrosis in the lungs of animals (*Guo et al. 2015; Shao et al. 2015*). However, paraquat is a broad-spectrum herbicide that has been shown to cause necrosis in organs other than the lungs (such as kidney and liver) which can cause significant mortality.

In addition to these models, certain non-chemical *in-vivo* approaches can induce pulmonary fibrosis. For example, an exposure of the thorax of animals to radiation has been shown to result in persistent fibrosis like changes in the lungs (*Paun et al. 2015; Lee et al. 2015*). However, as the fibrosis takes a long time to develop and the cost of the irradiating equipment can be high, this model is very expensive and difficult to run.

Intratracheal delivery of transgenes using viral vectors has shown some success, with delivery of genes for factors such as TGF-β1 eliciting fibrotic responses in the lungs of animals (*Kolb et al. 2001; Kolb et al. 2002*). Although delivery of these transgenes leads to a progressive and persistent fibrosis, the downside of such models can be that the animals may have an immune response to the viral vector, and the expression of the transgenes is much higher than physiologically possible.

Another animal model of pulmonary fibrosis that has been developed is the humanized mouse model of IPF, where cells from human patients of IPF are injected into severe combined immune deficient (SCID) mice. Infusion of human fibroblasts has been shown to lead to increases in fibrosis seen histologically and up-regulation of pro-fibrotic genes such as TGF-β1 and surfactant proteins at 63 days post-infusion (*Murray et al. 2013*). However, the main issue with this model is the length of time to generate fibrosis and the availability of cells from human patients with IPF.

Recently are growing in importance also the age-related models, considering that IPF is a disease affecting the elderly population. Indeed, it has been demonstrated that older mice are more inclined to developed lung fibrosis when exposed to pro-fibrotic stimuli (*Tashiro et al. 2017*). Moreover, a model with a specific deletion of one telomeric gene, demonstrated that telomere dysfunction (one of the principal characteristics of aging) in AECs type II is sufficient to cause lung fibrosis (*Naikawadi et al. 2016*). However, the ATS

guidelines do not consider necessary the prioritization of the use of aged mice for preclinical testing.

1.9.2.1   *The bleomycin (BLM)-induced pulmonary fibrosis model*

As mentioned in the previous paragraph, the BLM-induced pulmonary fibrosis model is the most used animal model to study pulmonary fibrosis and it is the most employed in preclinical studies during the drug development process for IPF. Indeed, the BLM model has proven invaluable in understanding many of the cellular and molecular pathways in fibrogenesis that are central to the current understanding of IPF pathogenesis. Furthermore, this model was used in the preclinical development of Nintedanib (*Wollin et al. 2015*).

BLM is a glycosylated linear non-ribosomal peptide antibiotic produced by the bacterium "Streptomyces verticillus" (*Umezawa et al. 1966*), with an important role in chemotherapy for the treatment of some forms of cancer such as germinative tumors and Hodgkin's lymphoma. However, its use can be life-threatening in up to 10% of the patients receiving the drug, since the treatment is associated with the occurrence of interstitial pulmonary fibrosis (also called fibrosing alveolitis) (*Balikian et al. 1982; Calaway et al. 2018*). Indeed, BLM induces pulmonary fibrosis by production of DNA-cleaving superoxide and hydroxide free radicals, which cause single and double stranded DNA breaks (*Claussen and Long, 1999*). This damage preferentially occurs in the lungs because of low levels of bleomycin hydrolase, a BLM-inactivating enzyme. Given the capabilities of the molecule to produce lung fibrosis in human, BLM was used to modelling IPF in a wide variety of experimental animals and has allowed the replication of some key hallmarks of the disease, such as damage to AECs, fibroblast and myofibroblast activation and collagen deposition (*Scotton and Chambers, 2010; Liu et al. 2017; Carrington et al. 2018*).

So far, BLM has been used in a variety of different species, including mice, rats, hamsters, rabbits, guinea pigs, dogs, and non-human primates, via a number of different administration routes. For instance, it has been delivered directly into the lung by intratracheal, oropharyngeal and inhaled administration, systemically by intravenous and intraperitoneal treatment or subcutaneously by mini-osmotic pumps. However, of these approaches, intratracheal instillation of BLM is the most frequently used route of administration because it better reproduces the human phenotype that is limited to the lungs, causing direct damage to AECs and leading to fibrotic changes mainly in the lung parenchyma (*Moore et al. 2013*). The recently published ATS workshop report on pulmonary fibrosis animal models confirmed that there is a consensus view of the murine

intratracheal BLM model as "the best-characterized animal model available for preclinical testing" (*Jenkins et al. 2017*).

The BLM model leads to an initial inflammatory phase, characterized by up-regulation of acute inflammatory cytokines together with an influx of neutrophils (*Kim et al. 2010*). This primary inflammatory phase lasts for approximately 7-10 days before subsiding into a fibrotic phase (from day 14) which more appropriately mimics some of the manifestation of IPF in human patients (**Figure 1.11**) (*Izbicki et al. 2020*). Terminal investigations are typically carried out three-four weeks after the initial BLM administration, approximately on day 21-28. Indeed, the fibrotic phase in the BLM model is self-limited and eventually reversible in a variable time period.

It is important to note that in the BLM model there is overlap between the inflammatory and fibrotic phases, with the initial strong inflammatory response taking up to 10 days post-injury to completely clear. Typically, the 7-day time point is used as a separation between the inflammatory and fibrotic phases (*Moeller et al. 2008*). However, since there is no clear distinction between the two phases, using this time point to differentiate between preventative and therapeutic studies is a limitation that needs to be considered, especially when using the BLM model to assess the efficacy of anti-fibrotic compounds. Thus, it is now apparent that their testing should be performed during the fibrotic phase, at least 7 days after BLM administration (*Moore et al. 2013*).
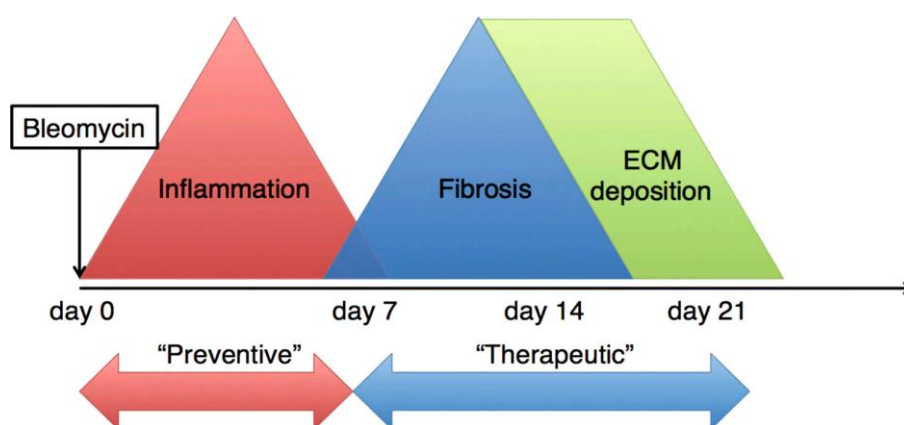
Figure 1.11 Schematic image of BLM-induced pulmonary fibrosis model (Image adapted from *Yanagihara et al. 2020*). The switch from inflammatory to fibrosis phase is around the seventh day post-BLM with fibrotic lesions appearance starting from day 14 and followed by fibrogenic changes with ECM deposition until day 21. These changes resolve after a variable time period. Interventions during the first seven days are considered as 'preventive' while interventions in the later stages are considered as 'therapeutic.' Anti-fibrotic treatments should be tested during 'therapeutic' timing.

Another important aspect to consider related to the "therapeutic window" for compound dosing is that the development of pulmonary fibrosis induced by a single intratracheal administration of BLM in mice is often unpredictable. In fact, there is a high degree of variability between individual animals in the extent of fibrosis, and the fibrosis tends to resolve spontaneously. This represents a limitation for pharmacological studies due to the restricted time window available for testing new anti-fibrotic drugs. Considering that fibrosis does not resolve in most patients with pulmonary fibrosis and the hypothesis that repeated events of lung injury are responsible of the disease development, one possibility to overcome this issue in mice could be to perform repeated administration of BLM instead of a single intratracheal administration. Indeed, the repeated intratracheal administration of BLM has been shown to produce a more robust and long-lasting response that could at least in part reproduce IPF progression. For example, Stellari and colleagues directly addressed this point and results from their investigations demonstrated that double intratracheal instillation of BLM produces a more severe and diffuse fibrosis compare to the single BLM instillation in mice (*Stellari et al. 2017*). Another proposal could be to consider the administration of BLM via oropharyngeal aspiration. Indeed, it has been reported that the oropharyngeal route leads to pulmonary fibrosis persisting for up to 6 months (*Scotton et al. 2013*), and the fibrotic response that develops after this method appears similar to the intratracheal instillation. Results from Ruscitti et al., demonstrated that lung fibrosis severity and duration after double oropharyngeal or intratracheal administration are comparable, while the oropharyngeal administration results in a more uniform distribution of fibrotic lesions through the lung lobes (*Ruscitti et al. 2020*).

Other aspects related to the sex, strain and age of the mice should be considered when using the BLM model. It has been demonstrated that male mice are more susceptible to BLM-induced pulmonary injury than female mice, which is similar to human IPF, though the precise mechanism is not fully understood (*Redente et al. 2011*). Therefore, the National Institutes of Health currently recommends use of both male and female animals in all research studies. The response to BLM is also strain-dependent: some strains, such as C57Bl/6 mice are more susceptible than BALB/c mice, presumably due to different expression patterns of cytokines and proteases (*Phan et al. 1992*). Furthermore, although IPF is a disease of advanced age most of the studies use young mice, generally aged 8-12 weeks, which are equivalent to teenager phase in a human life span. Some studies using BLM in aged mice (over 18 months) demonstrated more fibrosis and impaired resolution after injury, which may more closely reflect the human disease, however, due to the practical difficulties in the generation of aged mice combined with much higher cost, the

ATS guidelines do not consider necessary the prioritization of the standard use of aged mice for preclinical testing (*Jenkins et al. 2017*).

Finally, the most accurate analysis for lung fibrosis in preclinical models involves several endpoints, which should be as much as possible clinically relevant and validated. Current outcome measurements in the BLM and other experimental lung fibrosis models mainly involve the histological scores of fibrosis in stained tissue sections (commonly modified Ashcroft scoring), morphometric quantification, and biochemical analysis such as lung collagen or hydroxyproline (a major component of collagen) content. Although these endpoints give valuable information about the levels of fibrosis in the lungs of animals, they may not provide the whole picture for preclinical assessments of anti-fibrotic drugs. The ATS panel of experts suggests the possibility of integrating further clinically relevant assessments such as functional readouts, imaging techniques, measurement of arterial blood oxygen saturation with pulse oximetry, and most recently, the measurements of blood and molecular biomarkers which may predict disease progression and responses to new treatments (*Jenkins et al. 2017*). Furthermore, these techniques, as well as being more clinically relevant, provide researchers with the opportunity to longitudinally examine the progression of pulmonary fibrosis in a single animal, rather than having to sacrifice numerous animals to examine the fibrosis, and may also give a better indication of translation of the potential treatment from the *in-vivo* models to the clinic. Finally, other additional evaluations could include BALF analysis for the assessment of inflammatory cells counts as well as body weight, lung index (lung wet weight in mg compared to body weight in g) and survival rate (*Moeller et al. 2008*).

Regardless the limits that animal models may have, is fundamental to identify the best of them in terms of translatability and management, and characterize it as thoroughly as possible to understand what "questions" can be asked to the model to solve problems related to the disease that cannot be ask to human patients. Despite the growing ethical need to reduce the number of animals used in research, without animal models, complicated diseases such as IPF, could remain without a pharmacological solution for a long time. The idea to replace it with innovative and refined *in-vitro* models is promising and encouraging, but there is still a long way to go.

2. AIM OF THE WORK

IPF is a multifactorial, age-related and fatal lung disease of unknown origin, with a poor prognosis and very limited treatment options. To date, only two drugs are available on the market for the treatment of IPF: Nintedanib and Pirfenidone. Both therapies show pleiotropic mechanisms of action and have proven efficacy in slowing the rate of functional decline and disease progression in mild-to-moderate IPF patients. However, none of these two drugs is able to definitively reverse or cure the disease and are also associated with tolerability issues. Therefore, the incomplete understanding of the disease and lack of safe and effective treatment makes IPF a disease with a high medical need requiring novel approaches to treatment.

In addition, the preclinical models available to study IPF are not capable to completely reproduce human pathogenesis and the disease phenotype, showing some limits that impact negatively on the research of potential new drugs. The relevance of the preclinical models of IPF to evaluate the efficacy of new drugs has been widely discussed in the scientific community and it is still a matter of controversy and debate. Many compounds have shown efficacy in reducing the progression of pulmonary fibrosis in animal models, but only few of these compounds have confirmed their beneficial effects in clinical trials of IPF. Probably, one of the biggest issue that questions its value is that in the majority of preclinical studies compounds are tested under a prophylactic dosing regimen, whereas in IPF, patients are almost always treated after the fibrosis is well established. Moreover, the endpoints examined in preclinical models of IPF are mostly histological scoring and lung collagen content. However, the clinical evaluation of IPF most commonly relies on lung function measurements (e.g. FVC) and radiological findings on HRCT and, when available, histopathology. Despite these intrinsic limitations, the existing knowledge about IPF is largely arisen with the use of several types of molecular biology approaches performed on animal models of lung fibrosis. Undoubtedly, animal model of lung fibrosis represents an essential component to better understand the mechanisms involved in the disease and, at the same time, constitutes a necessary stage in the development of new drugs.

With this background, the aim of this PhD project was to deeply investigate the features of the most used preclinical model for IPF, the BLM-induced lung fibrosis mouse model, and explore more clinically relevant endpoints with the final goal to generate a robust preclinical model which is able to provide a better indication of a compound's potential efficacy, thus being suitable to support the Drug Discovery projects.

Starting from the recommendations recently published by the ATS panel of experts (*Jenkins et al. 2017*) regarding the best approach for the preclinical testing of potential

therapies for IPF, in the first part of the project the intratracheal BLM mouse model was investigated through the classical histopathological analysis in two experimental setups:

- A time course study, to follow the most important features that characterize the evolution, progression and the partial resolution of lung fibrosis induced by BLM.

- A pharmacological therapeutic study with Nintedanib, to evaluate the effect of an anti-fibrotic drug on the model and for its functional validation.

As a second step, since the ATS panel of experts suggested space for model refinement and proposed the oropharyngeal administration as a valuable alternative to intratracheal BLM instillation, the BLM mouse model was further investigated comparing the intratracheal and oropharyngeal routes of administration. The aim of this approach was to improve the distribution and progression of fibrotic lesions and have the possibility of including more relevant tools as final readouts such as CT imaging and lung function assessment. In this second part of the work, the oropharyngeal BLM model was explored in two steps consisting in a setup phase followed by the pharmacological validation with Nintedanib. Considering that the overall goal was to establish a robust preclinical model of pulmonary fibrosis with high translational potential, which was suitable to select and identify new pharmacological treatments for IPF, this second part of the work was also focused on the exploration and introduction of more clinically relevant endpoints such as lung function tests, CT imaging, oximetry and fibrotic clinical biomarkers to be coupled to the histological analysis commonly used at the preclinical level.

Overall this project aimed to generate an improved BLM model compared to that currently described in the literature and thanks to the introduction of clinically relevant endpoints should help to fill the gap between preclinical models and clinical needs and improve the translatability and the reliability of Drug Discovery compound screening in the search for novel anti-fibrotic drugs.

3. MATERIALS AND METHODS

3.1 *In-vivo* mouse model of pulmonary fibrosis

3.1.1 Animals

Female C57BL/6J mice, weighing 20-22 g at arrival, were supplied by Envigo RMS Italy, San Pietro al Natisone (Udine, Italy). American Thoracic Society's recommendations (*Jenkins et al. 2017*) on the use of animal models for the preclinical assessment of potential therapies for pulmonary fibrosis suggests the use of male mice, since they are more susceptible to BLM treatments and should require lower BLM concentrations compared with females. However, the National Institutes of Health recommends use of both male and female animals in all research studies. We used female mice since they are much less aggressive than males and do not require frequent interventions to separate the dominant.

Prior to use, animals were housed 5 per cage and acclimatized for at least 5 days to the local vivarium conditions (room temperature: 20-24 ºC; relative humidity: 40-70%; 12-h light-dark cycle), having free access to standard certified rodent chow and controlled tap water. Animals were checked for abnormalities or signs of health problems after arrival in the animal facility and were acclimatized for a period of at least 1 week before starting any experimental procedure.

During the experimental phase, mice were given daily high calories dietary supplement (DietGel Recovery purchased by Clear H20, Westbrook, ME, USA) and sterile sunflower seeds (Sunflower kernels w/o hulls, purchased by ssniff Spezialdiäten GmbH, Soest, DE) in addition to the standard rodent chow, since in our experience with the BLM model this food supplementation helps in reducing body weight loss and percentage of mortality. Moreover, mice health conditions (pain rating by visual analogue scale) was checked every day while the body weight was measured every two days throughout the duration of all the studies. All the experimental procedures and conditions involving experimental animals were reviewed and approved by the local ethics committees and authorized by the Italian Ministry of Health and were performed in full compliance with the international European ethics standards in conformity to directive 2010/63/EU, Italian D.Lgs 43 26/2014, and the revised "Guide for the Care and Use of Laboratory Animals" (Committee for the Update of the Guide for the Care and Use of Laboratory Animals and National Research Council, 2010).

3.1.2 Intratracheal (IT) administration

Mice were lightly anesthetized with 4% isoflurane in oxygen delivered in a box and then placed on an animal support stand facing upward by using a clean wire positioned under the animal's front incisors. The tongue was retracted with forceps to visualize the epiglottis.

For IT administration, 50 µl/mouse of saline (control group) or BLM solution were instilled directly through a tracheal cannula, using a small laryngoscope (Penn-Century Inc., Philadelphia, USA) to ensure a good positioning of the cannula into the tracheal lumen. Mice were monitored in cages until they had fully recovered. BLM sulphate, 15000 International Units (IU), powder for solution for injection/infusion (BAXTER Oncology GmbH, Germany), was dissolved in saline solution to obtain the correct dose of 0.0375 IU/mouse (25 ng/mouse). This procedure was performed at days 0 and 4.

3.1.3 Oropharyngeal (OA) administration

Mice were lightly anesthetized with 4% isoflurane in oxygen delivered in a box and then placed on an animal support stand facing upward by using a clean wire positioned under the animal's front incisors. The tongue was retracted with forceps to visualize the epiglottis. For OA administration, 50 µl/mouse of saline (control group) or BLM solution were instilled using a small laryngoscope and with a micropipette the liquid was placed onto the distal part of the oropharynx while the nose was gently closed. Mice were monitored in cages until they had fully recovered. BLM sulphate, 15000 International Units (IU), powder for solution for injection/infusion (BAXTER Oncology GmbH, Germany), dissolved in saline solution to obtain the correct dose of 0.0375 IU/mouse (25 ng/mouse). This procedure was performed at days 0 and 4.

3.1.4 Oral administration of drugs

Nintedanib (Carbosynt, Compton, UK), an FDA-approved drug, was dissolved in 1% of tween 80 (Sigma-Aldrich, St. Louis, MO, USA) in milliQ water and administered at 60 mg/kg once daily (o.d.) as free base or at 50 mg/kg twice daily (b.i.d.) as esylate by oral gavage, according to the experimental study.

3.2 Experimental design

3.2.1 Time course studies – Workflow

After the acclimatization period, animals were weighed and randomized in the different experimental groups. According to the route of BLM used, two different time course studies were performed.

3.2.1.1 Time course BLM IT study

Mice were instilled IT with saline (control group) or BLM solution, at day 0 and day 4. The dose used for the BLM was 0.0375 IU/mouse for each instillation. During the experimental

study, the health condition of the animals was checked every day while the body weight was measured every two days. Mice were euthanized by anesthetic overdose (4% isoflurane in oxygen) followed by bleeding from the abdominal aorta at 7, 14, 21 and 28 days from the first administration of BLM (**Figure 3.1**), and lungs were collected for the final experimental assessment. Specifically, in the BLM IT model the following readouts were evaluated:

- Hydroxyproline quantification as marker of fibrosis in lung tissue homogenate.
- Lung tissue histology: Ashcroft score and automated quantification of lung fibrosis.
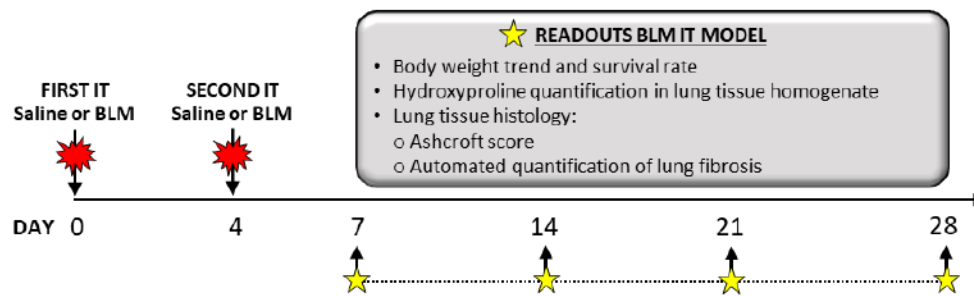
Time	Group Name	Challenge* (*IT administration at days 0 and 4)	N. Animals
T07	Saline	Saline solution	3
	BLM	BLM 0.0375 IU/mouse	5
T14	Saline	Saline solution	3
	BLM	BLM 0.0375 IU/mouse	5
T21	Saline	Saline solution	3
	BLM	BLM 0.0375 IU/mouse	5
T28	Saline	Saline solution	3
	BLM	BLM 0.0375 IU/mouse	5

Figure 3.1 Time course BLM IT Study. Experimental protocol and groups classification.

3.2.1.2 Time course BLM OA study

Mice were instilled OA with saline (control group) or BLM solution, at day 0 and day 4. The dose used for the BLM was 0.037 IU/mouse for each instillation. During the experimental study, the health condition of the animals was checked every day while the body weight was measured every two days. After in-life evaluations, mice were euthanized by anesthetic overdose (4% isoflurane in oxygen) followed by bleeding from the abdominal aorta at 7, 14, 21 and 28 days from the first administration of BLM (**Figure 3.2**), and plasma, BALF and lung samples were collected for the final experimental assessment. Specifically, in the BLM OA model the following readouts were evaluated:

- In-life evaluations:
  - Pulse oximetry
  - Micro-CT imaging
  - Lung function tests
- Biomarkers analysis in plasma and BALF samples
- Hydroxyproline quantification in lung tissue homogenate
- Lung tissue histology: Ashcroft score, automated quantification of lung fibrosis and artificial intelligence for fibrosis detection.
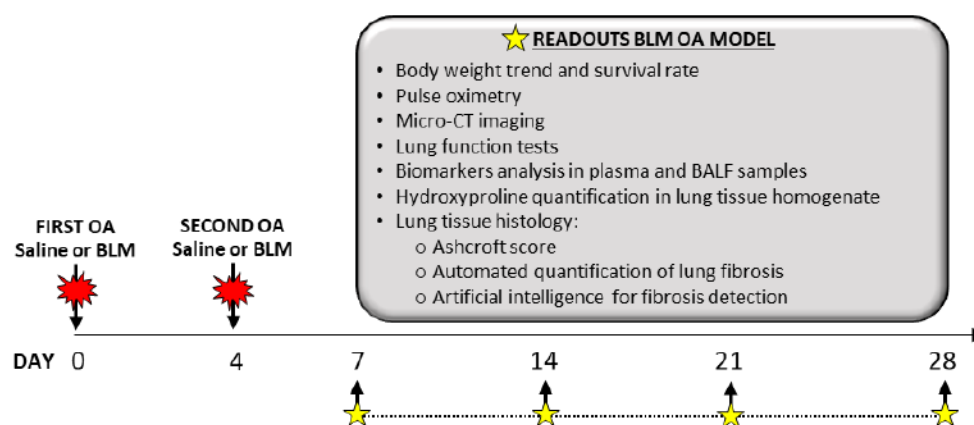
Time	Group Name	Challenge* (*OA administration at days 0 and 4)	N. Animals
T07	Saline	Saline solution	3
	BLM	BLM 0.0375 IU/mouse	10
T14	Saline	Saline solution	3
	BLM	BLM 0.0375 IU/mouse	10
T21	Saline	Saline solution	3
	BLM	BLM 0.0375 IU/mouse	10
T28	Saline	Saline solution	3
	BLM	BLM 0.0375 IU/mouse	10

Figure 3.2. Time course BLM OA Study. Experimental protocol and groups classification.

3.2.2 Therapeutic protocol study – Workflow

3.2.2.1 Therapeutic BLM IT study

After the acclimatization period, mice were instilled IT with saline or BLM solution, at day 0 and day 4. The dose used for the BLM was 0.0375 IU/mouse for each instillation. The therapeutic protocol started seven days after the first administration of BLM, when fibrosis was well established, and then continued for two weeks until day 21, when extensive fibrotic lesions were still evident. At day 7, mice treated with BLM were weighed,

randomized, and divided in two groups: one of them received daily Nintedanib and the other received daily vehicle for all the two weeks of treatment.

Specifically, the experimental groups were as follows:

- <u>Saline (control group)</u>: mice were instilled IT with saline solution and received vehicle (1% of tween 80 in milliQ water) administered orally o.d. for two weeks.

- <u>BLM</u>: mice were instilled IT with BLM and received vehicle (1% of tween 80 in milliQ water) administered orally o.d. for two weeks.

- <u>Nintedanib</u>: mice were instilled IT with BLM and received Nintedanib (60 mg/kg, free base) administered orally o.d. for two weeks.

During the experimental study, the health condition of the animals was checked every day while the body weight was measured every two days. Mice were sacrificed 21 days after the first administration of BLM by anesthetic overdose (4% isoflurane in oxygen) followed by bleeding from the abdominal aorta, and biological samples were collected for the final experimental readouts (*see paragraph 3.2.1.1*). A graphical explanation of the experimental protocol and the groups classification is reported in **Figure 3.3**.

Group Name	Challenge* (*IT administration at days 0 and 4)	Treatment* (*Oral administration from day 7 to 21)	N. Animals
Saline	Saline solution	Vehicle o.d.	20
BLM	BLM 0.0375 IU/mouse	Vehicle o.d.	30
Nintedanib	BLM 0.0375 IU/mouse	Nintedanib 60 mg/kg o.d.	30

Figure 3.3 Therapeutic BLM IT Study. Experimental protocol and groups classification.
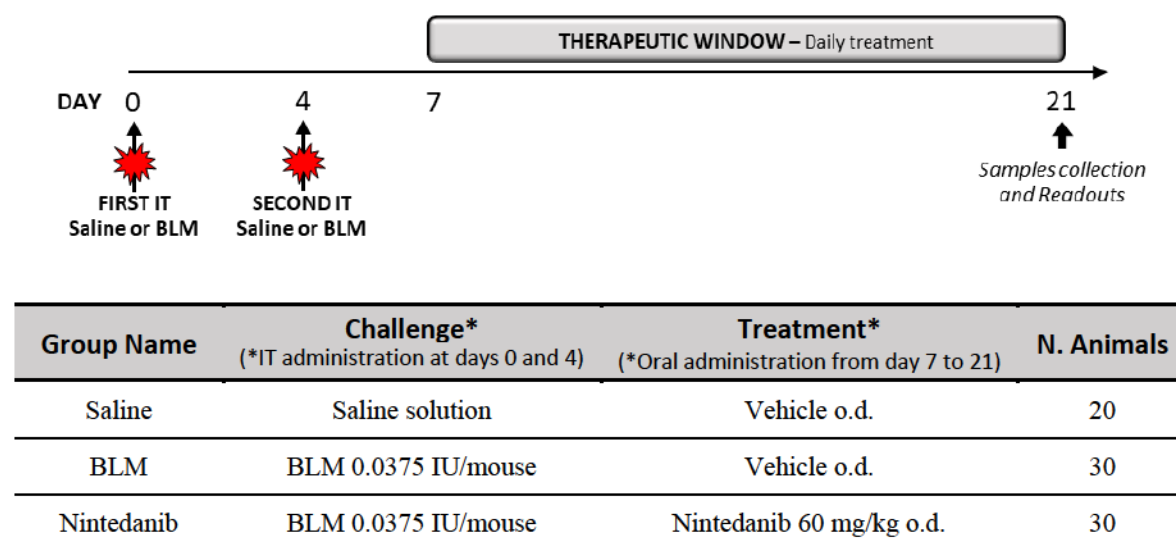
3.2.2.2 Therapeutic BLM OA study

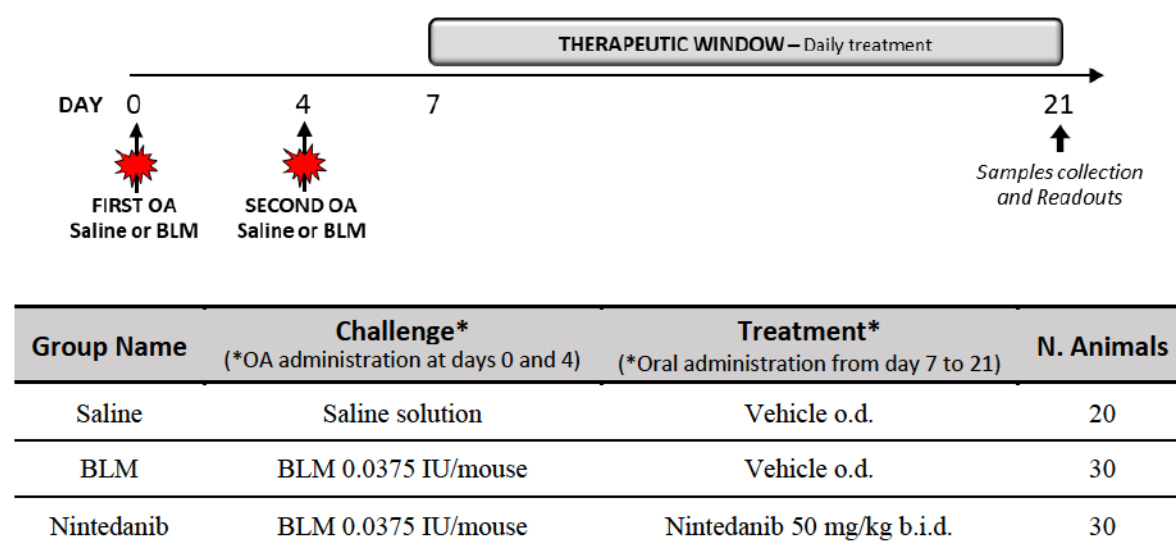After the acclimatization period, mice were instilled OA with saline or BLM solution, at day 0 and day 4. The dose used for the BLM was 0.0375 IU/mouse for each instillation. The therapeutic protocol started seven days after the first administration of BLM, when fibrosis was well established, and then continued for two weeks until day 21, when extensive fibrotic lesions were still evident. At day 7, mice treated with BLM were

weighed, randomized, and divided in two groups: one of them received daily Nintedanib and the other received daily vehicle for all the two weeks of treatment.

Specifically, the experimental groups were as follows:

-Saline (control group): mice were instilled OA with saline solution and received vehicle (1% of tween 80 in milliQ water) administered orally b.i.d. for two weeks.

-BLM: mice were instilled OA with BLM and received vehicle (1% of tween 80 in milliQ water) administered orally b.i.d. for two weeks.

-Nintedanib: mice were instilled OA with BLM and received Nintedanib (50 mg/kg, esylate) administered orally b.i.d. for two weeks.

During the experimental study, the health condition of the animals was checked every day while the body weight was measured every two days. After the in-life evaluations, mice were sacrificed 21 days after the first administration of BLM by anesthetic overdose (4% isoflurane in oxygen) followed by bleeding from the abdominal aorta, and biological samples were collected for the final experimental readouts (*see paragraph 3.2.1.2*). A graphical explanation of the experimental protocol and the groups classification is reported in **Figure 3.4**.

Group Name	Challenge* (*OA administration at days 0 and 4)	Treatment* (*Oral administration from day 7 to 21)	N. Animals
Saline	Saline solution	Vehicle o.d.	20
BLM	BLM 0.0375 IU/mouse	Vehicle o.d.	30
Nintedanib	BLM 0.0375 IU/mouse	Nintedanib 50 mg/kg b.i.d.	30

Figure 3.4 Therapeutic BLM OA Study. Experimental protocol and groups classification.

3.3 In-life evaluations

3.3.1 Pulse oximetry

The MouseOx® Pulse-oximeter (Starr Life Sciences, Oakmont, PA, USA) was used to monitor arterial blood oxygen saturation (SpO2) in mice, and to follow the effects of BLM on gaseous exchange in the lung. The collars of experimental animals were shaved at least a

day before the beginning of pulse oximetry monitoring. At indicated experimental time points, mice were anesthetized with 2% isoflurane and a small MouseOx collar clip sensor was placed on the animal's neck. The measurements were performed with anesthetized animal in the prone position placed on a heated mat at 37°C and were continued to allow recording of 2-3 minutes of stable signal from each animal. Pulse oximetry readings were recorded as a Windaq Waveform file at 15-Hz sample rate by MouseOx Plus's software and sorted by spreadsheet for readings that had no error codes. Arithmetic means of individual readings were then calculated for each animal and later used for statistical analysis.

3.3.2 Micro-CT imaging

Following anesthesia induction and maintenance with 2% isoflurane, mice lungs imaging was performed with a Quantum GX Micro-CT (PerkinElmer, Inc. Waltham, MA). For time course OA study, mice lungs were scanned at 7, 14, 21 and 28 days after the first BLM administration, while for therapeutic OA study, lungs imaging was performed longitudinally at day 7 and day 21. Images were acquired with an intrinsic retrospective two phase respiratory gating technique with the following parameters: X-ray tube voltage 90 KV, X-ray tube current 88 μA, total scan time of 4 min. The 'high speed' mode (acquiring projections without averaging in list-mode over a total angle of 360°) resulted in two 3D datasets, corresponding to the two different phases of the breathing cycle (i.e. end-inspiration and end-expiration). Data reported here refer to the end of expiration phase. The reconstructed datasets were imported and analyzed using Analyze software (Analyze 12.0; Copyright 1986–2017, Biomedical Imaging Resource, Mayo Clinic, Rochester, MN). Pulmonary image analysis was based on a semi-automatic segmentation to define airways and total lung volumes. Micro-CT images were rescaled into Hounsfield Units (HU) setting −1,000 HU as the density of air and 0 HU as the density of water. Pre-clinical HU density ranges (*Mecozzi et al. 2020*) were applied to semi-automatically segmented lungs for the quantitative assessment of parenchymal lesions. Normo-aerated tissue [−860 HU; −435 HU] and poorly-aerated tissue [−435 HU; −121 HU] were defined and normalized on total lung volumes.

3.3.3 Lung function tests

At selected experimental time points of the BLM-treatment regimen, respiratory system mechanics and Pressure-Volume (PV) relationships were measured using the FlexiVent System (SCIREQ Inc., Montreal Qc, Canada) (*Vanoirbeek et al. 2010*). Briefly, mice were anesthetized by intraperitoneal injection of ketamine (Anesketin®, Dechra Inc.,

Handelsweg, NL) and xylazine (Xilagesic®, Calier Inc., Barcelona, ES) solution (100 mg/kg and 10 mg/kg, respectively). Once surgical anesthesia was achieved, as assessed by loss of withdrawal reflex and absence of response to external stimuli, the mouse was tracheotomized using a 18-gauge metal cannula, connected via an endotracheal cannula to the FlexiVent and ventilated at a respiratory rate of 150 breaths/min and tidal volume of 10 ml/kg against a positive end-expiratory pressure of 3 cmH2O to achieve a mean lung volume close to that during spontaneous breathing. To prevent spontaneous breathing mice also received pancuronium bromide 1 mg/kg intraperitoneally. FlexiVent software version 8.1 was used to perform the perturbations.

The Deep Inflation perturbation provides a direct measurement of the subject's inspiratory capacity (IC) bringing the subject's lungs from end of expiration to TLC which is defined by default as a pressure of 30 cmH$_2$O. The Snapshot-150 perturbation is a brief (1.25 s for a mouse), single frequency forced oscillation (FOT). The single FOT measurements, fitting to single compartment model provides an accurate characterization of the respiratory system resistance (Rrs) and elastance (Ers). The PV loops are a family of maneuvers used to construct PV curves in a stepwise and executed in a pressure-driven manner (PVs-P). The PV curves assesses the distensibility of the respiratory system at rest over the entire inspiratory capacity, calculating the quasi-static compliance (Cst). The negative pressure-driven forced expiration (NPFE) maneuver was then performed by inflating the mouse lungs to a pressure of 30 cm H$_2$O over 1 s, holding this pressure for 2 s before connecting the animal's airways to the negative pressure reservoir (-50 cm H$_2$O) for 2 s. The NFPE maneuver mimics spirometry in humans generating some outcomes resembling those obtained in IPF patients, such as the forced expiratory volume in 0.1 s (FEV$_{0.1}$) and FVC. All maneuvers and perturbations were performed until three acceptable measurements (coefficient of determination ≥ 0.95) were achieved. For each parameter, an average of the three measurements was calculated and depicted per mouse.

3.4   Biological samples collection and processing

- PLASMA: Immediately after animals' sacrifice, blood samples were collected from the right heart ventricle and placed in a tube containing heparin as anticoagulant. Plasma was then separated by centrifuging the tubes at 2000 x g and 4°C for 10 minutes (Thermo Scientific Heraeus centrifuge). Plasma samples were aliquoted and stored at -80°C for quantitative determination of the biomarkers.

- BALF: Following blood collection, lungs were gently washed three times using a cannula inserted into the trachea with 0.6 ml of clear BAL solution [10X HBSS (Hanks' Balanced

Salt Solution), 10 mM EDTA (Ethylenediaminetetraacetic acid; Fluka analytical, Sigma-Aldrich, St. Louis, MO, USA), 10 mM HEPES ((4-(2-hydroxyethyl)-1-piperazineethanesulfonic acid; Gibco, ThermoFisher Scientific, Waltham, MA, USA) and distilled water]. Routine recovery of BALF did not significantly differ between animals with ~80% of instilled volume recovered. The obtained BALF was centrifuged at 1000 x g and 4°C for 10 minutes and the cell-free supernatant was aliquoted and stored at -80°C for quantitative determination of the biomarkers.

- LUNGS: The whole lungs were excised after BALF procedure and cardiac perfusion, and either fixed for histological analysis or stored for hydroxyproline content analysis in lung homogenates. According to the experimental protocol, samples were processed as follow:

- Sample processing for Hydroxyproline analysis: the whole lungs were removed, washed in saline solution, and weighted. Fresh lungs were quickly frozen in liquid nitrogen and stored at -80°C. To prepare lung tissue homogenate, each 100 mg of frozen lungs were homogenized in 1 ml of ice-cold 1X Phosphate Buffered Saline (PBS; Gibco, ThermoFisher Scientific, Waltham, MA, USA) containing Protease and Phosphatase Inhibitor Cocktail (Sigma-Aldrich, St. Louis, MO, USA), with gentleMACS™ Dissociator (Miltenyi Biotec, Germany). After this step, the total lung homogenates were collected, and aliquots were stored at -80°C for the quantitative determination of hydroxyproline content.

- Sample processing for histological analysis: the whole lungs were removed, inflated with a cannula through the trachea by gentle infusion with 0.6 ml of 10% formalin solution (Formaldehyde solution 4%, buffered, pH 6.9; Sigma-Aldrich, St. Louis, MO, USA) and fixed for at least 24 h at room temperature. Sample processing was performed by external laboratories: for BLM IT studies, activities were performed by laboratory unit of Prof. Donetti from Department of Biomedical Sciences for Health at University of Milan, Italy; for BLM OA studies, activities were performed by laboratory unit of Jane Schofield from Histology Department at Covance, Eye, UK. Both laboratories support Chiesi Farmaceutici for the histological processing activities.

After fixation, lungs have been dehydrated in graded ethanol series, clarified in xylene and paraffin embedded. Each longitudinally oriented lung was cut to obtain one representative slice of 5 μm thick, which subsequently were stained with Masson's Trichrome histological staining. Masson's Trichrome is a histological staining protocol that employs three different reagents for staining collagen and

ECM, muscle fibers, and erythrocytes. This staining protocol is usually employed for distinguishing collagen fibers in blue/green, and for this reason it is one of the staining protocols recommended for the histologic assessment of morphology in lung fibrosis related studies.

3.5 Protein analysis

3.5.1 Hydroxyproline

The total amount of hydroxyproline, as a measure of collagen content, was determined with the hydroxyproline Colorimetric Assay Kit (Sigma MAK008, USA) according to the manufacturer's protocol. Briefly, an aliquot of lung homogenate was hydrolyzed with the same concentration of 12N HCl at 100°C overnight. The hydrolyzed samples were transferred into a 96-well plate, allowed to evaporate to dryness and were first incubated 5 minutes with Chloramine T/Oxidation Buffer mixture at room temperature and then with 4-(Dimethylamino) benzaldehyde (DMAB)/ Perchloric Acid/Isopropanol solution for 60 minutes at 60°C. The absorbance of oxidized hydroxyproline was determined at 560 nm, using a microplate spectrophotometer (xMark, Biorad, California, USA). Standard curves were generated for each experiment using reagent hydroxyproline as a standard. Results were expressed as µg of hydroxyproline contained in total lung tissue.

3.5.2 Biomarkers analysis

The total amount of Surfactant Protein-D (SP-D; R&D systems, Bio-Techne, Minneapolis, MN, USA), Matrix Metalloproteinase-7 (MMP-7; Cusabio, Houston, TX, USA), and Collagen Type I (COL1; Cloud-Clone, Katy, TX, USA) were quantified in plasma or BALF samples with commercial Enzyme-linked immune-sorbent assay (ELISA) kits specific for mouse proteins according to the manufacturer's protocol. Briefly, antibody specific for the measured protein had been pre-coated onto a microplate. Standards and samples, at appropriate dilutions, were pipetted into the wells and any protein present was bound by the immobilized antibody. After removing any unbound substances with a series of washing cycles, a biotin-conjugated antibody, specific for the protein, was added to each well. After washing, avidin conjugated Horseradish Peroxidase (HRP) was added to the wells. Following a series of other washes to remove any unbound avidin-enzyme reagent, a substrate solution was added to the wells and a specific colour was developed in proportion to the amount of protein bound in the initial step. The colour development was stopped with a stop solution provided by the supplier and its intensity was measured at a specific wavelength (nm), using a microplate spectrophotometer (xMark, Biorad, California, USA).

For the determination of protein concentrations, a standard curve was plotted relating the intensity of the colour (O.D.) to the concentration of standards. Results were expressed as pg of protein per mL of sample.

3.6 Histological analysis

For histological analysis, Masson's trichrome stained slides representative of all the five lobes were digitalized through the image analysis system NDP.scan 3.2 with NanoZoomer S-60 scanner (Hamamatsu Photonics K.K, Japan). Scans were performed using the fully automated mode and 20x objective.

3.6.1 Ashcroft score

Fibrotic lung injury was assessed histologically on the whole-slide images through Ashcroft scoring system (*Hübner et al. 2008*) by an expert histopathology blinded to the experimental design. The analyses were performed by external laboratories: for time course BLM OA study the analysis was performed by AnaPath Services GmbH, Hammerstrasse, Switzerland; all other studies were analyzed by the Laboratory Unit of Prof. Donetti from Department of Biomedical Sciences for Health at University of Milan, Italy.

In order to cover the whole surface of each lung section, a grid with rectangles of dimensions 2x1 mm was placed over the tissue area. Only rectangles where at least half of the area was covered by parenchyma, excluding large blood vessels and bronchi, were evaluated. The severity of fibrotic tissue in each field was evaluated at 10x magnification using the Ashcroft scale from grade 0 to 8 (**Table 3.1**). In each examined field, the predominant degree of fibrosis that occupied more than half of the field area, was recorded. Ashcroft scores for each animal lung was expressed as the mean of the total number of fields. Mean Ashcroft scores for each group were obtained from the mean of each animal.

**Table 3.1** Description of the histological Ashcroft scoring system (Table taken from *Hübner et al. 2008)*.

Grade of Fibrosis	Histological features
0	Alveolar septa: No fibrotic burden at the most flimsy small fibers in some alveolar walls Lung structure: Normal lung
1	Alveolar septa: Isolated gentle fibrotic changes (septum ≤3× thicker than normal) Lung structure: Alveoli partly enlarged and rarefied, but no fibrotic masses prese
2	Alveolar septa: Clearly fibrotic changes (septum >3× thicker than normal) with knot-like formation but not connected to each other Lung structure: Alveoli partly enlarged and rarefied, but no fibrotic masses
3	Alveolar septa: Contiguous fibrotic walls (septum >3× thicker than normal) predominantly in whole microscopic field Lung structure: Alveoli partly enlarged and rarefied, but no fibrotic masses
4	Alveolar septa: Variable Lung structure: Single fibrotic masses (≤10% of microscopic field)
5	Alveolar septa: Variable Lung structure: Confluent fibrotic masses (>10% and ≤50% of microscopic field). Lung structure severely damaged but still preserved
6	Alveolar septa: Variable, mostly not existent Lung structure: Large contiguous fibrotic masses (>50% of microscopic field). Lung architecture mostly not preserved
7	Alveolar septa: Non-existent Lung structure: Alveoli nearly obliterated with fibrous masses but still up to five air bubbles
8	Alveolar septa: Non-existent Lung structure: Microscopic field with complete obliteration with fibrotic masses

3.6.2   Automated quantification of lung fibrosis

The quantification of lung fibrosis was carried out on whole-slide images by using Visiopharm® software (Visiopharm, Hoersholm, Denmark), a pathology image analysis software. The automated analysis was performed with an optimized and internally validated Analysis Protocol Packages (APPs). The APP was designed to distinguish healthy from fibrotic areas and then quantify the fibrotic tissue, detecting accumulation of connective tissue, excess of collagen deposition and cellular hyperproliferation. These features were easily visualized thanks to Masson's trichrome histological stain. The software was able to identify these types of morphological structures through the setting of specific color, intensity, and size thresholds. Briefly, the image analysis software runs, in tandem, three following APPs:

- Automatic identification of the lung section on the slides (total area measure).
- Automatic identification of the vessels and bronchi and exclusion of their collagen content.
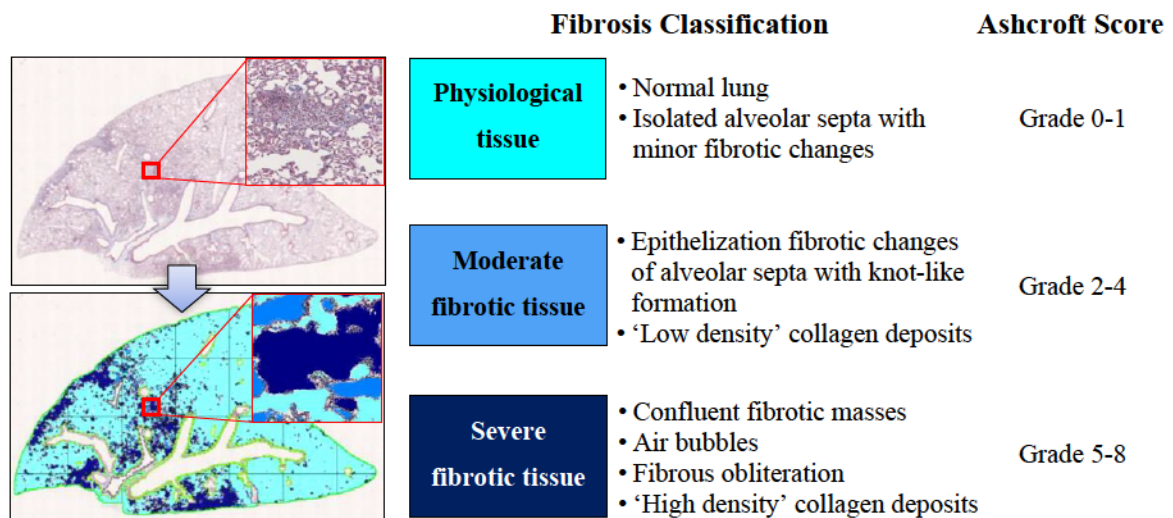- Automatic identification and quantification of fibrotic tissue.

Finally, the readout was represented by the percentage of lung parenchyma affected by fibrotic lesions on the total lung section. A schematic representation of the Visiopharm® APPs workflow is reported in **Figure 3.5**.
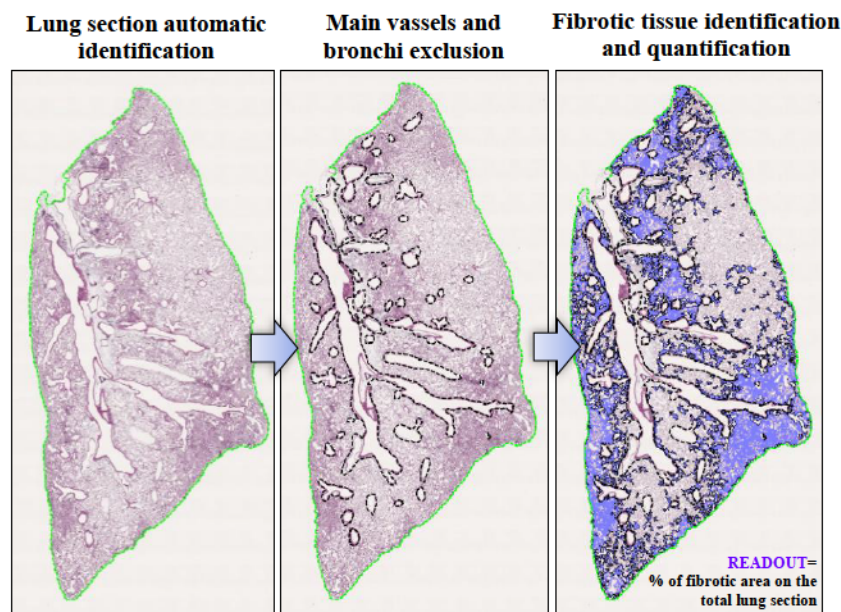
Figure 3.5. Workflow of the Visiopharm® APPs for automated quantification of lung fibrosis (Figure taken from Chiesi's internal presentation).

3.6.3 Artificial intelligence (AI)-based APP for fibrosis detection

Different grades of fibrosis severity on whole-slide images was assessed with the support of the AI deep learning Visiopharm® module. The AI-based APP was developed with the purpose of recognize and classify different degrees of fibrosis severity corresponding to the different grades described in the modified Ashcroft scale (**Figure 3.6**). Specifically, in addition to identify the lung parenchyma by excluding the basal collagen, main bronchi and blood cells, as described previously, the new APP was designed to identify the fibrotic regions and recognize different degrees of severity within these regions, classifying them as physiological, moderate and severe fibrosis.

	Fibrosis Classification	Ashcroft Score
Physiological tissue	• Normal lung • Isolated alveolar septa with minor fibrotic changes	Grade 0-1
Moderate fibrotic tissue	• Epithelization fibrotic changes of alveolar septa with knot-like formation • 'Low density' collagen deposits	Grade 2-4
Severe fibrotic tissue	• Confluent fibrotic masses • Air bubbles • Fibrous obliteration • 'High density' collagen deposits	Grade 5-8

Figure 3.6 Schematic classification of lung fibrosis severity distribution by AI-based Visiopharm® APPs (Figure taken from Chiesi's internal presentation).

3.7 Statistical analysis

All data were expressed as mean ± standard error of mean (SEM). Unpaired t-test or analysis of variance (ANOVA) followed by Sidak's or Dunnett's post hoc analysis was used to compare two or more experimental groups, respectively. The Pearson's correlation coefficient matrix (r value) was used to determine the degree of association between data. Statistical analyses were performed using GraphPad Prism 8 software (GraphPad Software Inc., San Diego, CA, USA). $p \leq 0.05$ was considered statistically significant.

4. RESULTS

4.1 Time course BLM IT study

The first experiment performed during my PhD period, with the aim to acquire a deeper characterization of the murine model of BLM-induced lung fibrosis, was a time course study that allowed to follow the evolution, progression and the partial resolution of fibrosis over time. Recently, the consensus view of the ATS workshop report on lung fibrosis animal models confirmed that "use of the murine IT BLM model in animals of both genders, using hydroxyproline measurements for collagen accumulation along with histologic assessments, is the best-characterized animal model available for preclinical testing" (*Jenkins et al. 2017*). In line with the ATS panel of experts, in this first study the lung fibrosis was induced in female mice by a double IT administration of BLM, at day 0 and at day 4 at a dose of 0.0375 IU/mouse for each instillation, which was reported to be able to induce fibrosis while being tolerated (*Stellari et al. 2017*). Histological analysis and hydroxyproline lung content were examined at different time points (days 7, 14, 21 and 28) from the first BLM IT administration. Moreover, body weight trend and survival rate were assessed throughout the study.

4.1.1 Body weight trend and survival

The body weight trend gave us a primary indication about the response of the animals to BLM-induced damage and was assessed throughout the duration of the study, along with the survival rate, being BLM a cytotoxic agent associated with several side effects, including body weight loss and increased mortality rate.

The double BLM IT administration induced a significant weight loss in the first days after challenge, reaching a peak around the seventh day after the first BLM administration, where mice treated with BLM lost on average $\simeq 11\%$ of their starting weight (**Figure 4.1 A**). In the following days, the BLM-treated animals recovered weight with a regular and progressive trend, while still maintaining a significant difference until the end of the experiment compared to Saline-treated mice, which conversely did not show any drop in body weight. During the experiment, no mortality was registered for both Saline and BLM groups (**Figure 4.1 B**). These observations suggest that double BLM IT was well tolerated by the animals.
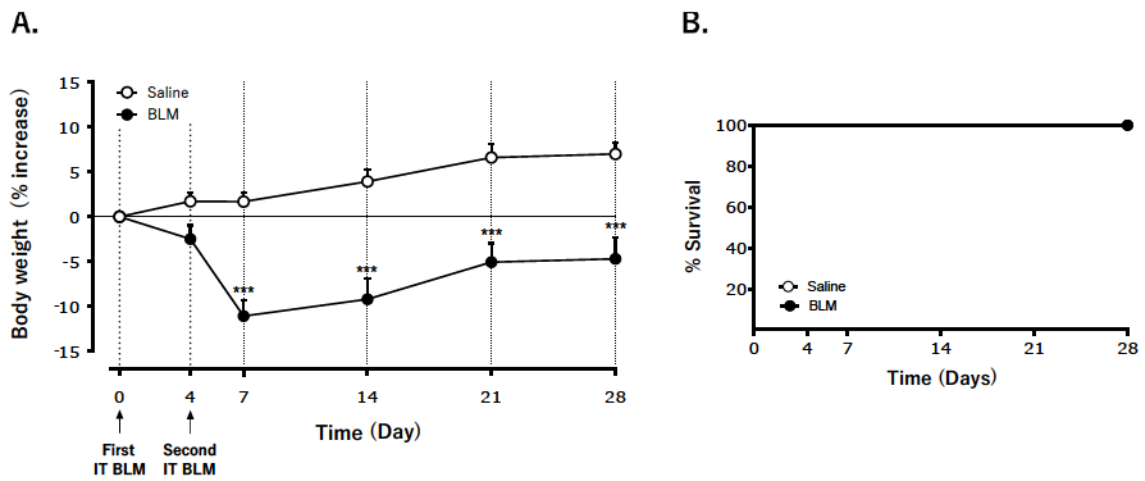
Figure 4.1 Effect of BLM IT administration on body weight loss and mortality of mice. **A.** Body weight trend. Each point represents the mean ± SEM values for both Saline (n=12; white circles) and BLM (n=20; black circles) groups of animals, expressed as percentage of body weight change calculated from day 0 onwards. Statistical analysis was assessed using two-way ANOVA followed by Sidak's test in comparison with the relative control values (Saline group); *** $p \leq 0.001$. **B.** Survival. Kaplan–Meier graph showing survival rate of mice from day 0 until day 28.

4.1.2 Histological analysis

The histological evaluation allowed us to demonstrate the presence of lung fibrosis and to visualize the severity and the distribution of the damage induced by double BLM IT instillation over time. Two types of analysis were performed on Masson's trichrome stained slides representative of all the five lobes:

- a visual analysis, based on the Ashcroft scoring scale (min 0 –max 8);

- an automated quantification of lung fibrosis (Visiopharm® software).

Moreover, a general qualitative evaluation was also performed to better understand histological changes induced by BLM IT over time. The **Figure 4.2** shows one representative image of BLM-treated lung tissue section for each analyzed time point, flanked by an image from one of the Saline groups (control animal). The image of lung tissue obtained from Saline-treated group revealed a preservation of the gross alveolar structures, while the stained connective tissue was present only at the perivascular and peri-bronchiolar level (physiological condition). Conversely, the staining from BLM-treated group revealed that double BLM IT administration induced an acute and severe inflammatory reaction in the lung at day 7, with hemorrhage and alveolar infiltration of different inflammatory cells, like neutrophils and macrophages/histiocytes. Moreover, at this time point, there was an initial collagen formation (scarce presence of reactive fibroblasts into provisional matrices normally present in the early stages of tissue remodeling after acute injury), mainly observed around large blood vessels, bronchi and in the sub-pleural area. At day 14, the tissue appeared more damaged with an increase of fibrosis compared to the previous time point. Fibrosis resulted more widespread throughout the parenchyma with the presence of thickened but still visible alveoli. Moreover, an increase in lymphocytes also in the alveolar spaces and the presence of reactive multi-nucleated macrophages was observed. At day 21, fibrotic tissue started branching and large areas of lung parenchyma were replaced with dense collagen deposition and fibrotic masses in which alveoli were not clearly identifiable. Finally, 28 day after the first BLM IT administration a reduction of severity and extent of total fibrosis was observed, although collagen fibres appeared to be organized in less extended but more compact fibrotic areas.

Overall, histopathological examination revealed that BLM IT administration induced a fibrotic pattern characterized by a patchy distribution of the fibrotic foci in the lung parenchyma of mice that led to a marked geographic heterogeneity in the distribution of fibrosis among the lobes, affecting more severely only one lobe in most of the cases, typically the left lung lobe, compared to the others.
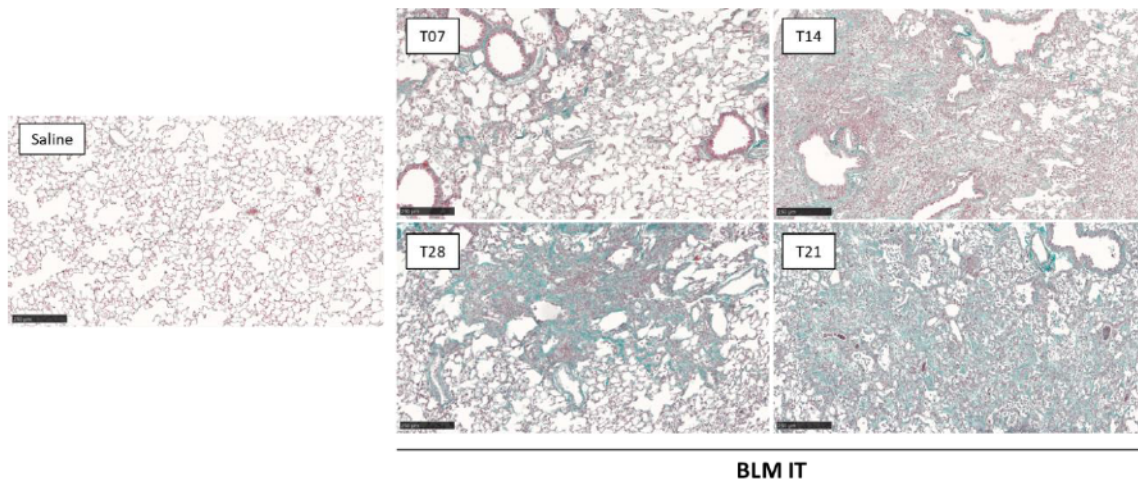
Figure 4.2 Histological appearance of the lung fibrosis induced by BLM IT over time. Representative Masson's trichrome-stained mouse lung tissue sections, obtained from control animals (Saline) and BLM-treated mice at different time points (T07, T14, T21 and T28); scale bar = 250 μm.

All these qualitative observations were confirmed and supported by the two histological analysis for the evaluation of lung fibrosis (**Figure 4.3 A-B**).

The Ashcroft score evaluation revealed that two IT instillations of BLM were able to induce the formation of myofibroblast-rich provisional matrices as early as day 7 after the first BLM IT administration (**Figure 4.3 A**). At this time point, the score in the BLM group was 2.8 ± 0.1 (a damage more severe than an "isolated alveolar septa with gentle fibrotic changes" as defined by Hübner et al.) compared to 0.3 ± 0.2 of the Saline group ($p \leq 0.001$). The Ashcroft score value observed in BLM group increased over time, reaching a peak of fibrosis severity at day 14 (3.6 ± 0.3 vs 0.3 ± 0.1; $p \leq 0.001$), which remained comparable until day 21 (3.5 ± 0.2 vs 0.2 ± 0.1; $p \leq 0.001$). Scores observed at these time points corresponds to a moderate degree of fibrosis with alveolar septa variable, partial enlarged and rarefied, and presence of single fibrotic masses ($\leq 10\%$ of microscopic field) (*Hubner et al. 2008*). At day 28, the Ashcroft score of the BLM-treated group significantly decreased compared to that observed on days 14 and 21 ($p \leq 0.05$), although still maintaining a significant difference compared to the Saline group (2.6 ± 0.4 vs 0.2 ± 0.1; $p \leq 0.05$).

These results were confirmed by the automated analysis performed using the Visiopharm® software for the quantification of lung fibrosis (**Figure 4.3 B**). The area of fibrotic tissue observed at day 7 after the first IT BLM administration was about 32% of the total lung area. This area increased at day 14, reaching 43% fibrotic tissue, and remained stable until day 21 (39%). Similarly to the Ashcroft score evaluation, the fibrotic area gradually

decreased at day 28 (30%), probably highlighting an initial resolution of fibrosis. As expected, the control groups treated with Saline exhibited a normal lung with minimal parenchymal changes (average value of fibrotic tissue was 10.2% for all points of observation).
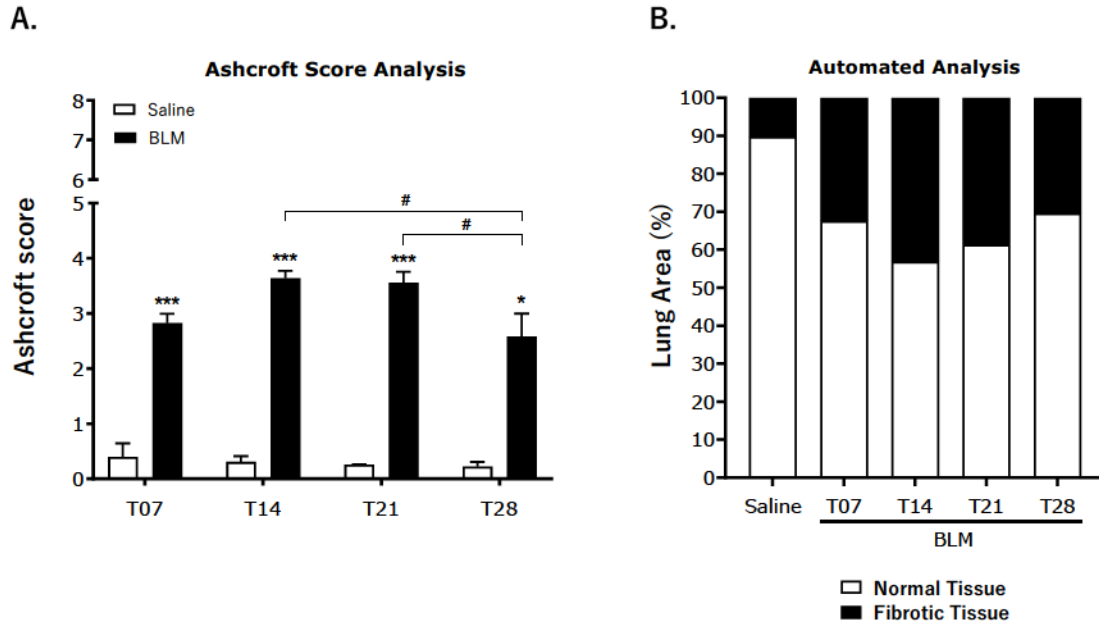

Figure 4.3 Histological analysis of pulmonary fibrosis in Masson's Trichrome stained lung sections performed in female mice at different time points (T07, T14, T21, and T28) from the first BLM IT administration. **A.** Ashcroft score analysis. Data are expressed as mean $\pm$ SEM (n=3 Saline (white bars); n=5 BLM (black bars)). Statistical analysis was assessed using unpaired Student's t-test in comparison with the relative control values (Saline group); *** $p \leq 0.001$, * $p \leq 0.05$. # $p \leq 0.05$ refers to one-way ANOVA (Dunnett's t test) comparisons among BLM-treated groups. **B.** Automated quantification of lung fibrosis by Visiopharm® software. Data are expressed as mean value; Saline bar is reported as mean value of all the control animals.

4.1.3   Quantification of Hydroxyproline lung content

Hydroxyproline (Hyp) is a non-proteinogenic amino acid that constitutes one of the most important components of collagen, where it helps to stabilize the protein helical structure. Considering its high content within the triple helix of collagen, the Hyp quantification was used to obtain an approximation of the amount of collagen in the lungs.

Moreover, since BLM IT administration gives a patchy distribution of fibrosis in the lungs, it has been decided to perform the analysis of Hyp content in the whole lung homogenate of mice for all the analyzed time points, instead of processing half lung tissue for the histology and the other half for Hyp analysis from the same animal. This should allow to have a more reproducible comparison both between the experimental groups and the different studies.

The levels of the total lung Hyp measured in the BLM groups increased among the different time points compared to the Saline-treated groups (**Figure 4.4**). In particular, while at day 7 no significant increase was evident (320.2 ± 22.6 vs 253.7 ± 5.6 µg/mg lung, NS), a significant difference between the two different groups of treatment was observed from day 14 (362.1 ± 13.2 vs 252.6 ± 10.5 µg/mg lung, $p \leq 0.01$), and especially at day 21 where Hyp content was more than doubled in the BLM group compared to the Saline group (503.6 ± 45.9 vs 229.0 ± 10.7 µg/mg lung, $p \leq 0.01$). Furthermore, levels of Hyp content among the BLM-treatment groups were significantly increased at day 21 compared to day 7 ($p \leq 0.01$), where instead, at this latter time point the fold of increase between Saline and BLM was less than 2. At day 28, a slight decreasing trend of Hyp levels was observed in the BLM group (478.5 ± 72.9 vs 244 ± 8.2 µg/mg lung, NS), suggesting a preliminary reduction of the collagen content of fibrotic lesions, mainly visible in some animals than others as suggested by the higher variability observed at this late time point.
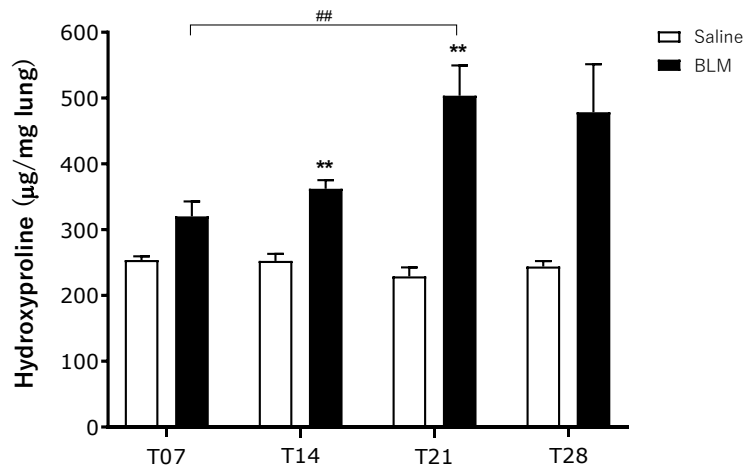
Figure 4.4 Quantification of Hyp content in lung homogenate performed in female mice at different time points (T07, T14, T21, and T28) from the first BLM IT administration. Data are expressed as mean ± SEM (n=3 Saline (white bars); n=5 BLM (black bars)). Statistical analysis was assessed using unpaired Student's t-test in comparison with the relative control values (Saline group); ** $p \leq$ 0.01. ## $p \leq 0.01$ refers to one-way ANOVA (Dunnett's t test) comparisons among BLM-treated groups.

4.2 Therapeutic BLM IT study

After the evaluation of the effects of BLM over time, a therapeutic study with an approved drug like Nintedanib to assess the effect of an anti-fibrotic compound on the model was designed. This study aimed to provide the pharmacological validation of the model and, at the same time, to allow a better indication of a compound potential efficacy, with the final aim to have a model suitable to support the Drug Discovery projects. Based on the results obtained from the time course study and in order to ensure an adequate therapeutic window to test new anti-fibrotic compounds, it was decided to start treatment after the initial acute inflammatory phase (day 7 after the first BLM IT administration), as recommended by the ATS expert group (*Jenkins et al. 2017*), and to set day 21 as the final time point of the therapeutic window, considering that at this point the fibrotic response was still evident and more consistent in all the readouts evaluated. More technical details are described in the Materials and Methods section (see paragraph 3.2.2.1).

### 4.2.1 Body weight trend and survival

The double BLM IT administration induced a significant weight loss in the first days after challenge, reaching a peak around the seventh day, where mice treated with BLM lost on average $\simeq$13% of their starting weight. In the following days, the BLM-treated mice recovered weight with a regular and progressive trend, while still maintaining a significant difference until day 17 compared to Saline-treated animals, which conversely did not show any drop in body weight. The oral treatment with Nintedanib (60 mg/kg o.d.) did not induce any significant effect on body weight of mice compared to BLM group; however, mice treated with Nintedanib tended to recover more slowly the weight loss induced by BLM (**Figure 4.5 A**). Moreover, as shown in the survival graph in **Figure 4.5 B**, a 15% of mortality was recorded in the BLM group, whereas a mortality of 10% was observed in mice treated with Nintedanib, suggesting a possible protective effect of Nintedanib with this dose. Compared to the time course study where no mortality was observed, the slight mortality obtained in this study could be due to the daily manipulation of the animals following the treatments that could have impacted in terms of tolerability on top of the BLM effect.
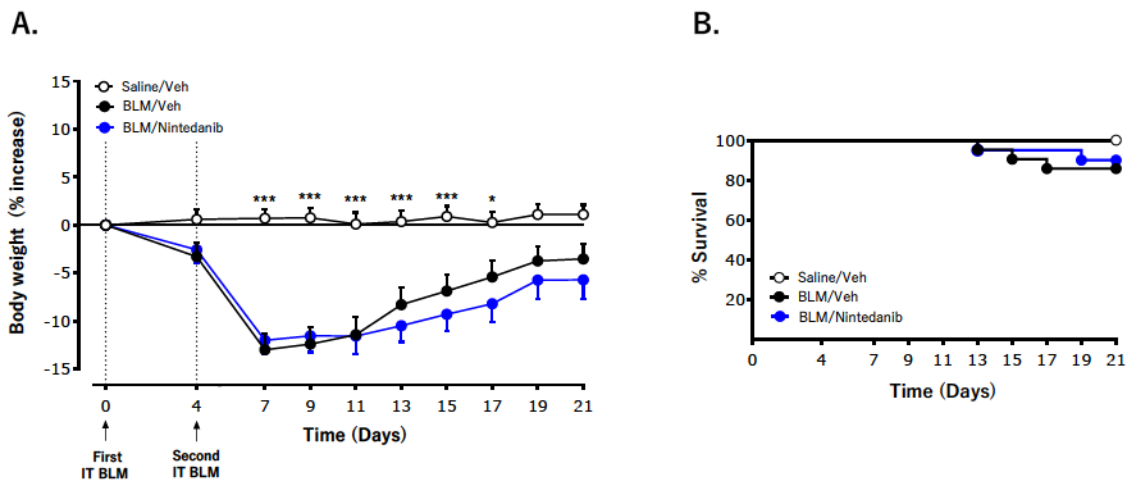
Figure 4.5 Effect of Nintedanib on body weight loss and mortality in BLM treated mice. Female mice were daily treated by oral gavage with either Nintedanib (60 mg/kg o.d.) or vehicle (1% of Tween 80 in milliQ water), starting from day 7 after BLM IT administration up to day 21. **A.** Body weight trend. Each point represents the mean ± SEM values for Saline/Veh (n=20; white circles), BLM/Veh (n=30; black circles) and BLM/Nintedanib (n=30; blue circles) groups of animals, expressed as percentage of body weight change calculated from day 0 onwards. Statistical analysis was assessed using two-way ANOVA followed by Dunnett's test in comparison with the BLM group; *** p ≤ 0.001, * p ≤ 0.05. **B.** Survival. Kaplan–Meier graph showing survival rate for each group of treatment from day 0 until day 21. BLM, bleomycin; Veh, vehicle.

4.2.2 Histological analysis

As shown in **Figure 4.6**, the Masson's trichrome stained lung slides obtained in this study revealed that at day 21 BLM-induced lung fibrosis mainly consisted of collagen deposition in alveolar walls and in the pulmonary interstice and evident fibrotic masses. Moreover, an inflammatory reaction of different degrees of entity (presence of macrophages and lymphocytes), was always seen. In the cases of more severe fibrosis, bronchiolization of the alveoli and an overexpression of the bronchiolar-associated lymphoid tissue were also observed. Overall, in most cases, a strong difference in the distribution of fibrosis among the various lobes was noted. In BLM-treated mice, areas of normal lung parenchyma were replaced with dense collagen agglomerates where alveoli were not well identifiable. However, in the Nintedanib group (for almost all the animals) the collagen deposition appeared diffuse through the tissue. Moreover, in this group the alveoli were clearly visible even if the septa were more thickened than in the Saline-control group, which exhibited a normal histological conformation and preservation of the various pulmonary elements, as expected.
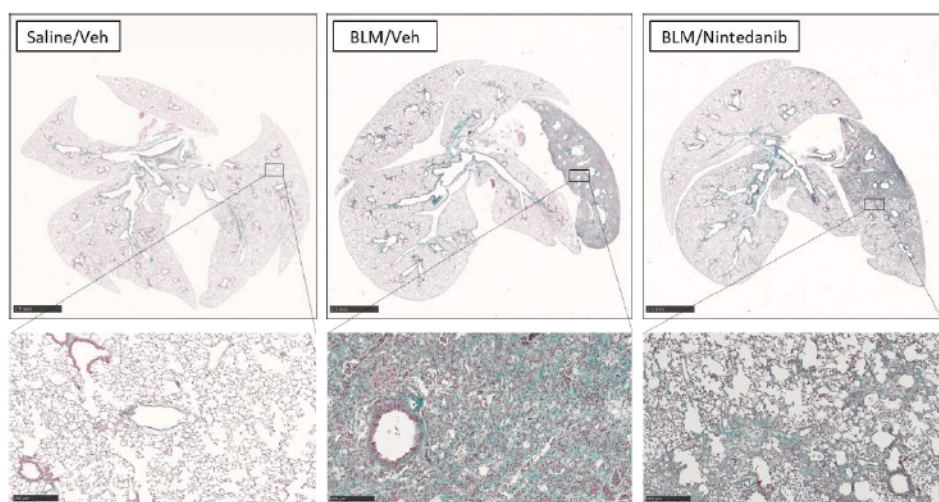

Figure 4.6 Representative whole-slide images of Masson's trichrome stained mouse lung section of each experimental group with enlarged details (scale bar = 250 μm) at 21 days after BLM IT administration; the name of the group is reported in the upper left corner label.

These qualitative observations were confirmed and supported by the two histological analysis performed in this study (**Figure 4.7 A-B**). Indeed, at day 21, the Ashcroft score analysis highlighted a significant increase of the average Ashcroft's score in the BLM mice treated by double IT instillation compared to those treated with Saline (3.7 ± 0.3 vs 0.3 ± 0.1, $p \leq 0.001$). Interestingly, in several BLM samples the most affected lung lobe by fibrosis was mostly the left one. For this reason, a strong heterogeneity in fibrosis values

for the five different lobes was observed, thus, in the same animal there were high scores in one lobe and low values in the other lobes at the same time. The oral treatment with Nintedanib at the dose of 60 mg/kg o.d. significantly reduced the value of Ashcroft score compared with the BLM group (3.2 ± 0.2, 16% of inhibition vs BLM group, $p \leq 0.01$) (**Figure 4.7 A**).

Results from the automated quantification of lung fibrosis performed by Visiopharm® software mirrored the Ashcroft score evaluation, indicating that BLM treatment significantly increased the percentage of lung fibrosis over the entire lung section of about 4-fold compared to the Saline-treated mice (39.6 ± 2.6 % fibrosis on total lung area vs 10.6 ± 0.7 % fibrosis on total lung area, $p \leq 0.001$). In particular, the software analysis showed that, at day 21, Nintedanib (60 mg/kg o.d.) significantly reduced the amount of lung fibrosis produced by BLM IT instillations (29.2 ± 2.2 % fibrosis on total lung area, 36% of inhibition vs BLM group, $p \leq 0.01$) (**Figure 4.7 B**).
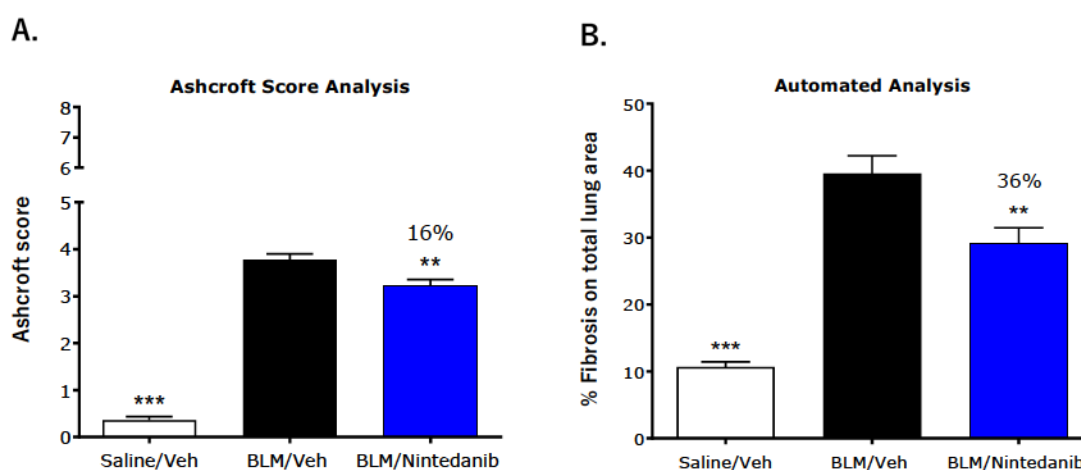

Figure 4.7 Effect of Nintedanib on histological analysis assessed on Masson's Trichrome stained mouse lung sections at 21 days after BLM IT administration. Female mice were daily treated by oral gavage with either Nintedanib (60 mg/kg o.d.) or vehicle (1% of Tween 80 in milliQ water), starting from day 7 after BLM IT administration up to day 21. **A.** Ashcroft score analysis **B.** Percentage of lung fibrosis on the total lung area identified with the automated quantification by Visiopharm® software. Data represent mean ± SEM values for Saline/Veh (n=10; white bar), BLM/Veh (n=15; black bar) and BLM/Nintedanib (n=15; blue bar) groups of animals. Statistical analysis was assessed using one-way ANOVA followed by Dunnett's test in comparison with the BLM group; *** $p \leq 0.001$, ** $p \leq 0.01$. BLM, bleomycin; Veh, vehicle.

4.2.3 Quantification of Hydroxyproline lung content

Figure 4.8 represents the effect of Nintedanib on the lung Hyp content at day 21 after the BLM-induced lung injury. Due to the heterogeneity in the distribution of fibrosis among the lung lobes given by BLM IT instillations, the Hyp content was assessed in the whole lung homogenate of dedicated animals that were not destined to the histological analysis.

At day 21, BLM treatment significantly increased the Hyp content of about 2-fold compared with the Saline group (490.4 ± 18.9 vs 247.9 ± 17.0 µg/mg lung, $p \leq 0.001$). Treatment with Nintedanib (60 mg/kg o.d.) caused a significant reduction of Hyp content compared to the BLM group (398.3 ± 25.9 µg/mg lung, 38% of inhibition vs BLM group, $p \leq 0.01$).
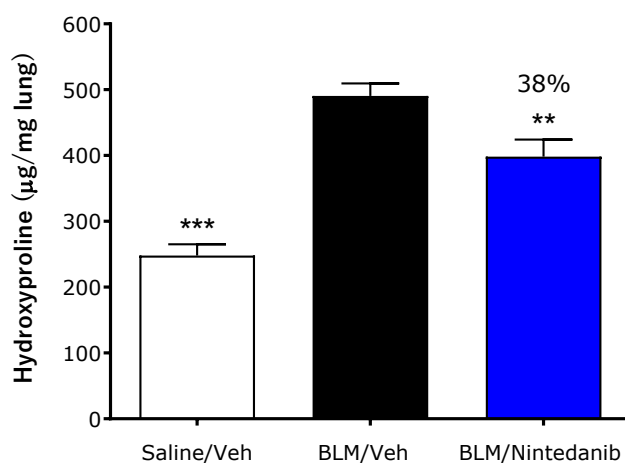
Figure 4.8 Effect of Nintedanib on Hyp content in lung homogenate of mice at day 21 after BLM IT administration. Female mice were daily treated by oral gavage with either Nintedanib (60 mg/kg o.d.) or vehicle (1% of Tween 80 in milliQ water), starting from day 7 after BLM IT administration up to day 21. Bar graph representing the Hyp content (µg/mg lung) quantified in whole lung homogenate of mice at day 21 after BLM IT administration. Data represent mean $\pm$ SEM values for Saline/Veh (n=10; white bar), BLM/Veh (n=15; black bar) and BLM/Nintedanib (n=15; blue bar) groups of animals. Statistical analysis was assessed using one-way ANOVA followed by Dunnett's test in comparison with the BLM group; *** $p \leq 0.001$, ** $p \leq 0.01$. BLM, bleomycin; Veh, vehicle.

4.3 Time course BLM OA study

The characterization of the BLM IT model proved useful in better understanding the development of BLM-induced lung fibrosis and gave us an exact timeline of the morphological events that occurred after the injury. In addition, the information acquired with this model helped to provide the necessary indications to define the therapeutic protocol for the pharmacological validation with Nintedanib. However, even if it represents a reproducible model in the observed evaluations and validated for primary screening, the BLM IT model highlighted a number of limitations. First, IT administration induced a marked heterogeneous and severe distribution of fibrosis in the lung parenchyma of mice, affecting more severely only one lobe than the other lung lobes, which precluded the possibility to use the same lung for different readouts. In addition, based on internal evidence, BLM IT model was not suitable for micro-CT analysis. Indeed, due to lack of aeration in some regions attributable to absence of clear boundaries and jagged or severely damaged parenchyma, the lung regions of most severe fibrosis (Ashcroft grade > 5) were not detectable with 3D imaging technology.

To overcome these issues and since the ATS panel of experts suggested space for model refinement and proposed the OA administration as a valuable alternative to the IT instillation, in this part of the work the BLM mouse model was further investigated by comparing the IT and OA routes of administration. This approach aimed to try to improve the distribution and progression of fibrotic lesions having the possibility to introduce more relevant tools as final readouts such as micro-CT imaging and lung function assessment.

The BLM OA model was explored using the same experimental BLM IT protocol, in two steps consisting of a setup phase followed by the pharmacological validation with Nintedanib tested under therapeutic regimen. More technical details are described in the Materials and Methods section (see paragraph 3.2.1.2).

4.3.1 Body weight trend and survival

The double BLM OA administration induced a significant weight loss in the first days after challenge, reaching a peak around the seventh day, where mice treated with BLM lost on average ≃7% of their starting weight (**Figure 4.9 A**). In the following days, the BLM-treated animals recovered weight with a regular and progressive trend until the end of the experiment, while still maintaining a significant difference compared to Saline-treated mice, which conversely did not show any drop in body weight. During the experiment, no mortality was registered with the OA protocol for both Saline and BLM groups (**Figure 4.9 B**). These results were in line with those obtained with the BLM IT protocol, suggesting that the two BLM OA administrations at the dose of 0.0375 IU/mouse were also well tolerated by the animals.
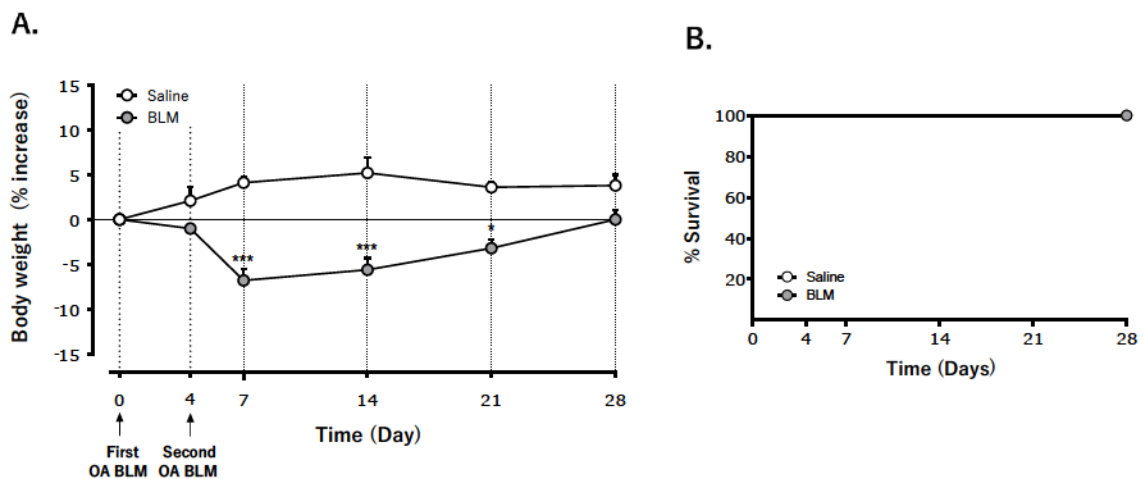
Figure 4.9 Effect of BLM OA administration on body weight loss and mortality of mice. **A**. Body weight trend. Each point represents the mean ± SEM values for both Saline (n=12; white circles) and BLM (n=40; grey circles) groups of animals, expressed as percentage of body weight change calculated from day 0 onwards. Statistical analysis was assessed using two-way ANOVA followed by Sidak's test in comparison with the relative control values (Saline group); *** p ≤ 0.001, * p ≤ 0.05. **B**. Survival. Kaplan–Meier graph showing survival rate of mice from day 0 until day 28.

4.3.2 Pulse oximetry

Pulse oximetry is a simple, non-invasive test that uses infrared sensing of hemoglobin emission and movement to determine many vital signs including SpO2, and it is widely used in the management of IPF patients to monitor and maintain SpO2 at a level above 90% to prevent the development of secondary disorder such as pulmonary hypertension.

To assess the effects of BLM on gaseous exchange in the lung, mice were monitored in real-time for the percentage of SpO2 using the MouseOx® Pulse-oximeter (see paragraph 3.3.1).

The double OA instillation of BLM led to a reduction in pulse oximetry readings of mice as compared with Saline-control animals (**Figure 4.10**). Specifically, results revealed a significant decrease in SpO2 below 90%, reflecting hypoxemia, at day 7 (88.8 ± 0.9 % vs 98.7 ± 0.1 %, $p \leq 0.001$) and day 14 (89.3 ± 1.8 % vs 98.8 ± 0.2 %, $p \leq 0.001$) after BLM first dose. From day 21, a slight progressive trend towards increasing of SpO2 levels in BLM mice was observed, which however, were still significantly lower compared to saline group (91.8 ± 1.9 % vs 98.7 ± 0.2 %, $p \leq 0.05$). At day 28, no significant changes were observed in the BLM-treated mice compared to the respective control animals (92.7 ± 2.5 % vs 98.5 ± 0.2 %, NS), although SpO2 levels were still below 95%. As expected, baseline (T0) SpO2 measurements from all the untreated experimental animals were $\simeq 99\%$, reflecting condition of normal oxygen saturation levels.
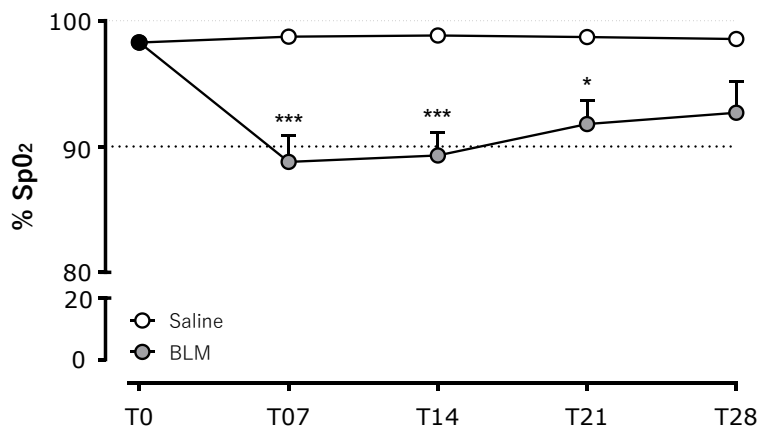
Figure 4.10 Effect of BLM OA administration on pulse oximetry. Female mice were assessed for Sp02 levels at baseline (untreated animals, black circle; T0) and at different time points (T07, T14, T21, and T28) from the first BLM OA administration. Each point represents the mean ± SEM values for both Saline (n=12; white circles) and BLM (n=40; grey circles) groups of animals. Statistical analysis was assessed using two-way ANOVA followed by Sidak's test in comparison with the relative control values (Saline group); *** $p \leq 0.001$, * $p \leq 0.05$.

4.3.3 Micro-CT imaging

In-vivo lung micro-CT is being increasingly embraced in pulmonary research because it provides a valuable tool to acquire longitudinal information on lung fibrosis onset, progression and subsequent therapy evaluation in preclinical models of pulmonary fibrosis. Micro-CT delivers visual and quantitative 3D information about the whole lung, including regional differences, with high resolution and sensitivity, yielding translational data that align well with imaging assessments routinely performed in IPF patients.

In this time course study, micro-CT imaging was performed at days 7, 14, 21 and 28 from the first BLM or Saline OA administration to assess the parenchymal changes of mice over time. As mentioned in the Material and Methods section (see paragraph 3.3.2), for quantitative 3D assessment of the parenchymal lesions induced by BLM, preclinical HU density ranges were applied to semi-automatically segmented lung parenchyma distinguishing in normal-aerated ([−860, −435] HU) and poorly-aerated ([−435, −121] HU) regions (*Mecozzi et al. 2020*). These compartments of tissue, colored in blue and pink respectively, were defined and normalized on total lung volume of mice (**Figure 4.11 A-B**). Representative micro-CT images at the different time points clearly demonstrate that BLM OA treated mice showed a homogeneous increase of the poorly-aerated tissue compared to Saline-treated group (**Figure 4.11 A**).

Specifically, as shown in the graph of **Figure 4.11 B**, the quantification of lung aeration degrees confirmed the progressive increase in percentage of poorly-aerated regions for BLM mice as early as day 7 (27.3%) after the first BLM OA instillation, with a peak at 14 and 21 days (51.9% and 47%, respectively), that tended to decrease at day 28 (33.6%). As expected, the Saline-control animals exhibited mainly normo-aerated tissue, reflecting physiological conditions, with minimal poorly-aerated regions (the average value of poorly-aerated tissue was 18.6% for all points of observation).

A.

B.
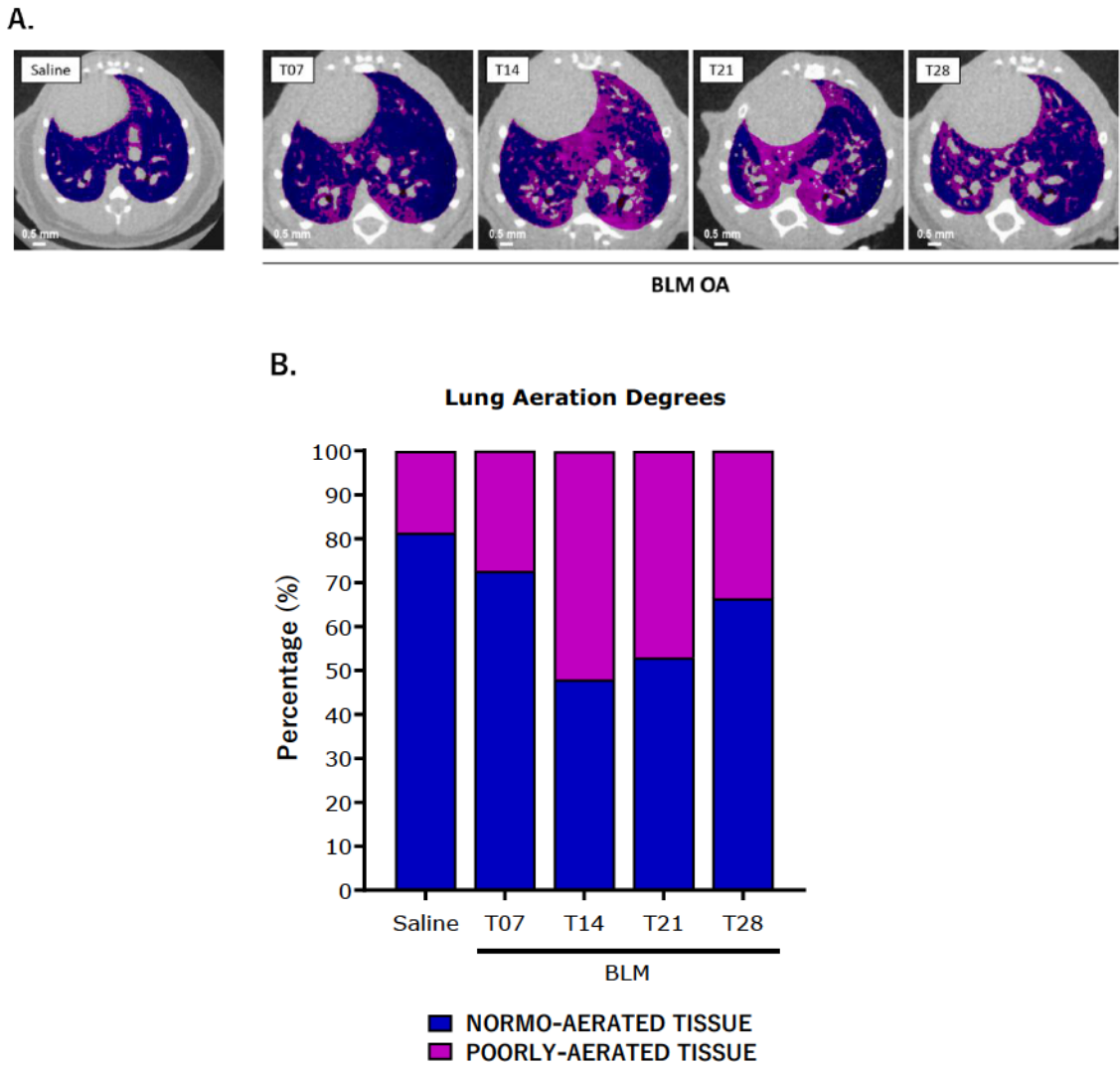
Figure 4.11 Micro-CT imaging evaluation of the parenchymal lesions induced by BLM OA administration over time. **A.** Representative transverse micro-CT lung images of female mouse acquired from control animals (Saline) and BLM-treated mice at different time points (T07, T14, T21 and T28). Normo-aerated ([−860, −435] HU) and poorly-aerated ([−435, −121] HU) regions are reported in blue and pink, respectively; scale bar = 0.5 mm. **B.** Quantification of normo- and poorly-aerated tissue on total lung volumes of mice. Data are expressed as mean value (n=3 Saline; n=10 BLM); Saline bar is reported as mean value of all the control animals.

4.3.4 Lung function tests

Lung function tests routinely implemented in the clinical setting are the first step in the diagnosis of IPF. A decline in FVC in patients with IPF is considered evidence of disease progression and predictable of mortality. Moreover, in clinical studies, the lung function is considered the primary endpoint to assess the success of therapeutics directed towards IPF. Characterizing lung function in preclinical models of pulmonary fibrosis could be essential to follow variations over time and improve clinical predictability of new therapeutic candidates.

In this study, lung function tests were performed on days 7, 14, 21 and 28 of the BLM-treatment regimen using FlexiVent System (see paragraph 3.3.3), in order to assess the time course of lung functional alterations in the development of BLM-induced lung fibrosis.

A complete overview of all lung function parameters measured is reported in **Table 4.1.** Consistently with an increased stiffness of the lungs, mice treated with double BLM OA showed a significant decrease in IC compared to Saline-control animals on day 14 and 21 ($p \leq 0.001$ and $p \leq 0.01$, respectively), while no changes in IC were detected on days 7 and 28 after the first BLM OA administration. Furthermore, in BLM-treated mice, IC on days 14 and 21 was significantly lower compared with days 7 ($p \leq 0.01$) and 28 ($p \leq 0.05$) (**Figure 4.12 A**). Conversely, when compared with Saline-treated animals, the double BLM OA caused a significant increase in both Rrs and Ers measures. In particular, Rrs was significantly higher in BLM-treated mice on days 14, 21 and 28 compared with Saline-treated animals ($p \leq 0.01$). Moreover, Rrs was significantly greater in BLM-treated mice on day 14 compared with days 7 and 28 ($p \leq 0.01$ and $p \leq 0.05$, respectively) (**Figure 4.12 B**). Ers was significantly increase as early as day 7 ($p \leq 0.05$) after the first BLM administration, and especially on days 14 and 21 in BLM mice compared with Saline-treated animals ($p \leq 0.001$ and $p \leq 0.01$, respectively). At day 28, no significant difference was obtained between the two experimental groups, mainly due to the higher variability observed in BLM animals at this late time point. Moreover, Ers was significantly greater in BLM mice on days 14 and 21 compared with days 7 ($p \leq 0.01$) and 28 ($p \leq 0.05$) (**Figure 4.12 C**).

Data from Cst measures revealed a significant reduction as early as day 7 after BLM treatment ($p \leq 0.05$), that remained significantly attenuated on days 14 and 21 ($p \leq 0.001$) and until day 28 ($p \leq 0.05$). Among BLM-treated mice, Cst on days 14 and 21 was significantly lower compared with days 7 ($p \leq 0.001$) and 28 ($p \leq 0.01$) (**Figure 4.12 D**).

Finally, consistently with a typical restrictive airway pattern seen in human IPF patients, BLM-treated mice showed a significant reduction in both $FEV_{0.1}$ and FVC measures.

Specifically, significant changes on $FEV_{0.1}$ and FVC were observed on days 14 ($p \leq 0.001$), 21 ($p \leq 0.001$) and 28 ($p \leq 0.05$ and $p \leq 0.01$, respectively) after the first BLM OA administration, while no difference was measured on day 7 (**Figure 4.12 E-F**, respectively). As expected, no significant changes in all these functional parameters were detected among Saline-exposed mice.

Table 4.1 Overview of all lung function parameters measured by FlexiVent System in female mice at different time point (T07, T14, T21 and T28) from the first BLM OA administration.

Time point	Group	*Deep inflation* IC (mL)	*Snapshot-150* Rrs (cmH2O.s/mL)	Ers (cmH2O.s/mL)	*PVs-P* Cst (mL/cmH2O)	*NPFE* FEV$_{0.1}$ (mL)	FVC (mL)
T07	Saline	0.79 ± 0.01	0.54 ± 0.02	28.2 ± 0.08	0.06 ± 0.002	0.96 ± 0.02	1.06 ± 0.02
	BLM	0.75 ± 0.02	0.61 ± 0.03	$\mathbf{33.5 \pm 1.8^{*}}$	$\mathbf{0.05 \pm 0.003^{*}}$	0.84 ± 0.04	0.98 ± 0.03
T14	Saline	0.76 ± 0.02	0.57 ± 0.01	31.3 ± 1.4	0.06 ± 0.004	0.95 ± 0.02	1.08 ± 0.02
	BLM	$\mathbf{0.59 \pm 0.02^{***}}$	$\mathbf{0.87 \pm 0.05^{**}}$	$\mathbf{47.4 \pm 1.9^{***}}$	$\mathbf{0.03 \pm 0.003^{***}}$	$\mathbf{0.70 \pm 0.03^{***}}$	$\mathbf{0.88 \pm 0.03^{***}}$
T21	Saline	0.76 ± 0.01	0.53 ± 0.02	30.1 ± 1.4	0.06 ± 0.002	0.97 ± 0.02	1.10 ± 0.02
	BLM	$\mathbf{0.57 \pm 0.04^{**}}$	$\mathbf{0.78 \pm 0.06^{**}}$	$\mathbf{46.4 \pm 4.0^{**}}$	$\mathbf{0.03 \pm 0.004^{***}}$	$\mathbf{0.72 \pm 0.04^{***}}$	$\mathbf{0.87 \pm 0.04^{***}}$
T28	Saline	0.79 ± 0.01	0.54 ± 0.02	27.8 ± 1.5	0.06 ± 0.002	0.96 ± 0.02	1.08 ± 0.03
	BLM	0.70 ± 0.03	$\mathbf{0.67 \pm 0.03^{**}}$	35.3 ± 3.7	$\mathbf{0.05 \pm 0.003^{*}}$	$\mathbf{0.80 \pm 0.04^{*}}$	$\mathbf{0.92 \pm 0.04^{**}}$

Data are expressed as mean ± SEM (n=3 Saline; n=10 BLM). Statistical analysis was assessed using unpaired Student's t-test in comparison with the relative control values (Saline group); *** $p \leq 0.001$, ** $p \leq 0.01$, * $p \leq 0.05$. PVs-P, stepwise pressure-driven PV loop; NPFE, negative pressure-driven forced expiration; IC, inspiratory capacity; Rrs, resistance of the respiratory system; Ers, elastance of the respiratory system; Cst, quasi-static compliance; $FEV_{0.1}$, forced expiratory volume in 0.1 s; FVC, forced vital capacity.
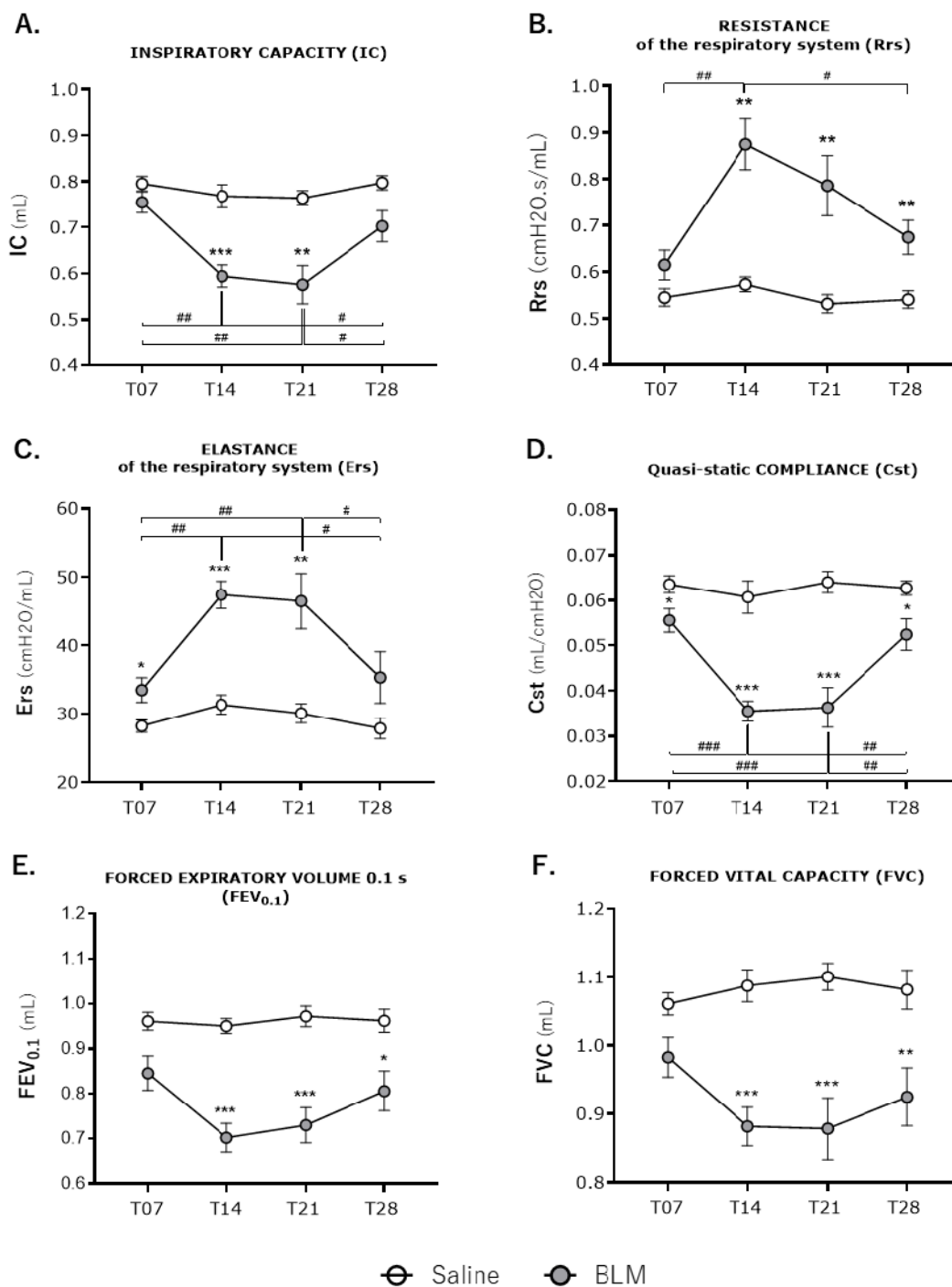
Figure 4.12 Lung function parameters measured by Flexivent System in female mice at different time points (T07, T14, T21, and T28) from the first BLM OA administration. **A.** Inspiratory capacity (IC); **B.** Resistance of the respiratory system (Rrs); **C.** Elastance of the respiratory system (Ers); **D.** Quasi-static compliance (Cst); **D.** Forced expiratory volume in 0.1 s ($FEV_{0.1}$); **E.** Forced vital capacity (FVC). Data are expressed as mean ± SEM (n=3 Saline (white circles); n=10 BLM (grey circles)). Statistical analysis was assessed using unpaired Student's t-test in comparison with the relative control values (Saline group); *** $p \leq 0.001$, ** $p \leq 0.01$, * $p \leq 0.05$. ### $p \leq 0.001$, ## $p \leq 0.01$, # $p \leq 0.05$ refers to one-way ANOVA (Dunnett's t test) comparisons among BLM-treated groups.

4.3.5 Histological analysis

In addition to the two histological analyses already evaluated with the BLM IT protocol on Masson's trichrome stained slides representative of all the five lobes (Ashcroft score analysis and automated quantification of lung fibrosis), in the BLM OA model another histological evaluation was performed by AI-based Visiopharm® APPs to further recognize and classify different degrees of fibrosis severity within the lung parenchyma in a way independent from the operator compared to the Ashcroft scoring system.

Moreover, a general qualitative evaluation was also carried out to assess the morphological changes induced by BLM OA over time, and the distribution of fibrosis in the lung parenchyma. The **Figure 4.13** shows one representative image of BLM-treated lung tissue section for each analyzed time point, flanked by an image from one of the Saline groups (control animal). The lung sections obtained from Saline-treated mice revealed a normal conformation of the different pulmonary structures, while trichrome staining highlighted in green the presence of collagen normally developed around the main bronchi and blood vessels (physiological condition). Conversely, the staining from BLM-treated group revealed that double BLM OA administration induced several changes in lung parenchyma as early as day 7. At this time point, the main changes were: focal or diffuse infiltration of inflammatory cells such as lymphocytes and macrophages/histiocytes in the alveoli, and increased peri-bronchial and perivascular inflammatory reaction; reactive hyperplasia of the alveolar epithelium cells, sometimes accompanied by atypia, associated with inflammation; scarce presence of reactive fibroblasts observed mainly in the peri-bronchiolar or subpleural areas. Provisional matrix, when present, was always accompanied by an inflammatory reaction with an increase in lymphocytes around the bronchi and vessels; the accumulation of macrophages in the alveoli was also frequent. At day 14, an increase in fibrosis was observed compared to the BLM lung sections obtained at day 7. Fibrosis was more widespread throughout the lung parenchyma and not only around the bronchi and vessels or in the subpleural area. The inflammation was widespread with an increase in lymphocytes also in the alveolar spaces, and the presence of reactive multi-nucleated macrophages was observed. In some cases, bronchiolization of the alveolar epithelium was observed. At day 21, maintenance of moderate to severe fibrosis, associated with inflammation, was observed. Notably, areas of lung parenchyma were replaced with dense collagen deposition and fibrotic masses in which alveoli were not clearly identifiable. Finally, 28 days after the first administration of BLM OA a reduction in fibrosis and inflammatory response was observed in most lung sections; in these samples, the fibrosis was poor and the

inflammation was mild, that remained mainly around the bronchi and in some sporadic areas of lung parenchyma.

Compared to the BLM IT protocol, where alveolar space alterations varied from partly enlarged air spaces to partial and complete obliteration due to fibrotic proliferation, the fibrotic lesions in OA-treated mice occurred as diffuse single fibro-proliferative loci. Fibrosis in mice treated with double BLM OA instillation appeared more homogeneous, less variable among animals and uniformly distributed throughout the lung lobes at all the time points of observation.
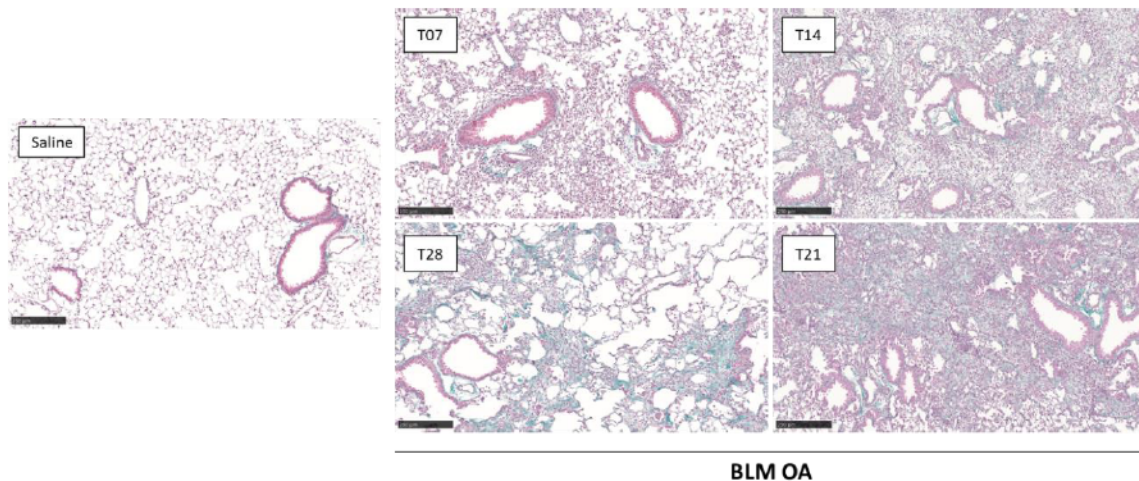
BLM OA

Figure 4.13 Histological appearance of the lung fibrosis induced by BLM OA over time. Representative Masson's trichrome-stained mouse lung tissue sections, obtained from control animals (Saline) and BLM-treated mice at different time points (T07, T14, T21 and T28); scale bar = 250 μm.

All these qualitative observations were confirmed and supported by the three histological analysis for the evaluation of lung fibrosis (**Figure 4.14 A-B-C**).

The Ashcroft score evaluation did not reveal any significant differences between IT and OA protocols. The analysis indicated that two OA instillations of BLM were able to induce the the formation of myofibroblast-rich provisional matrices as early as day 7 after the first BLM OA administration (**Figure 4.14 A**). At this time point, the score in the BLM group was 2.2 ± 0.2 compared to 0.2 ± 0.1 of the Saline group ($p \leq 0.001$). The Ashcroft score in BLM-treated group increased over time, reaching the maximum value at day 14 (3.8 ± 0.2 vs 0.2 ± 0.1; $p \leq 0.001$), which corresponded to a moderate degree of fibrosis, and remained comparable until day 21 (3.6 ± 0.2 vs 0.1 ± 0.1; $p \leq 0.001$). At these latter time points, the Ashcroft score value of BLM mice was significantly different compared to that observed on days 7 ($p \leq 0.001$). Moreover, at day 28, the Ashcroft score of the BLM group significantly

decreased compared to that observed on days 14 and 21 (p ≤ 0.01 and p ≤ 0.05, respectively), although still maintaining a significant difference compared to the Saline group (2.8 ± 0.3 vs 0.1 ± 0.1; p ≤ 0.05). The Saline-treated group, as expected, showed normal lung architecture (Score <1) at all points of observation with no prominent changes in the lung parenchyma.

These results were confirmed by the automated analysis performed using the Visiopharm® software for the quantification of lung fibrosis (**Figure 4.14 B**). The area of fibrotic tissue calculated at day 7 after the first BLM OA administration was about 25% of the total lung area. This area increased at day 14, reaching 34% fibrotic tissue, and remained stable until day 21 (31%). In line to the Ashcroft score evaluation, the fibrotic area gradually decreased at day 28 (21%). As expected, the control groups treated with Saline exhibited a normal lung with an average value of fibrotic tissue of 10.2% for all points of observation.

Finally, as showed in **Figure 4.14 C**, the AI analysis for the classification of lung fibrosis severity distribution demonstrated that days 14 and 21 after the first OA administration were the time points with the highest degrees of fibrosis severity (Ashcroft scores 5-8), with 12% and 10% of severe tissue, respectively, while the moderate tissue was ≃7% for both time points. The AI evaluation also confirmed a decreased severity at day 28. Indeed, at this time point the severe fibrotic tissue was only 6% of the total lung area (4% of moderate tissue), which was comparable to 7% of the day 7 (6% of moderate tissue). The control group treated with Saline, as expected, showed 99% of physiological tissue for all points of observation, with less than 1% of severe tissue.
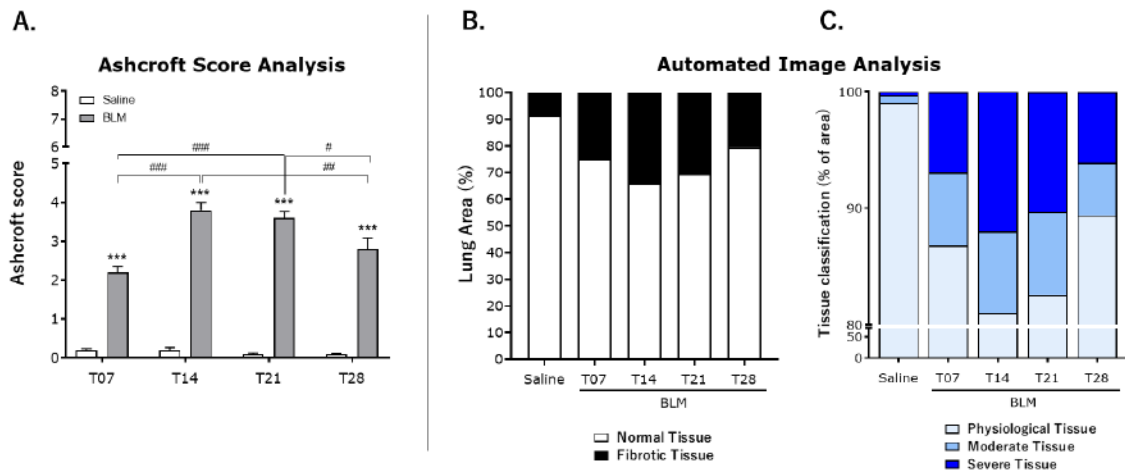
Figure 4.14 Histological analysis of pulmonary fibrosis in Masson's Trichrome stained lung sections performed in female mice at different time points (T07, T14, T21, and T28) from the first BLM OA administration. **A.** Ashcroft score analysis. Data are expressed as mean ± SEM (n=5 Saline (white bars); n=10 BLM (grey bars)). Statistical analysis was assessed using unpaired Student's t-test in comparison with the relative control values (Saline group); *** p ≤ 0.001. ### p ≤0.001, ## p ≤0.01, # p ≤0.05 refers to one-way ANOVA (Dunnett's t test) comparisons among BLM-treated groups. **B.** Automated quantification of lung fibrosis by Visiopharm® software. **C.** Tissue classification of lung fibrosis severity distribution using AI-based Visiopharm® APPs. Data are expressed as mean value; Saline bar is reported as mean value of all the control animals.

4.3.6 Quantification of Hydroxyproline lung content

The homogeneous distribution of fibrotic lesion observed in the OA model should allow to investigate different *ex-vivo* parameters in the same animal using for example the left lung for histology and right lobes for either Hyp content, or other fibrotic markers determinations. However, in this study the analysis of Hyp content was performed in the whole lung homogenate of mice for all the analyzed time points, thus, additional dedicated animals have been destinated for this analysis.

The levels of the total lung Hyp measured in the BLM groups increased among the different time points compared to the Saline-treated groups (**Figure 4.15**). In particular, while at day 7 no significant increase was evident (278.1 ± 24.1 vs 223.6 ± 19.2 µg/mg lung, NS), a significant difference between the two different groups of treatment was observed from day 14 (341.6 ± 20.1 vs 215.9 ± 8.9 µg/mg lung, $p \leq 0.001$), and especially at day 21 where Hyp content was about double in the BLM group compared to Saline group (417.1 ± 35.4 vs 217.2 ± 24.8 µg/mg lung, $p \leq 0.001$). Moreover, levels of Hyp content among the BLM-treatment groups were significantly increased at day 21 compared to day 7 ($p \leq 0.01$). At day 28, an initial trend towards decreasing Hyp levels appeared in the BLM group, although still showed a significant difference compared to the saline group (362.0 ± 22.4 vs 217.6 ± 18.5 µg/mg lung, $p \leq 0.01$). Overall, the same levels of Hyp was observed for both the IT and OA protocols over time.
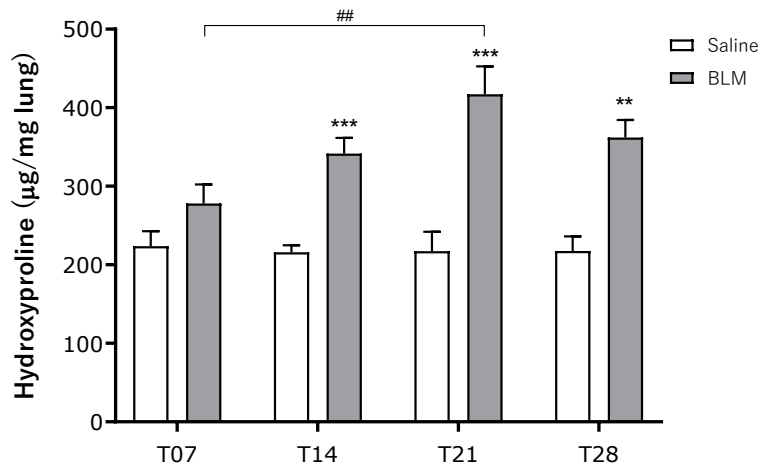
Figure 4.15 Quantification of Hyp content in lung homogenate performed in female mice at different time points (T07, T14, T21, and T28) from the first BLM OA administration. Data are expressed as mean ± SEM (n=3 Saline (white bars); n=10 BLM (grey bars)). Statistical analysis was assessed using unpaired Student's t-test in comparison with the relative control values (Saline group); *** $p \leq 0.001$, ** $p \leq 0.01$. ## $p \leq 0.01$ refers to one-way ANOVA (Dunnett's t test) comparisons among BLM-treated groups.

4.3.7 Biomarkers analysis

Recent advances in the field of clinical biomarkers suggested that quantification of proteins could play an important role in the diagnosis, classification, prognosis, and treatment response of lung diseases such as IPF. As mentioned in paragraph 1.8.1, over the last two decades, a plethora of systemic biomarkers was tested regarding their use in IPF. Among them, the most promising are a range of molecules involved in epithelial damage and repair, inflammation, myofibroblast accumulation and ECM deposition. Therefore, the evaluation of clinically relevant biomarkers associated with diagnosis and progression of IPF could improve the predictability and translatability of preclinical models when considering assessment of novel mechanisms and compounds. In this perspective, we examined over time the potential role of selected relevant biomarkers in IPF such as SP-D, MMP-7 and COL1 from different biological compartments, i.e. plasma and BALF, using commercial ELISA assays according to the manufacturers' protocol (see paragraph 3.5.2). Results showed that all these candidate proteins were significantly regulated during the onset and progression of fibrosis in mice treated with double BLM OA when compared with Saline-control animals (**Figure 4.16 A-B-C**).

Specifically, SP-D concentration in plasma was significantly increase as early as day 7 after the first BLM OA administration (327 528.0 ± 30 381.5 pg/mL vs 8 663.0 ± 1 854.7 pg/mL, $p \leq 0.001$), and on days 14 and 21 in BLM mice compared with Saline groups (312 390.0 ± 50 352.4 pg/mL vs 8 969.7 ± 2 194.4 pg/mL; 297 485.0 ± 56 346.3 pg/mL vs 8 198.3 ± 907.8 pg/mL, respectively; $p \leq 0.001$). At day 28, significant differences between the two experimental groups was still evident (92 259.5 ± 31 951.6 pg/mL vs 7 960.1 ± 1 271.1 pg/mL, NS). However, SP-D was significantly greater in BLM mice on days 7, 14 and 21 compared with day 28 ($p \leq 0.001$, $p \leq 0.001$ and $p \leq 0.01$, respectively) (**Figure 4.16 A**).

Data from MMP-7 levels measured in BALF revealed a significant increase at day 7 after BLM treatment (2 057.6 ± 150.0 pg/mL vs 286.2 ± 38.6 pg/mL, $p \leq 0.001$), that remained significantly elevated on day 14 (1 436.1 ± 124.6 pg/mL vs 311.6 ± 46.6 pg/mL, $p \leq 0.001$). At day 21, a decrease in MMP-7 levels in BLM mice was observed, although they were still significantly higher compared with Saline group (678.0 ± 88.9 pg/mL vs 283.2 ± 45.2 pg/mL, $p \leq 0.05$). At day 28, no significant difference was obtained between the two experimental groups (435.9 ± 67.5 pg/mL vs 261.7 ± 35.9 pg/mL, NS). Among BLM-treated mice, MMP-7 on day 7 was significantly higher compared with days 14 ($p \leq 0.01$), 21 ($p \leq 0.001$) and 28 ($p \leq 0.001$), while at day 14 was significantly higher compared with days 21 ($p \leq 0.001$) and 28 ($p \leq 0.001$) (**Figure 4.16 B**).

Finally, BLM-treated mice showed significant differences for COL1 levels in all the time points analyzed compared with Saline groups. Specifically, levels of COL1 measured in BALF was significant increased at days 7 (42 626.6 ± 3 694.7 pg/mL vs 441.1 ± 84.8 pg/mL, p ≤ 0.001), 14 (42 995.3 ± 7 623.7 pg/mL vs 459.7 ± 79.8 pg/mL, p ≤ 0.001) and 21 (32 675.5 ± 4 257.9 pg/mL vs 472.2 ± 97.2 pg/mL, p ≤ 0.001) after the first BLM OA administration. At day 28, a trend towards decreasing in COL1 levels was observed although a significant difference between the two experimental groups was still evident (14 109.1± 5 209.3 pg/mL vs 460.1 ± 88.8 pg/mL, p ≤ 0.05). Moreover, COL1 was significantly greater in BLM mice on days 7 and 14 compared with day 28 (p ≤ 0.01) (**Figure 4.16 C**). As expected, no significant changes in all these selected proteins were detected among Saline-treated mice.
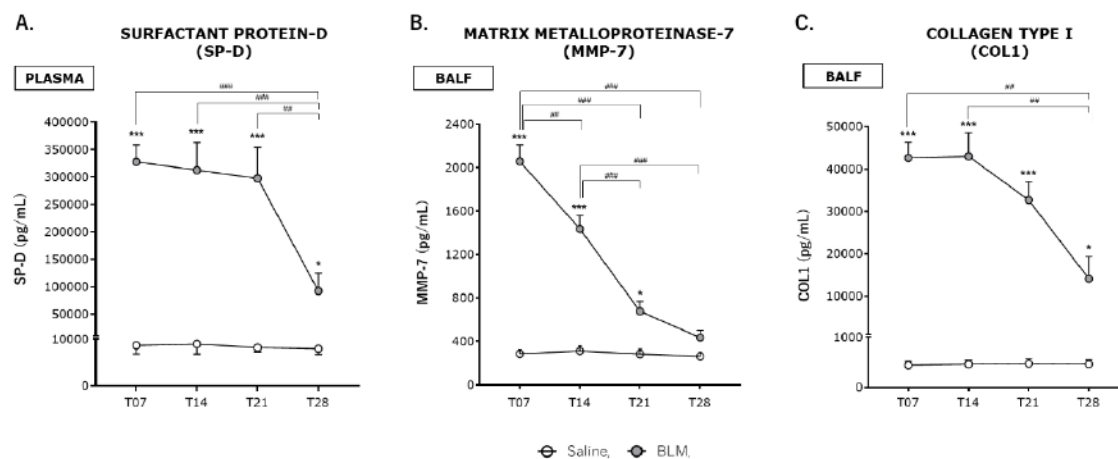
Figure 4.16 Quantification of selected biomarkers measured by ELISA assay in plasma (**A**) and BALF (**B-C**) samples obtained from female mice at different time points (T07, T14, T21, and T28) from the first BLM OA administration. **A.** Plasma levels of surfactant protein-D (SP-D). **B.** BALF levels of matrix metalloproteinase-7 (MMP-7). **C.** BALF levels of collagen type I (COL1). Data are expressed as mean ± SEM (n=3 Saline (white circles); n=10 BLM (grey circles)). Statistical analysis was assessed using unpaired Student's t-test in comparison with the relative control values (Saline group); *** p ≤ 0.001, * p ≤ 0.05. ### p ≤ 0.0.1, ## p ≤ 0.01, # p ≤ 0.05 refers to one-way ANOVA (Dunnett's t test) comparisons among BLM-treated groups. BALF, bronchoalveolar lavage fluid; BLM, bleomycin; Veh, vehicle.

4.4 Therapeutic BLM OA study

The characterization of the BLM OA model with the introduction of novel readouts to assess the progression of lung fibrosis over time, allowed to study the BLM model in a deeper and more comprehensive way, increasing also the translational value of the model since most of the new introduced readouts are routinely used in clinical settings. Based on the results obtained, the OA model turned out to be comparable to the previous BLM IT fibrosis model and suitable for evaluating fibrosis through multiple readouts in the same lung. Moreover, fibrosis in BLM OA treated mice appeared more homogeneous and uniformly distributed throughout the lung lobes.

Considering these advantages, the next step was the pharmacological validation with Nintedanib to test the therapeutic effect of this compound on the OA protocol with the integration of novel more clinically relevant readouts. The experimental protocol of this study was the same used in the previous IT model, which was reported to be suitable for screening anti-fibrotic compounds (*Fragni et al. 2020, abstract presented at the 19th Fraunhofer Seminar 2020*). BLM was administered via OA route at day 0 and day 4 at the dose of 0.0375 IU/mouse for each instillation, and it was defined day 7 after the first BLM OA instillation as the start of treatment and day 21 as the end of the therapeutic window for the assessment of the final readouts. However, as suggested from internal evidence and from the literature (*Wollin et al. 2021*), in this pharmacological study we optimized the dose of Nintedanib from 60 mg/kg o.d. free base to 50 mg/kg b.i.d. esylate.

4.4.1 Body weight trend and survival

The double BLM OA administration induced a significant weight loss in the first days after challenge, reaching a peak between days 7 and 13, where mice treated with BLM lost on average $\simeq 10\%$ of their starting weight. In the following days, the BLM-treated mice recovered weight with a regular and progressive trend, while still maintaining a significant difference until the end of the experiment compared to Saline-treated animals, which conversely did not show any drop in body weight. The oral daily treatment with Nintedanib (50 mg/kg b.i.d.) did not induce any significant effect on body weight of mice compared to BLM group, showing the same recovery trend. (**Figure 4.17 A**). In addition, as shown in the survival graph in **Figure 4.17 B**, both BLM and Nintedanib groups of treatments showed the same mortality rate of 15%. As for the pharmacological BLM IT study, the mortality obtained in this study could be justified by the daily manipulation of the animals due to the treatments, which here was twice daily and which could have an impact in terms of tolerability on top of the BLM effect.
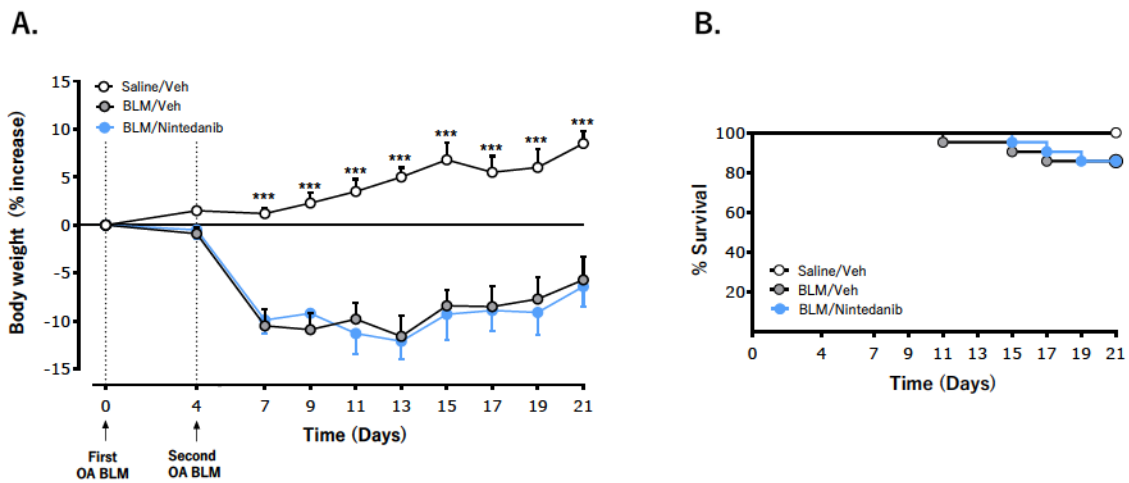
Figure 4.17 Effect of Nintedanib on body weight loss and mortality in BLM treated mice. Female mice were daily treated by oral gavage with either Nintedanib (50 mg/kg b.i.d.) or vehicle (1% of Tween 80 in milliQ water), starting from day 7 after BLM OA administration up to day 21. **A.** Body weight trend. Each point represents the mean ± SEM values for Saline/Veh (n=20; white circles), BLM/Veh (n=30; grey circles) and BLM/Nintedanib (n=30; light blue circles) groups of animals, expressed as percentage of body weight change calculated from day 0 onwards. Statistical analysis was assessed using two-way ANOVA followed by Dunnett's test in comparison with the BLM group; *** $p \leq 0.001$. **B.** Survival. Kaplan–Meier graph showing survival rate for each group of treatment from day 0 until day 21. BLM, bleomycin; Veh, vehicle.

4.4.2 Pulse oximetry

To assess the effect of Nintedanib on functional oxygen saturation, mice were monitored real-time at baseline (T0), and at different time points (T07, T14, and T21) post BLM first dose (**Figure 4.18 A-B**).

BLM treatment led to a progressive reduction in SpO2 levels as compared with Saline-control mice and baseline (T0) measurements from all the untreated experimental animals. Consistent with the results obtained from time course study, a significant decrease in SpO2 was observed in BLM mice compared to Saline-treated animals on days 7 and 14 after BLM first dose (92.3 ± 1.1 % vs 98.6 ± 0.3 %; 92.7 ± 1.8 % vs 98.9 ± 0.1 %, respectively; $p \le 0.001$), which remained significantly lower until day 21 (93.5 ± 1.4 % vs 98.7 ± 0.1 %, $p \le 0.01$) (**Figure 4.18 A**). Pulse oximetry readings of mice treated orally with Nintedanib (50mg/kg b.i.d.) were similar to those of BLM groups on days 7 and 14 (93.8 ± 0.5 %; 93.6 ± 1.8 %, respectively, NS). At day 21, however, measurements of SpO2 levels revealed that Nintedanib treatment was able to significantly improve oxygen saturation in the lungs of mice compared to the BLM group (97.8 ± 0.6 %) (**Figure 4.18 B**).
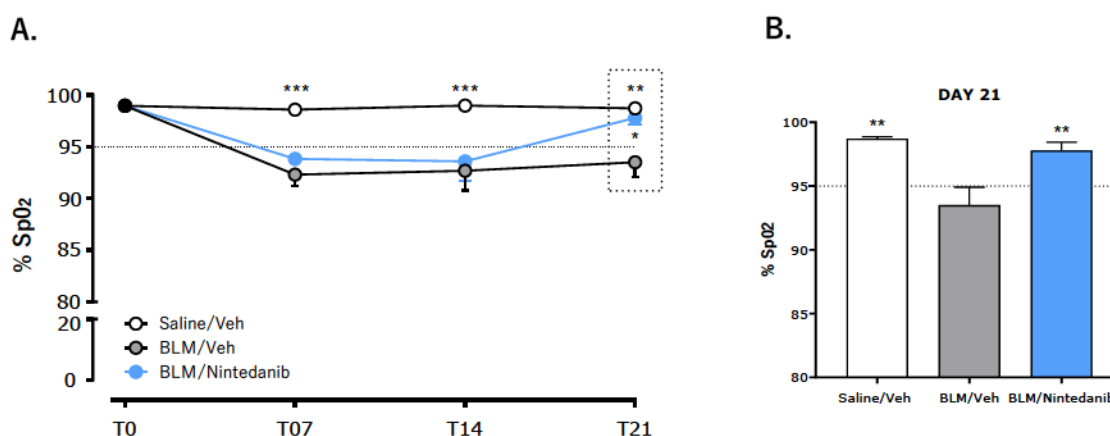

Figure 4.18 Effect of Nintedanib on pulse oximetry. Female mice were daily treated by oral gavage with either Nintedanib (50 mg/kg b.i.d.) or vehicle (1% of Tween 80 in milliQ water), starting from day 7 after BLM OA administration up to day 21. **A.** Percentage of Sp02 levels measured at baseline (untreated animals, black circles; T0) and at different time points (T07, T14, T21) from the first BLM OA administration. **B.** Effect of Nintedanib on SpO2 levels at day 21. Data represent mean ± SEM values for Saline/Veh (n=20; white circles or bar), BLM/Veh (n=30; grey circles or bar) and BLM/Nintedanib (n=30; light blue circles or bar) groups of animals. Statistical analysis was assessed using two-way and one-way ANOVA followed by Dunnett's test in comparison with the BLM group; *** $p \le 0.001$, ** $p \le 0.01$, * $p \le 0.05$. BLM, bleomycin; Veh, vehicle.

4.4.3 Micro-CT imaging

Figure 4.19 shows representative micro-CT lung images of Saline, BLM, and Nintedanib mice at day 21 after the first BLM OA administration, clearly highlighting the differences in tissue aeration degrees between the different groups of treatment, where normo- and poorly-aerated regions were extracted as previously described. Specifically, the images indicate that the regions of normo-aerated tissue, highlighted in blue, are scarce in the BLM group compared to the poorly-aerated ones (pink), which instead are significantly marked compared to Saline group. Treatment with Nintedanib at day 21 clearly reduces these regions.
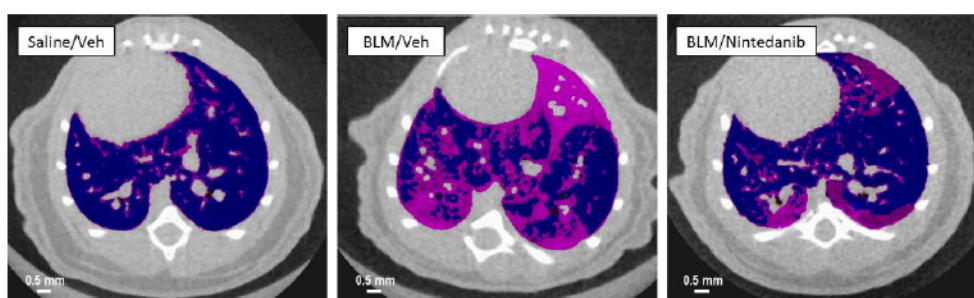
Figure 4.19 Representative transverse micro-CT lung images of female mouse acquired from each experimental group at 21 days after BLM OA administration. Normo-aerated ([−860, −435] HU) and poorly-aerated ([−435, −121] HU) regions are reported in blue and pink, respectively (scale bar = 0.5 mm); the name of the group is reported in the upper left corner label.

In this study, we performed the micro-CT analysis longitudinally at the beginning (day 7) and at the end of the therapeutic window (day 21), in order to assess and quantify the anti-fibrotic effect of Nintedanib on normo- and poorly-aerated compartments of tissue, reported in blue and pink colors, respectively (**Figure 4.20 A-B**).

As showed in **Figure 4.20 A** (blue box), while the percentage of normo-aerated tissue after BLM OA treatment was significantly decreased between day 7 and day 21 in the BLM group (72.4 ± 1.6 % vs 56.1 ± 3.1 %, respectively; $p \leq 0.001$), with Nintedanib remained stable between these days (69.1 ± 1.7 % vs 66.7 ± 2.1 %, respectively; NS), showing a significant increase of the normo-aerated tissue compared to the BLM group at day 21 ($p <0.01$). As a consequence, the percentage of poorly-aerated tissue, corresponding to the fibrotic area, increased significantly in the BLM group between days 7 and 21 (27.6 ± 1.6 % vs 43.9 ± 3.1 %, respectively; $p \leq 0.001$), while Nintedanib was able to stabilize the damaged tissue in this timeframe avoiding its increase (30.9 ± 1.7 % vs 33.2 ± 2.1 %, respectively; NS) (**Figure 4.20 B**, pink box). Indeed, at day 21, treatment with Nintedanib

significantly inhibited the increase in poorly-aerated tissue compared to the BLM group (40% of inhibition vs BLM group, p <0.01). As expected, Saline-control group exhibited a normo-aerated compartment significantly higher compared to BLM group at days 7 and 21 (84.4 ± 0.6 % vs 82.8 ± 0.3 %, respectively; p ≤ 0.001), while the poorly-aerated compartment was significantly lower at these days (15.6 ± 0.6 % vs 17.2 ± 0.3 %, respectively; p ≤ 0.001). No differences were observed among the Saline-treated groups over time.

LONGITUDINAL MICRO-CT
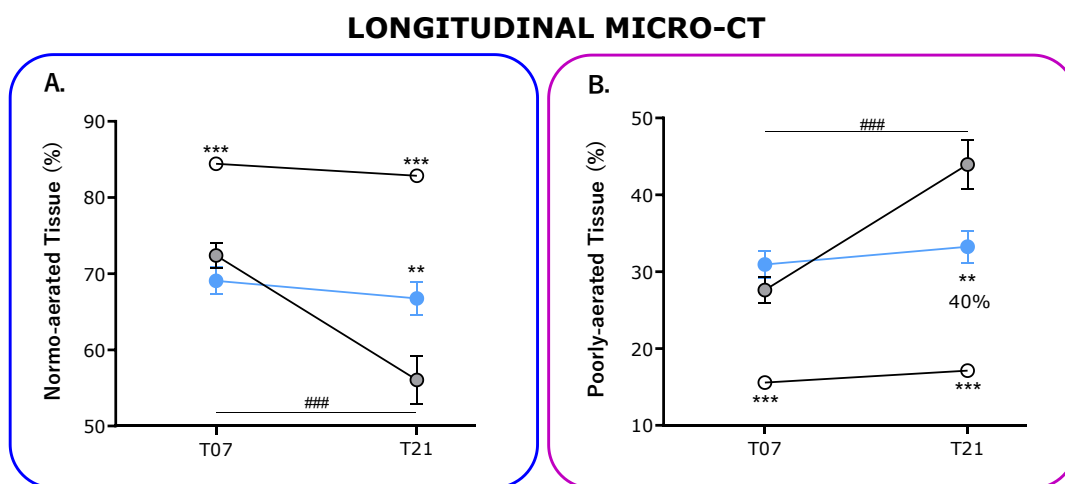
Figure 4.20 Effect of Nintedanib on lung aeration degrees assessed longitudinally by micro-CT. Female mice were daily treated by oral gavage with either Nintedanib (50 mg/kg b.i.d.) or vehicle (1% of Tween 80 in milliQ water), starting from day 7 after BLM IT administration up to day 21. **A.** Percentage of normo-aerated tissue on total lung volumes of mice assessed longitudinally at days 7 (T07) and 21 (T21) after BLM OA administration. **B.** Percentage of poorly-aerated tissue on total lung volumes of mice assessed longitudinally at days 7 (T07) and 21 (T21) after BLM OA administration. Data represent mean ± SEM values for Saline/Veh (n=20; white circles), BLM/Veh (n=30; grey circles) and BLM/Nintedanib (n=30; light blue circles) groups of animals. Statistical analysis was assessed using two-way ANOVA followed by Dunnett's test in comparison with the BLM group; *** p ≤ 0.001, ** p ≤ 0.01. ### p ≤ 0.001 refers to BLM-treated groups. BLM, bleomycin; Veh, vehicle.

4.4.4 Lung function tests

To assess the effect of Nintedanib on BLM-induced pulmonary dysfunction, lung function tests were performed on day 21 after the first BLM OA administration by FlexiVent System. Although in this experiment all parameters previously described were analyzed (**Table 4.2**), it has been decided to show only FVC measures, since it is also the most relevant parameter used in clinical practice (**Figure 4.21**).

Consistently with an expected increase in lung stiffness and a restrictive pattern typical of the fibrotic disease, in BLM mice a decline in FVC of 0.34 ± 0.02 mL compared to the Saline group (mean FVC: 1.14 ± 0.02 mL) was observed. At day 21, treatment with Nintedanib at the dose of 50 mg/kg b.i.d. was able to significantly limit BLM-induced alterations in lung function parameter, significantly improving the FVC of 44% compared with the BLM group of mice (0.19 ± 0.03 mL; difference vs BLM: 0.15 mL; $p \leq 0.001$).

Table 4.2 Overview of all lung function parameters measured by FlexiVent System in female mice at day 21 after BLM OA administration.

Group	Deep inflation	Snapshot-150		PVs-P	NPFE	
	IC (mL)	Rrs (cmH2O.s/mL)	Ers (cmH2O.s/mL)	Cst (mL/cmH2O)	$FEV_{0.1}$ (mL)	FVC (mL)
Saline/Veh	$\mathbf{0.83 \pm 0.02}$***	$\mathbf{0.54 \pm 0.01}$***	$\mathbf{26.6 \pm 0.7}$***	$\mathbf{0.07 \pm 0.002}$***	$\mathbf{1.03 \pm 0.02}$***	$\mathbf{1.14 \pm 0.02}$***
BLM/Veh	0.56 ± 0.02	0.80 ± 0.05	47.1 ± 3.2	0.04 ± 0.002	0.71 ± 0.03	0.80 ± 0.02
BLM/Nintedanib	$\mathbf{0.68 \pm 0.03}$**	$\mathbf{0.63 \pm 0.03}$*	$\mathbf{36.4 \pm 2.1}$**	$\mathbf{0.05 \pm 0.003}$**	$\mathbf{0.84 \pm 0.03}$**	$\mathbf{0.95 \pm 0.03}$***

Data are expressed as mean $\pm$ SEM (n=20 Saline/Veh; n=30 BLM/Veh; n=30 BLM/Nintedanib). Statistical analysis was assessed using one-way ANOVA followed by Dunnett's test in comparison with the BLM group; *** $p \leq 0.001$, ** $p \leq 0.01$, * $p \leq 0.05$. PVs-P, stepwise pressure-driven PV loop; NPFE, negative pressure-driven forced expiration; IC, inspiratory capacity; Rrs, resistance of the respiratory system; Ers, elastance of the respiratory system; Cst, quasi-static compliance; $FEV_{0.1}$, forced expiratory volume in 0.1 s; FVC, forced vital capacity. BLM, bleomycin; Veh, vehicle.

FORCED VITAL CAPACITY (FVC)
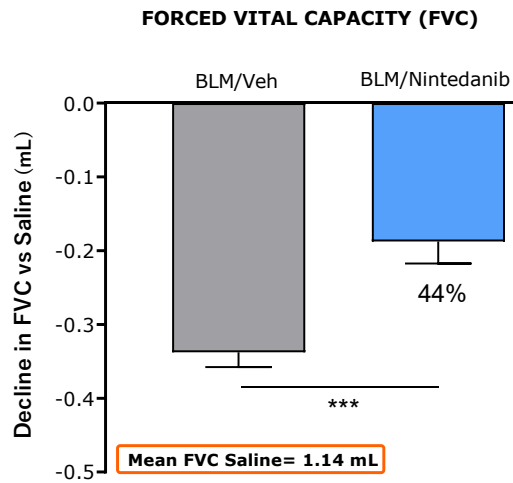
Figure 4.21 Effect of Nintedanib on decline in FVC at day 21 after BLM OA administration. Female mice were daily treated by oral gavage with either Nintedanib (50 mg/kg b.i.d.) or vehicle (1% of Tween 80 in milliQ water), starting from day 7 after BLM OA administration up to day 21. Data represent mean ± SEM values for BLM/Veh (n=30; grey bar) and BLM/Nintedanib (n=30; light blue bar) groups of animals, expressed as difference of mL vs mean of Saline group. Statistical analysis was assessed using unpaired Student's t-test in comparison with the BLM group; *** p ≤ 0.001. BLM, bleomycin; Veh, vehicle.

4.4.5 Histological analysis

As shown in **Figure 4.22**, the Masson's trichrome stained lung slides obtained in this study revealed that at day 21 BLM-induced lung fibrosis mainly consisted by collagen deposition in alveolar walls and in the pulmonary interstice and fibrotic masses associated with dense clusters of inflammatory cells. In BLM-treated mice, areas of normal lung parenchyma were replaced with dense collagen agglomerates where alveoli were not well identifiable. However, in the Nintedanib group the collagen deposition appeared diffuse through the tissue. Moreover, in this group the alveoli were clearly visible even if the septa were more thickened than in the Saline-control group, which exhibited a normal histological conformation and preservation of the various pulmonary elements, as expected. Overall, BLM OA instillations produced a homogeneous distribution of diffuse fibrosis throughout the lung lobes, although within each treatment groups there was an individual, animal-specific variability in response to BLM treatment.
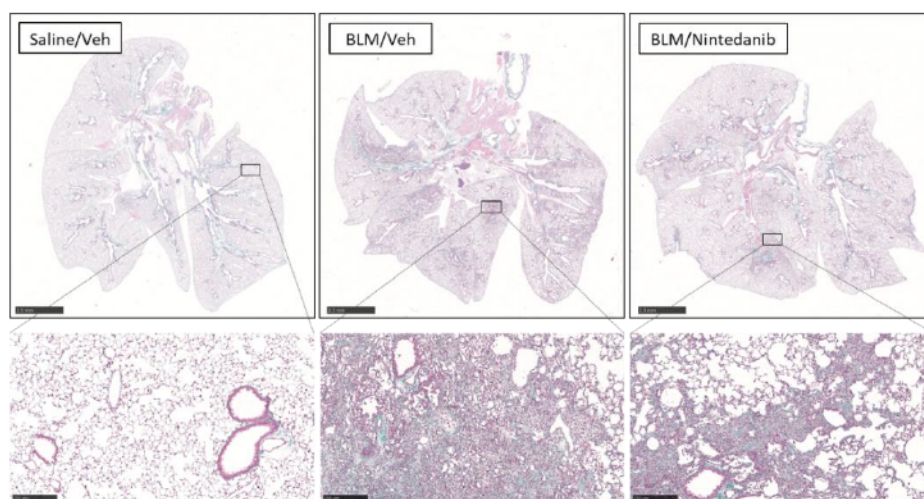
Figure 4.22 Representative whole-slide images of Masson's trichrome stained mouse lung section of each experimental group with enlarged details (scale bar = 250 µm) at 21 days after BLM OA administration; the name of the group is reported in the upper left corner label.

These qualitative observations were confirmed by the histological analysis performed in this study (**Figure 4.23 A-B-C**). At day 21, the Ashcroft score analysis highlighted a significant increase of the average Ashcroft's score in the BLM mice treated by double OA instillation compared to the control mice treated with Saline (3.6 ± 0.1 vs 0.7 ± 0.2, $p \leq 0.001$). The oral treatment with Nintedanib at the dose of 50 mg/kg b.i.d. significantly reduced the value of Ashcroft score compared with the BLM group (3.1 ± 0.1, 18% of inhibition vs BLM group, $p \leq 0.05$) (**Figure 4.23 A**).

The differences between these two groups were even more evident looking at the two analyses performed by Visiopharm® software (right part of **Figure 4.23 B-C**).

Results from the automated quantification of lung fibrosis showed that, at day 21, Nintedanib (50 mg/kg b.i.d.) caused a significant reduction of 33% of lung fibrosis percentage compared to BLM group (31.8 ± 3.6 % vs 42.1 ± 3.1 % fibrosis on total lung area, $p \leq 0.01$), as shown in **Figure 4.23 B**. In line with Ashcroft score analysis, BLM treatment resulted in a significant increase of the percentage of lung fibrosis over the entire lung section area of about 4-fold compared to the Saline-control group (10.9 ± 1.4 % fibrosis on total lung area, $p \leq 0.001$).

The AI-based Visiopharm® APPs analysis further demonstrated the effect of Nintedanib treatment in reducing lung fibrosis severity (**Figure 4.23 C**). Indeed, in the group treated with Nintedanib there was a significant reduction in the percentage of severe fibrotic tissue on behalf of a significant increase of physiological tissue compared to the BLM group (8.4 ± 1.1 % vs 4.1 ± 1.1 %; 93.1 ± 0.7 % vs 86.1 ± 0.9 %, respectively; $p \leq 0.001$). No significant differences on moderate tissue were reported between these two groups (2.9 ± 0.4 % vs 5.4 ± 0.8 %, NS). As expected, the control group treated with Saline showed significant differences compared to BLM group in all the three different tissue classification: physiological, moderate, and severe (98.9 ± 0.4 %; 0.7 ± 0.1 %; 0.4 ± 0.2 %, respectively; $p \leq 0.001$).
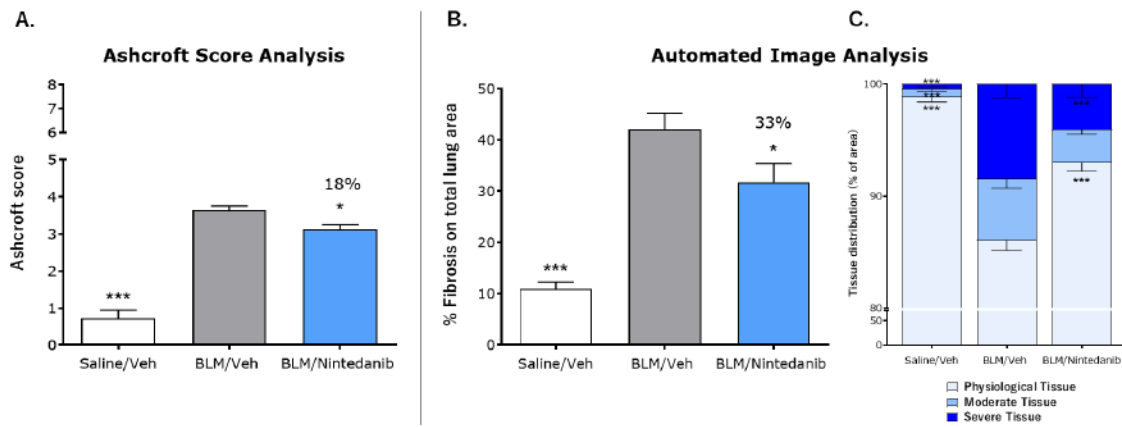
Figure 4.23 Effect of Nintedanib on histological analysis assessed on Masson's Trichrome stained mouse lung sections at 21 days after BLM OA administration. Female mice were daily treated by oral gavage with either Nintedanib (50 mg/kg b.i.d.) or vehicle (1% of Tween 80 in milliQ water), starting from day 7 after BLM OA administration up to day 21. **A.** Ashcroft score analysis. **B.** Percentage of lung fibrosis on the total lung area identified with the automated quantification by Visiopharm® software. **C.** Tissue classification of lung fibrosis severity distribution using AI-based Visiopharm® APPs. Data represent mean ± SEM values for Saline/Veh (n=10; white bar), BLM/Veh (n=15; black bar) and BLM/Nintedanib (n=15; light blue bar) groups of animals. Statistical analysis was assessed using one-way ANOVA followed by Dunnett's test in comparison with the BLM group; *** $p \leq 0.001$, * $p \leq 0.05$. BLM, bleomycin; Veh, vehicle.

4.4.6 Quantification of Hydroxyproline lung content

Figure 4.24 shows the effect of Nintedanib on the lung Hyp content at day 21 after BLM OA administration, which was assessed in the whole lung homogenate of mice not destined to the histological analysis.

At day 21, BLM treatment significantly increased the Hyp content by more than 2-fold compared with the Saline group (411.1 ± 25.6 µg/mg lung vs 169.3 ± 7.1 µg/mg lung, $p \leq 0.001$). Treatment with Nintedanib (50 mg/kg b.i.d.) caused a significant reduction of Hyp content compared to the BLM group (308.8 ± 13.1 µg/mg lung, 42% of inhibition vs BLM group, $p \leq 0.01$).
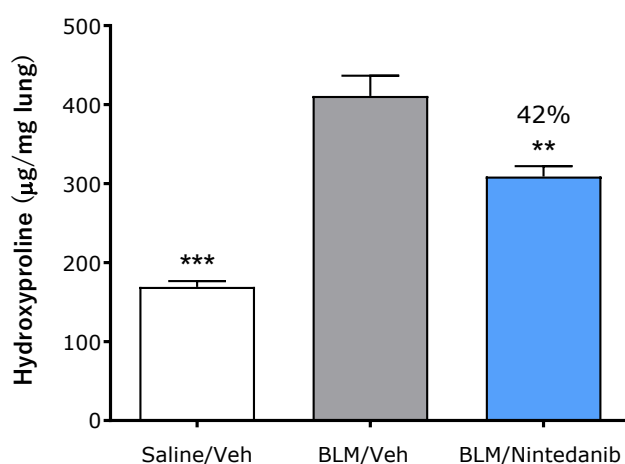
Figure 4.24 Effect of Nintedanib on Hyp content in lung homogenate of mice at day 21 after BLM OA administration. Female mice were daily treated by oral gavage with either Nintedanib (50 mg/kg b.i.d.) or vehicle (1% of Tween 80 in milliQ water), starting from day 7 after BLM OA administration up to day 21. Bar graph representing the Hyp content (µg/mg lung) quantified in whole lung homogenate of mice at day 21 after BLM OA administration. Data represent mean ± SEM values for Saline/Veh (n=10; white bar), BLM/Veh (n=15; grey bar) and BLM/Nintedanib (n=15; light blue bar) groups of animals. Statistical analysis was assessed using one-way ANOVA followed by Dunnett's test in comparison with the BLM group; *** $p \leq 0.001$, ** $p \leq 0.01$. Hyp, hydroxyproline; BLM, bleomycin; Veh, vehicle.

4.4.7 Biomarkers analysis

To assess the effect of Nintedanib on fibrotic biomarkers of lung fibrosis, plasma levels of SP-D, and BALF levels of MMP-7 and COL1 were quantified on day 21 after the first BLM OA administration by using ELISA assays (**Figure 4.25 A-B-C**, respectively).

Results indicated that the levels of these relevant biomarkers of pulmonary fibrosis were all significantly elevated in the BLM-treated compared to Saline-control animals. Specifically, mice treated with BLM showed a 49-fold increase in plasma SP-D content (270 760.8 ± 67 914.5 pg/mL vs 5 484.0 ± 196.4 pg/mL, $p \leq 0.01$), a 2.4-fold increase in BALF content of MMP-7 (585.1 ± 94.2 pg/mL vs 245.9 ± 20.7 pg/mL $p \leq 0.01$), and a 73-fold increase in BALF content of COL1 (32 062.4 ± 7 788.1 pg/mL vs 440.7 ± 81.4 pg/mL $p \leq 0.01$).

At day 21, the oral treatment with Nintedanib at the dose of 50 mg/kg b.i.d. significantly reduced the levels of all these biomarkers of pulmonary fibrosis (SP-D: 74 626.9 ± 15 462.4 pg/mL, 74% of inhibition vs BLM group; MMP-7: 314.1 ± 43.1 pg/mL, 80% of inhibition vs BLM group; COL1: 12 008.0 ± 2 672.4 pg/mL, 63% of inhibition vs BLM group; $p \leq 0.05$).
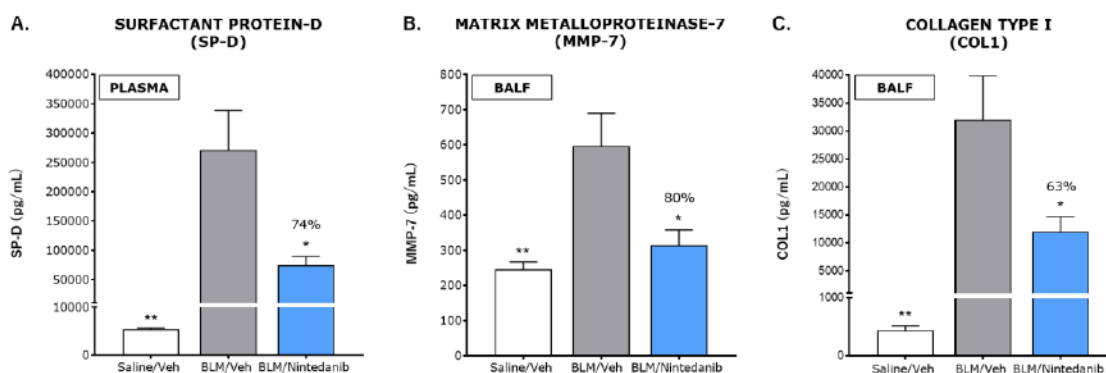

Figure 4.25 Effect of Nintedanib on selected biomarkers at day 21 after BLM OA administration. Female mice were daily treated by oral gavage with either Nintedanib (50 mg/kg b.i.d.) or vehicle (1% of Tween 80 in milliQ water), starting from day 7 after BLM OA administration up to day 21. **A.** Plasma levels of surfactant protein-D (SP-D). **B.** BALF levels of matrix metalloproteinase-7 (MMP-7). **C.** BALF levels of collagen type I (COL1). Data represent mean ± SEM values for Saline/Veh (n=10; white bar), BLM/Veh (n=15; grey bar) and BLM/Nintedanib (n=15; light blue bar) groups of animals. Statistical analysis was assessed using one-way ANOVA followed by Dunnett's test in comparison with the BLM group; ** $p \leq 0.01$, * $p \leq 0.05$. BALF, bronchoalveolar lavage fluid; BLM, bleomycin; Veh, vehicle.

4.4.8 Correlations analysis

As a final step of this study, the correlation between the respective indicators of lung function, histology, pulse oximetry, 3D imaging, and fibrotic biomarkers was analyzed (**Figure 4.26**).

Impaired airway function was accompanied by an aggravation of pulmonary fibrosis. In particular, lung function measurements, such as FVC, showed a significant negative correlation with lung histology by Ashcroft scores and with poorly-aerated tissue derived from the micro-CT scans, expressed as poorly-aerated lung volume (Pearson r was -0.85 and -0.76, respectively, and p value was < 0.0001). Furthermore, FVC also had a strong negative correlation with levels of the fibrotic biomarkers measured in plasma and BALF samples. Pearson r values between FVC and levels of SP-D, MMP-7, and COL1 were -0.70 (p < 0.0001), -0.51 (p = 0.0052), and -0.67 (p = 0.0001), respectively. A similar correlation was observed for Hyp in lung tissue, as the Pearson r value for FVC was -0.73 (p < 0.0001). Taken together, the levels of these biomarkers, including lung Hyp content, were strongly and positively correlated with each other.

Similar to lung function measurements, Sp02 readings showed significant and negative correlations with histology (Pearson r -0.58, p = 0.0020), imaging (Pearson r -0.76, p < 0.0001), fibrotic biomarkers (Pearson r SP-D -0.56, p = 0.0032; Pearson r MMP-7 -0.56, p = 0.0029; Pearson r COL1 -0.64, p = 0.0005), and lung Hyp content (Pearson r -0.59, p = 0.0017). Conversely, Sp02 measures were positively and significantly correlated with FVC (Pearson r was 0.60 and the p value was = 0.0014).

From another point of view, SP-D, MMP-7, COL1, and especially Hyp, showed positive and significant correlations both with Ashcroft scores and poorly-aerated lung volume. Pearson r values between levels of SP-D, MMP-7, COL1 and Hyp and Ashcroft score were 0.56 (P = 0.0019), 0.43 (p = 0.0237), 0.59 (p = 0.0010) and 0.73 (p < 0.0001), respectively, while for poorly-aerated lung volume were 0.61 (p = 0.0006), 0.63 (p = 0.0004), 0.70 (p < 0.0001) and 0.69 (p < 0.0001), respectively.

Finally, a strong and significant positive correlation was demonstrated between Ashcroft scores and the poorly-aerated lung volume, indicating that the severity of fibrosis was related to the increase in poorly-aerated tissue (Pearson r was 0.83 and the p value was < 0.0001).
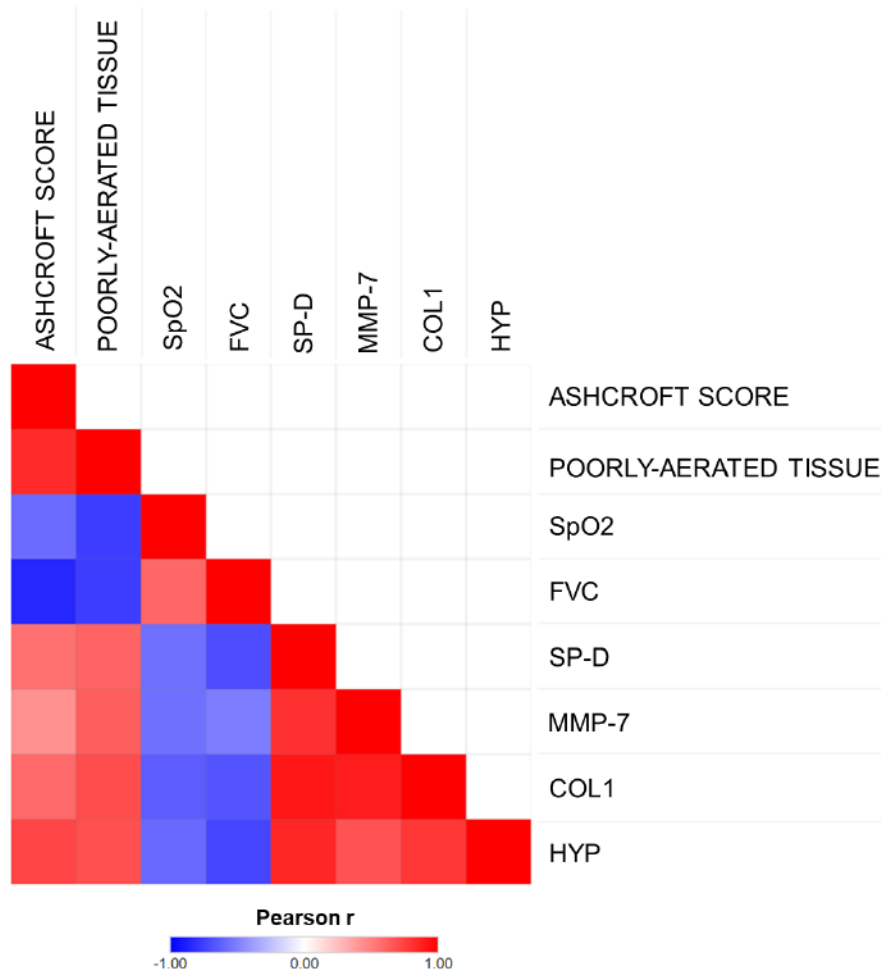
Figure 4.26 Correlations between histology, micro-CT imaging, pulse oximetry, lung function, fibrotic biomarkers and Hyp at day 21 after BLM OA administration. Female mice were daily treated by oral gavage with either Nintedanib (50 mg/kg b.i.d.) or vehicle (1% of Tween 80 in milliQ water), starting from day 7 after BLM OA administration up to day 21. Correlations were determined using Pearson's correlation coefficient matrix tests. Correlations include Saline/Veh, BLM/Veh and BLM/Nintedanib groups of animals. Significance of the correlation analysis was set at $p < 0.05$. SpO2, oxygen saturation; FVC, forced vital capacity; SP-D, surfactant protein-D; MMP-7, matrix metalloproteinase-7; COL1, collagen type I; Hyp, hydroxyproline.

5. DISCUSSION AND CONSLUSION

IPF is a fatal and complex disease of unknown etiology which makes drug development challenging. Although in the last decade the knowledge regarding the pathogenesis of IPF has considerably improved, potential new targets have been identified and two drugs received formal approval from regulatory authorities entering in the daily clinical practice, the medical need for treating this devastating disease remains very high.

Many potentially effective anti-fibrotic compounds have shown promising results in preclinical models of pulmonary fibrosis, but only few of them have been successfully translated to the clinic (*Seibold et al. 2010; Daniels et al. 2010*). Preclinical studies are crucial steps in the drug discovery process and the selection of the best drug candidate for clinical development relies on how well experimental animal models are able to predict clinical outcomes. The ATS panel of experts formalized recommendations for preclinical assessment to drug development, suggesting an integrated approach using relevant animal models and appropriate readouts for measuring evolution of lung fibrosis over time and the potential efficacy of anti-fibrotic drugs.

Although BLM-induced lung fibrosis murine models are accepted as the first line for drug testing, their clinical transability is debated. Several challenges in the research field may explain this translational problem. Animal models of pulmonary fibrosis have the inherent limitation that no one exactly mimics human disease. Indeed, the lesion that develop in the lungs of animals result in a fibrotic condition that tends to spontaneously resolve over time, losing the feature of progression typical of IPF disease (*Moeller at al. 2008*). Moreover, most of the compounds tested preclinically for the treatment of IPF are evaluated in models where a single fibrotic insult is used, however in humans the development of IPF is thought to be progressive and due to repeated micro-injuries (*Selman et al. 2002*). Therefore, models that use repeated smaller insults that result in a progressive development of fibrosis may provide a better model of pulmonary fibrosis.

Second, most often only prophylactic testing of the drug is performed. This point could explain the poorly predictivity of pulmonary fibrosis preclinical models. Therapeutic testing when fibrosis is appearing or omnipresent should better mimic the real-life situation and be more relevant to evaluate the anti-fibrotic properties of a putative compound (*Jenkins et al. 2017*). A recent study published by Kolb and colleagues highlighted that the vast majority of studies using the BLM model to test anti-fibrotic efficacy of drugs do not consider the element of appropriate therapeutic timing (*Kolb et al. 2020*). Out of 221 studies published between 1980 and 2006, only 10 were designed using a therapeutic treatment regimen, which means starting the administration of an experimental therapy at least 7 days after BLM instillation.

Lastly, despite technological advances, only endpoint measurements such as biochemical evaluation of lung Hyp levels as marker of collagen accumulation or histological assessments of fibrotic tissue deposition are generally used to assess the burden of lung disease and the efficacy of the drug. These endpoints often exhibit high variability, limited sensibility of drug efficacy, and are unable to give temporal and spatial information of the pathology over the entire lung. More importantly, they differ substantially from the endpoints used in clinical trials (e.g. CT and functional readouts such as lung function decline or impairment in gas exchange), stressing the need for more clinically relevant readouts which would improve the translatability between human IPF and animal models, and therefore the preclinical screening efficiency of new therapies.

Bridging the gap between preclinical research and clinical needs by assessing clinically relevant readouts in a robust animal model should have a significant impact on the efficiency in identifying new therapeutic targets and compounds, ultimately leading to better patient care. To address this point, in this PhD work, we (1) reproduced the mouse model of pulmonary fibrosis most described in the literature, the IT BLM model, and analyzed its main limitations; (2) looking at the clinic, we optimized the BLM model with the introduction of clinically more relevant parameters (i.e., lung function tests, micro-CT imaging, oximetry and fibrotic clinical biomarkers) through a new BLM OA protocol and finally, (3) we explored the added value of these more relevant readouts with the pharmacological validation with Nintedanib, which was tested under therapeutic regimen. Ultimately, the final goal aimed to generate an improved BLM model of pulmonary fibrosis compared to that currently described in the literature, in order to enhance its robustness, reliability and translatability to be used as a model of screening within the IPF projects of Chiesi Famaceutici for the identification of novel anti-fibrotic drugs.

5.1 Characterization of the BLM IT model and its limitations

The first experiment performed during this PhD project was a time course study of a BLM-induced lung fibrosis murine model which, as largely explained in the introduction, is the most used and best characterized and recommended model for preclinical testing of anti-IPF drugs. It has also been employed in the preclinical study of Pirfenidone and Nintedanib, the only two drugs approved for IPF. This experiment represented an important step to understand the key points of development, progression and resolution of lung fibrosis induced by BLM. Furthermore, this experiment allowed to identify the best therapeutic window to test potential anti-fibrotic molecules.

In the model used in this study, lung fibrosis was induced by two IT administrations of BLM. In the literature it is reported that repetitive multiple doses of BLM over time can increase the duration of the fibrotic stage with however longer time investment (*Yanagihara et al. 2020*). For example, Degryse and colleagues reported more robust and marked fibrotic features in the lungs of mice undergoing repetitive IT administration (every other week for a total of eight doses) compared with single dosing, but this protocol involves a significant amount of time and has high management cost (*Degryse et al. 2010*). Therefore, the choice to adopt a double administration was dictated by the possibility to mimic the recurrent episodes of lung injury that occur in IPF and to reproduce the chronic aspect of the disease more effectively, while maintaining an easy to handle model suitable for compound screening. Indeed, a double administration of BLM produces a more robust and reproducible lung fibrosis with longer resolution times with respect to models that employ a single dose (*Stellari et al. 2017*).

The BLM IT administration induced a significant weight loss in the first days of treatment. This outcome reflected the cytotoxic effect of BLM and allowed to assess the animal state of health and understand the extent of damage caused by BLM during the experiment. The weight loss in animals is actually an indication of a stress and pain conditions and is considered as a parameter for severity assessment (*Talbot et al. 2020*). A weight loss induced by BLM in lung fibrosis experiments is a well-known effect from literature (*Bauer et al. 2015; Cowley et al. 2019*). In this study, the highest body weight reduction was reached on day 7, with an average weight loss of ≃11%, which indicates a quite moderate BLM effect, considering that local authorities define a body-weight reduction of 20% or more, as a parameter of severe suffering that requires a human endpoint decision. Despite the initial weight loss, after day 7 the BLM-treated mice tended to recover weight with a regular trend until the end of the experiment. Even if a decrease in survival rate was observed in other experiments reported in literature with this model (*Bauer et al. 2015; Cowley et al. 2019*), in this study no mortality was observed in BLM mice, thus reflecting good tolerability of the animals with this clinically-approved BLM and dosing regimen.

Morphological and molecular characterization of lung fibrosis is an important endpoint for preclinical assessment in a BLM-model of pulmonary fibrosis. According to the ATS panel of experts, Hyp measurements for collagen accumulation along with histologic assessments in the lung tissue represent the optimal primary endpoints for preclinical assessment of novel therapeutic agents (*Jenkins et al. 2017*).

The assessment of Hyp content in lung homogenate is the fastest and easiest way to estimate collagen content, because Hyp is one of the key components of this complex

protein and it is estimated that each milligram of Hyp is equivalent to 6.94 milligrams of collagen (*Campa et al. 1990*). In the time course experiment, we decided to process both lungs for Hyp analysis, in order to have a more reproducible data, thus allocating a separate group of animals for the histological assessment. An elevated Hyp concentration was observed in BLM-treated mice starting from day 7 with an upward trend over time, reaching a statistically significant effect on day 14 and particularly on day 21, where the levels were ~2-fold increased. These data are consistent with those reported in the literature where other time course studies of BLM-induced lung fibrosis showed an increase in Hyp concentration of about 1.5-fold, reaching a peak effect at days 14-21 post-BLM administration (*Izbicki et al. 2002; Bauer et al. 2015*).

The Hyp data mirrors the features observed in the histological analysis. In fact, 7 days after the first administration of BLM, the amount of ECM and collagen, marked by the trichrome staining, was visually lower than at the other time points, in line with the Hyp data, and still associated with a significant presence of inflammation. At day 14, when the inflammation was less evident, the histological images showed the advanced of the fibrotic process with the production of components of the ECM and an initial alteration of the pulmonary structure. The fibrotic process continued and worsened in the following time point, day 21, leading to the formation of dense fibrotic agglomerates. This framework clearly describes the classical development of the BLM model, as reported by other studies, that indicate a switch from inflammation to fibrosis around the seventh day post-BLM with fibrotic lesions appearance starting from day 14. Terminal investigations are typically carried out on day 21 or 28 after the initial BLM dose. (*Carrington et al. 2018; Yanagihara et al. 2020*).

To implement the classical lung fibrosis scoring represented by the Ashcroft score, we developed an automated image APPs with Visiopharm® Software designed to distinguish and quantify the fibrotic lung lesions on the whole-slide images (see paragraph 3.6.2) (*Pontis et al. 2019*). Similar evaluations using fully automated histo-morphometric image analysis methodology are already described in the literature to quantify fibrosis in animal models of pulmonary fibrosis (*Seger et al. 2018*). With this approach, we were able to provide a robust and broader assessment of the lung lesions by quantifying pulmonary fibrosis in a reliable and observer-independent manner. Results, in fact, were in line with the other evaluations, making these readouts consistent among each other. However, the automated analysis also shows the advantage of being less time-comsuming compared to the Ashcroft score analysis.

The results obtained with this first time course study allowed us to define the correct therapeutic window for intervening with anti-fibrotic drugs and led to the possibility of proceeding with a pharmacological study using an FDA-approved drug like Nintedanib. This experiment was needed for the pharmacological validation of the model and, at the same time, provided the bases to assess the efficacy of new anti-fibrotic compounds. Pharmacological interventions before and during the inflammatory phase would act only at level of BLM-induced inflammation and could have a preventive effect on the establishment of lung fibrosis. As mentioned previously, many drugs that have been proven to be effective with this protocol (defined "preventive protocol treatment") have failed in clinical trials. For example, compounds such as prednisolone which is an anti-inflammatory agent, and other compounds having similar mechanisms of action have shown some efficacy in pre-clinical models when dosed prophylactically (*Chaudhary et al. 2006; Oku et al. 2008*). However, anti-inflammatory therapy have only shown very weak benefit, if any, in the treatment of pulmonary fibrosis in the clinic (*Douglas et al. 2000*; *Demedts et al. 2005*), and their use is currently not recommended in the treatment of IPF (*Raghu et al. 2011*). So, many published papers in the context of BLM preclinical models suggested to investigate the effects of an anti-fibrotic agent in a protocol that consisted in administering drugs 7 days post-BLM and so at the beginning of the histological evidence of fibrosis and after the peak of the inflammatory phase ("curative protocol treatment") (*Jenkins et al. 2017; Bonniaud et al. 2018; Yanagihara et al. 2020*). Based on these considerations and according to our results, we defined day 7 after the first BLM IT administration as the start of the treatment and day 21 as the final time point of the therapeutic window for the assessment of the readouts, considering that the fibrotic response was still evident and robust in all the readouts evaluated. The 7-day time point, thus, was used as a separation between the inflammatory and fibrotic phases (*Kolb et al. 2020*).

During the pharmacological experiment, the animals treated with Nintedanib showed a similar body weight trend compared with the BLM mice. However, the animals treated with Nintedanib tended to recover more slowly the weight loss compared to BLM group. This difference could be related to the adverse effects of the drug, that are reported in clinical trials (*Richeldi et al. 2014*), even if these effects were not mentioned in preclinical validation studies with Nintedanib (*Surber et al. 2020*). Moreover, compared to the time course study where no mortality was observed, the slight mortality obtained in the BLM and Nintedanib groups (ranging from 10 to 15%) could be due to the daily manipulation of the animals following the treatments that could have impacted in terms of tolerability on top of the BLM effect.

In line with the time course studies, lung Hyp content was significantly increased of about 2-fold in BLM-treated mice compared to the control animals. Nintedanib showed a significant modulation of this surrogate marker of collagen content in the lungs (36% of inhibition), an effect which is however not in agreement with Ackermann and colleagues who did not observe any difference in Hyp lung content between animals treated with BLM and those treated with Nintedanib (*Ackermann et al. 2017*). Park and colleagues, on the other hand, observed only a slight effect of Nintedanib on this marker in another BLM model of pulmonary fibrosis (*Park et al. 2020*). Therefore, although the ATS guidelines have confirmed Hyp as the optimal primary endpoint for preclinical assessment of new anti-fibrotic drugs, in the literature Hyp measurement is not always reported, probably due to the poor sensitivity of this readout in demonstrating the efficacy of tested compounds.

The results obtained on Hyp levels in this pharmacological study were however supported by the histological analysis that highlighted a significant inhibition in reducing the percentage (36%) and the severity (16%) of the fibrotic lesions after the treatment with Nintedanib, when measured by the automated image analysis and by Ashcroft scoring system, respectively. The effect of Nintedanib on the histological analysis resulted from our study is in line with the results reported in other studies investigating Nintedanib under therapeutic regimen. In particular, using a similar experimental condition, Ackermann and colleagues showed a significant reduction in fibrotic scores with Nintedanib compared to animals treated with BLM (2.08 vs 4.89, p<0.001) (*Ackermann et al. 2017*), a results also confirmed by Wollin and colleagues during the preclinical validation of Nintedanib (*Wollin et al. 2014*). Also, Seger and colleagues reported a significant reduction in the percentage of fibrotic masses with Nintedanib using a fully automated image analysis software (*Seger et al. 2018*). However, as expected, the treatment failed to completely revert the fibrotic process limiting to a partial effect as also observed in clinical treatment. Indeed, as mentioned in the Introduction section, this drug is able to slow down the progression of IPF, improving some functional respiratory parameters of the lung without resolving the disease.

The characterization of the BLM IT model proved to be useful in better understanding the development of BLM-induced lung fibrosis and gave us the necessary indications to define the therapeutic protocol, however, it highlighted several limitations. In our experiments, the IT administration induced a marked heterogeneous distribution of fibrosis in the lung parenchyma of mice, affecting generally only one lobe, leaving the others poorly fibrotic (see paragraph 4.1.2 and **Figures 4.2-4.6**). Although the patchy fibrotic lesions observed in the BLM IT protocol may better reproduces the features of the human disease, this

heterogeneous distribution pattern could be limiting for drug screening since generating a high variability among experimental animals. Indeed, the heterogeneous distribution observed in the IT protocol precludes the possibility to use the same lung for different readouts, as for example histology and biochemical analysis performed on the left and on the right lobe, respectively. A common approach in preclinical studies is doubling the number of mice for experiment, although a direct link between fibrosis degree and other fibrosis markers is precluded as well as represents an unethical approach considering the 3R principle of animal research. An additional limitation emerged from the BLM IT model is related to the readouts evaluated, histology and Hyp content, that revealed some disadvantages such as the limited sensitivity to pharmacological treatments and, most critical, the inability to get a direct link to clinics. Hence the need for novel, more sensitive, and clinically relevant readouts.

5.2 Bridging the gap between preclinical research and clinical needs: introduction of clinically relevant readouts with the BLM OA mouse model

Looking to the clinic, HRCT imaging and functional endpoints are used to diagnose and monitor patients with IPF. In human, FVC is widely considered an accepted surrogate endpoint in IPF clinical trials and it is routinely used as a primary endpoint to measure disease progression and to assess the success of therapeutics directed towards IPF. Also, HRCT scans are invaluable to diagnose and stage IPF. HRCT can assess the nature and extent of parenchymal abnormalities, narrow the differential diagnosis, and in some patients, substantiate a specific diagnosis, obviating the need for SLB.

Significant recent progress in the challenging field of IPF has also been achieved in the identification of novel protein biomarkers. In IPF, biomarkers may have the potential to enable differential diagnosis (e.g., between IPF and non-IPF fibrosing ILDs), more effective patient stratification (e.g., determine the subtype of ILD or identify patients at risk of progression), and better up-front selection of therapy. Most importantly, they may allow physicians to monitor early treatment response, which remains a huge unmet need.

With this scenario, to build a stronger translational bridge to the clinic, we have explored in our model some of these clinically relevant readouts, introducing lung function measurements, longitudinal micro-CT imaging, fibrotic biomarkers analysis, and finally, oximetry readings, to be coupled with the traditional preclinical endpoints. Moreover, to overcome the first mentioned limit, related to the heterogeneity and variability of fibrosis distribution following the IT BLM instillation, and to further refine the model, we

investigated a new BLM route of administration, the OA aspiration, as also suggested by the ATS panel of experts (*Jenkins et al. 2017*).

No statistically significant difference on overall mouse survival was found between IT and OA BLM administrations in the time course studies (**Figures 4.1 A-4.9 A**). Similarly, both routes of BLM administration, as compared to Saline-treated animals, resulted in significant and comparable weight loss (**Figures 4.1 B-4.9 B**). Again, no difference upon the differential administration route of BLM was noted on Hyp levels (**Figures 4.4-4.15**). However, histological observations of the lung parenchyma revealed a marked difference in the fibrosis distribution among various lobes in BLM IT compared to OA treated mice over time (**Figures 4.2-4.13**). Fibrosis in OA treated mice appeared more homogeneous, less variable among animals and uniformly distributed throughout the lobes at the different time points. The difference in lung fibrosis distribution between IT vs OA administration may depends on the different techniques for BLM delivery. In the IT instillation technique, the solution is forced by adding a constant pressure and, for this reason, it could reach the right or the left lung randomly. Also, IT administration could result in a peri-operative mortality, as it concerns almost exclusively handling, skill and chance. OA administration, instead, requires lower technical skills compared to IT; it is much easier and faster to perform and benefits from the physiological breath (*Barbayianni et al. 2018*); as a consequence BLM may better distribute in the whole lung, resulting in a more uniform distribution of moderate and severe lesions across lung lobes.

Previously we reported the development of an automated image APPs with Visiopharm® software to quantify the percentage of total lung parenchyma affected by fibrotic lesions. In the last years, advances in machine learning have enabled the synergy of AI and digital pathology (*Berigei et al. 2021*). Therefore, as a further refinement of the histological evaluations, we introduced AI-based analysis to complement the automated analysis of lung fibrosis quantification, while also providing information on fibrosis severity. With the support of the AI deep learning Visiopharm® module, we developed a new APP that identifies and classifies three degrees of fibrosis severity corresponding to the different grades described in the modified Ashcroft scale (*Hübner et al. 2008*). This approach, results to be more reliable, more accurate and less time-consuming compared to the classical histological analysis based on scoring attributed by the pathologist. Overall, all the histological analysis performed did not reveal any significant differences among each other and between IT and OA protocols (**Figures 4.3-4.14**). Although still few studies have reported a direct comparison between these two routes of administration (*Jenkins et al. 2017*; *Egger et al. 2015*; *Barbayianni et al. 2018*), our data are in line with those obtained

from others existing reports. Lakatos and colleagues suggested the advantage of OA model against IT instillation in a detailed comparative study using silica suspension in C57Bl/6 mice, an evidence also confirmed subsequently by Bale and colleagues (*Lakatos et al. 2006*; *Bale et a. 2016*).

The real breakthrough in the refinement and improvement of this BLM model has been achieved with the introduction of novel readouts, which are highly relevant in the clinical context of IPF.

Publications suggest that lung function analysis is an important tool in the evaluation of mouse respiratory disease models (*Devos et al. 2017*) but, despite its undiscussed translational value, this readout is rarely used at the preclinical level, because it is expensive and requires a very specific technical competency. Here, to further increase the traslational value of our model, we have introduced the lung function tests by Flexivent system and explored a number of parameters to identify temporal changes in respiratory system mechanics that are also observed in IPF patients. In the time course BLM OA experiment, we found that alteration in respiratory system mechanics and pressure-volume relationships of BLM mice were observed as early as 7 days after the start of BLM administration reaching a peak effect at days 14 and 21. Among the parameters evaluated (see **Table 4.1**), we considered as the most relevant for fibrosis FVC, which is also the primary endpoint used in clinical trials to assess the efficacy of anti-fibrotic treatments in IPF patients.

In clinical practice, HRCT imaging plays a key role for the diagnosis of IPF (*Lynch et al. 2018*). This technology provides a non-invasive evaluation of both the morphometry and functionality of lungs, exploiting the inherent contrast between air and tissue (*Zhou et al. 2015*). Despite micro-CT is still not fully implemented in preclinical studies, recently, this 3D imaging technology has been applied in some animal models of lung diseases including fibrosis and emphysema (*Clark et al. 2014; Vande Velde et al. 2016*), emerging as a powerful tool for the longitudinal assessment of disease progression (*De Langhe et al. 2012; Dekoster et al. 2020*). In the time course study, we have found that poorly-aerated tissue could be a good marker for fibrosis quantification. Indeed, the quantification of fibrosis based on the percentage of poorly-aerated regions revealed a progressive increase in damaged tissue for BLM OA mice with a peak at 14-21 days that tended to decrease on day 28, a condition that was also reported by Ruscitti and colleagues (*Ruscitti et al. 2020*). Moreover, Dekoster and colleagues performed similar evaluations using a mouse model of pulmonary fibrosis induced by silica instillation, in which they also reported positive

correlations between these micro-CT-derived measurements and lung function data (*Dakoster et al. 2020*).

In IPF, biomarkers can be categorized according to possible pathogenic pathways, broadly including those associated with AECs damage and dysfunction, ECM remodelling and fibroproliferation, as well as immune dysregulation (*Jee et al. 2019*). Molecular biomarkers have rapidly become a buzzword in pulmonary medicine. Clinical scientists and drug companies repeatedly mention that they are the most critical missing link in improving drug development in chronic lung disease in general, and in IPF in particular. To date there is no validated biomarkers for IPF. There are several promising candidates under study, but none of them has reached clinical practice use yet. Hence, there is a tremendous unmet need in stablishing markers for disease early diagnostics, progression and outcome of IPF (*Ley et al. 2014*), and currently, several groups are focusing their research on developing and establishing these signatures. The PROLIFIC collaboration, as mentioned in the Introduction section, is an example of the innovative and intensive research to advance the application of biomarkers to clinical trials in IPF and to promote translational discoveries into clinical practice. The goal of this research is to develop well-qualified multiplex assays to detect important biomarkers in patients with IPF. The assays, composed of 12 specific biomarkers (epithelial damage (CYFRA 21-1, SP-D, CA-19-9, KL-6), fibrosis (MMP-7, Tenascin C, Periostin), inflammation (CCL18, CXCL13, slCAM1), and thrombosis (PAI-1)) selected based on published scientific reports describing their prognostic utility for the disease itself and their potential predictive utility for how well a drug works, will be used to uncover early indicators of a drug's activity (*Schmidt, 2020*).

To this end, we sought to comprehensively assess in our BLM-induced lung fibrosis model some of the biomarkers most described in IPF (see paragraph 1.8.1) to further increase the outcome measures during drug testing. We first identified some of these candidate biomarkers, then selected also by PROLIFIC, such as KL-6/MUC1, sICAM, SP-A and SP-D, MMP-7 and different types of collagen; we explored their modulation in several biological compartments during the initiation, establishment, and resolution of fibrosis (all data are not shown) and then, we selected those that were significantly modulated by BLM treatment. In clinical trials, biological tissues or fluids such as whole blood, serum, BALF and induced sputum are used to evaluate biomarkers levels in IPF patients (*Inoue et al. 2020*), therefore, also in our studies we measured the levels of these markes in the following biological matrices, BALF and plasma. From the different selected proteins, three were significantly regulated during the onset and resolution of fibrosis when measured in plasma and BALF. Specifically, in the time course study, we found that

plasma SP-D, and BALF MMP-7 and COL1 levels were significantly increased in BLM-treated mice as early as day 7 and remained increased as the injury was maintained. Although very few studies are reported in the literature regarding the role of potential biomarkers in the animal models of pulmonary fibrosis, results observed in our study on these biomarkers seem to be in line with the results obtained in other BLM or other similar models of pulmonary fibrosis (*Dekoster et al. 2020; Fernandez et al. 2016; Liu et al. 2017*). The fact that these pro-fibrotic biomarkers are up-regulated both in IPF patients and in our BLM model further suggests the translational potential of the model.

Pulse oximetry saturation can predict prognosis of IPF and provides a non-invasive assessment of SpO2 (*Takei et al. 2020*). It is commonly used in IPF patients, as secondary endpoint, to monitor and maintain SpO2 at a level above 90% to prevent the development of secondary disorder such as pulmonary hypertension (*Alhamad et al. 2020*). The measurements of SpO2 with the MouseOx® Pulse-oximeter provided us a useful measure of the deleterious effects of BLM on the lungs of mice. The data are obtained in a rapid, quantitative, and real-time manner without the need to euthanize the mice. Therefore, this assay has many advantages both in following the natural progression of the injury and for testing potential therapies for lung injury. Our data demonstrated that OA administration of BLM produced a significant decrease in SpO2 below 90% reflecting hypoxemia beginning on day 7. Similar results were also observed by Foskett and colleagues in another mouse model of BLM-induced pulmonary fibrosis where, however, SpO2 levels were evaluated only until day 12 post BLM (*Foskett el al. 2014*). Our results demonstrated a significant decrease of these levels until day 21 after the first BLM administration when comparted to the control groups.

As a final step of this PhD project, we performed a therapeutic study with Nintedanib to assess the robustness of these clinically relevant readouts in the model.

Analogously to IPF clinical trials, we demonstrated that treatment with Nintedanib limited BLM-induced functional alterations, significantly improving the FVC of 44%, eliciting efficacy comparable to that observed in IPF patients (*Richeldi et al. 2014*).

Also with the longitudinal micro-CT analysis, we observed that Nintedanib treatment stabilized tissue damage by significantly inhibiting the increase of poorly-areated regions of 40%. Moreover, Nintedanib significantly reduced the levels of plasma SP-D, and BALF MMP-7 and COL1 and improved the SpO2 levels.

We have demonstrated for the first time the value of evaluating these clinically relevant readouts all together in a preclinical model of pulmonary fibrosis, strengthening the

assessment of the efficacy of a new anti-fibrotic compound compared to histology and Hyp alone, and making the model more robust for drugs screening.

5.3 Final conclusions

The incomplete understanding of the disease and the lack of safe and effective treatments make IPF a disease with considerable unmet need requiring a novel approach to treatment. However, drug discovery in this field had to face a lot of challenges probably due to a very complex disease, difficult to fully understand and to resemble with animal models. Considering these intrinsic limits of drug discovery for IPF, the goal of this PhD project was to generate a more reliable, predictable and robust animal model of pulmonary fibrosis through the introduction of clinically relevant endpoints, not commonly evaluated at the preclinical level, in order to make the model closer to human disease and more suitable for the identification of new anti-fibrotic drugs.

In this PhD work, we have proposed a new protocol for lung fibrosis development induced by double OA administration of BLM, which gives a more uniform distribution of fibrotic lesions through the lung compared to IT instillation. This new protocol presents several improvements in comparison to the existing BLM fibrosis models. It indeed turned out to be easy to perform, able to induce a robust fibrosis and suitable for screening anti-fibrotic compounds, exhibiting two weeks of therapeutic intervention, where putative drug candidate can be administered following a therapeutic regimen. Furthermore, one of the main advantages is to have multiple relevant readouts from the same subject reducing the variability and the number of mice used, allowing a direct link between disease and biochemical analysis or molecular events. In this context, the OA model is fully in compliance with the main "3R principle", Replacement, Refinement, Reduction of animal research (*Flecknell, 2002; Tannenbaum and Bennett, 2015*), since the number of animals can be reduced.

The crucial and decisive step for the refinement of our BLM model in an attempt to bridge the gap between preclinical models and the clinic was accomplished thanks to the introduction of novel clinically relevant parameters, that can be fully integrated in a drug discovery process.

In particular, pulmonary function test, which is not commonly measured at preclinical level especially to assess the efficacy of drugs, should be considered an important tool with a high translational value, considering its importance in clinical trials and in the management of IPF patients. Our results demonstrate that in mice it is possible to measure the same functional parameters applied in patients with IPF; in this model, the pharmacological

validation with Nintedanib demonstrates not only that this drug is able to modulate significantly FVC, in line with the clinical data, but that this readout is robust, consistent and more sensitive compared to the histological analysis and, similarly to the clinical practice, could be considered a primary endpoint also in a preclinical model for drug discovery process.

The Ashcroft score analysis, widely used at preclinical level as histological outcome, reveals some disadvantages such as a time-consuming processing, operator-dependent results and, most critical a low sensibility to detect the drugs efficacy. The introduction of the automated analysis of images, especially the AI-based analysis, improve consistently the histological outcome, gaining in accuracy, sensitivity and automation of the method. The effect of compounds is better appreciated since the automated analysis gives the possibility to gain further information on the effects of a drug on lung histology compared to the simple Ashcroft scoring system, such as the ability to reduce the severe and moderate components of fibrosis. Despite the improvement achieved by automated analysis, we believe that Ashcroft score analysis still remains a very key element in preclinical models and, considering its significant and positive degree of correlation with the automated analysis (Pearson r 0.87, $p < 0.0001$; data not shown), coupling these different histological evaluations can provide a more comprehensive and reliable view of fibrosis and drugs efficacy.

Finally, the introduction of different readouts in the model that all go to the same direction showing a significant correlation among each other has from one side increased the robustness of the model and from the other side has allowed to bring this preclinical model to a level of complexity that mirrors the one observed in human IPF.

Overall this PhD work has enhanced the translational and predictivity value of the BLM model increasing the chance of selecting promising compounds to advance to clinical trials and has concretely led to significant benefits to drug discovery process in the IPF research, improving the quality and the reliability of the search of novel anti-fibrotic drugs.

Our studies could provide the way for a new drug discovery approach and cast a new light on the importance to examine clinical endpoints in preclinical trials, giving a better indication of new anti-fibrotic drugs to push into the clinic.

6. REFERENCES

Ackermann M., Kim Y. O., Wagner W. L., Schuppan D., Valenzuela C. D., Mentzer S. J., Kreuz S., Stiller D., Wollin L., Konerding M. A. *"Effects of nintedanib on the microvascular architecture in a lung fibrosis model"*. Angiogenesis. **2017**; 20(3): 359-372.

Alhamad E. H., Cal J. G., Alrajhi N. N., Aharbi W. N., AlRikabi A. C., AlBoukai A. A. *"Clinical characteristics, comorbidities, and outcomes in patients with idiopathic pulmonary fibrosis"*. Ann Thorac Med. **2020**; 15(4):208-214.

Alhamad E. H., Lynch J. P., Martinez F. J. *"Pulmonary function tests in interstitial lung disease: what role do they have?"*. Clin Chest Med. **2001**; 22(4):715-50, ix.

Alsafadi H. N., Staab-Weijnitz C. A., Lehmann M., Lindner M., Peschel B., Königshoff M., Wagner D. E. *"An ex vivo model to induce early fibrosis-like changes in human precision-cut lung slices"*. Am J Physiol Lung Cell Mol Physiol. **2017**; 312(6):L896-L902.

American Thoracic Society. *"Idiopathic pulmonary fibrosis: diagnosis and treatment"*. *International consensus statement.* Am J Respir Crit Care Med. **2000**; 161:646-664.

Aoki J., Inoue A., Okudaira S. "Two pathways for lysophosphatidic acid production". Biochim Biophys Acta. **2008**; 1781(9):513-8.

Appel J. Z., Lee S. M., Hartwig M. G., Li B., Hsieh C. C., et al. *"Characterization of the innate immune response to chronic aspiration in a novel rodent model"*. Respir Res. **2007**;8(1):87.

Armanios M., Blackburn E. H. *"The telomere syndromes"*. Nat Rev Genet. **2012**; 13(10):693-704.

Bale S., Sunkoju M., Reddy S. S., Swamy V., Godugu C. *"Oropharyngeal aspiration of bleomycin: An alternative experimental model of pulmonary fibrosis developed in Swiss mice"*. Indian J Pharmacol. **2016**;48(6):643-648.

Balestrini J. L., Chaudhry S., Sarrazy V., Koehler A., Hinz B. *"The mechanical memory of lung myofibroblasts"*. Integr Biol (Camb). **2012**; 4(4):410-21.

Balikian J. P., Jochelson M. S., Bauer K. A., Skarkin A. T., Garnick M. B., Canellos G. P., Smith E. H. *"Pulmonary complications of chemotherapy regimens containing bleomycin"*. AJR Am J Roentgenol. **1982**; 139(3):455-61.

Barbayianni I., Ninou I., Tzouvelekis A., Aidinis V. *"Bleomycin Revisited: A Direct Comparison of the Intratracheal Micro-Spraying and the Oropharyngeal Aspiration Routes of Bleomycin Administration in Mice"*. Front Med (Lausanne). **2018**; 5:269.

Bargagli E., Margollicci M., Luddi A., Nikiforakis N., Perari M. G., et al. *"Chitotriosidase activity in patients with interstitial lung diseases"*. Respir Med. **2007**;101(10):2176-81.

Bascom R., Hitz K., Dimmock A. E. F., Makhay M., et al. *"Description of Protocol to Evaluate MN-001'S (tipelukast) Efficacy, Safety and Tolerability in Subjects with Idiopathic Pulmonary Fibrosis"*. Am J Respir Crit Care Med. **2020**; 201:A1493.

Bascom R., Hitz K., Dimmock A. E. F., Makhay M., Matsuda K. *"A Single-Center, Randomized, Placebo-Controlled Study to Evaluate the Efficacy, Safety, and Tolerability of MN-001 (Tipelukast) in Subjects with Idiopathic Pulmonary Fibrosis"*. Am J Respir Crit Care Med. **2021**; 203:A1898.

Bauer Y., Tedrow J., de Bernard S., Birker-Robaczewska M., Gibson K. F., Guardela B. J., Hess P., et al. *"A Novel Genomic Signature with Translational Significance for Human Idiopathic Pulmonary Fibrosis"*. Am J Respir Cell Mol Biol. **2015**; 52 (2), 217-231.

Baumgartner K. B., Samet J. M., Coultas D. B., Stidley C. A., Hunt W. C., Colby T. V., Waldron J. A. *"Occupational and environmental risk factors for idiopathic pulmonary fibrosis: a multicenter case-control study"*. Am J Epidemiol. **2000**; 152(4):307-15.

Baumgartner K. B., Samet J. M., Stidley C. A., Colby T. V., Waldron J. A. *"Cigarette smoking: a risk factor for idiopathic pulmonary fibrosis"*. Am J Respir Crit Care Med. **1997**; 155:242-248.

Behr J., Bendstrup E., Crestani B., Günther A., Olschewski H., et al. *"Safety and tolerability of acetylcysteine and pirfenidone combination therapy in idiopathic pulmonary fibrosis: a randomised, double-blind, placebo-controlled, phase 2 trial"*. Lancet Respir Med. **2016**; 4(6):445-53.

Bennett B., Blease K., Ye Y., Azaryan A., Ramirez-Valle F., Ceres R., et al. *"CC-90001, a Second Generation Jun N-Terminal Kinase (JNK) Inhibitor for the Treatment of Idiopathic Pulmonary Fibrosis"*. Am J Resp Crit Care Med. **2017**; 195:A5409.

Berigei S., Roop B., Nandy S., Knipe R. S., et al. *"Artificial Intelligence Algorithm for Automated Fibrosis Quantification in Preclinical Bleomycin Model of Pulmonary Fibrosis"*. Am J Respir Crit Care Med. **2021**; 203:A4231.

Blaauboer M. E., Boeijen F. R., Emson C. L., Turner S. M., Zandieh-Doulabi B., et al. *"Extracellular matrix proteins: a positive feedback loop in lung fibrosis?"*. Matrix Biol. **2014**; 34:170-8.

Bonniaud P., Fabre A., Frossard N., Guignabert C., Inman M., Kuebler W. M., Maes T., et al. *"Optimising Experimental Research in Respiratory Diseases: An ERS Statement"*. Eur Respir J. **2018**; 51(5):17021-33.

Bonniaud P., Kolb M., Galt T., Robertson J., Robbins G., et al. *"Smad3 null mice develop airspace enlargement and are resistant to TGF-beta-mediated pulmonary fibrosis"*. J Immunol. **2004**; 173(3):2099-108.

Brownell R., Moua T., Henry T. S., Elicker B. M., White D., Vittinghoff E., et al. *"The use of pretest probability increases the value of high-resolution CT in diagnosing usual interstitial pneumonia"*. Thorax. **2017**; 72(5):424-429.

Business Wire. "*Kadmon Announces Positive Topline Results from Phase 2 Study of KD025 in Idiopathic Pulmonary Fibrosis*" **2018**; (https://www.businesswire.com/news/home/20180212006192/en/Kadmon-Announces-Positive-Topline-Results-Phase-2).

Calaway A. C., Foster R. S., Adra N., Masterson T. A., Albany C., et al. *"Risk of Bleomycin-Related Pulmonary Toxicities and Operative Morbidity After Postchemotherapy Retroperitoneal Lymph Node Dissection in Patients With Good-Risk Germ Cell Tumors"*. J Clin Oncol. **2018**; 36(29):2950-2954.

Camelo A., Dunmore R., Sleeman M. A., Clarke D. L. *"The epithelium in idiopathic pulmonary fibrosis: breaking the barrier"*. Front Pharmacol. **2014**; 4:173.

Campa J. S., McAnulty R. J., Laurent G. J. *"Application of high-pressure liquid chromatography to studies of collagen production by isolated cells in culture"*. Anal Biochem. **1990**; 186(2): 257-263.

Carrington R., Jordan S., Pitchford S. C., Page C. P. *"Use of animal models in IPF research"*. Pulm Pharmacol Ther. **2018**; 51:73-78.

Cavazza A., Rossi G., Carbonelli C., Spaggiari L., Pacie M., Roggeri A. *"The role of histology in idiopathic pulmonary fibrosis: An update"*. Respir Med. **2010**; 104 Suppl 1:S11-22.

Chaudhary N. I., Schnapp A., Park J. E. *"Pharmacologic differentiation of inflammation and fibrosis in the rat bleomycin model"*. Am J Respir Crit Care Med. **2006**; 173(7):769-76.

Chen C. Z., Raghunath M. *"Focus on collagen: in vitro systems to study fibrogenesis and antifibrosis state of the art"*. Fibrogenesis Tissue Repair. **2009**; 2:7.

Chen Y. W., Huang S. X., de Carvalho A. L. R. T., Ho S. H., Islam M. N., Volpi S., Notarangelo L. D., et al. *"A three-dimensional model of human lung development and disease from pluripotent stem cells"*. Nat Cell Biol. **2017**; 19(5):542-549.

Cheresh P., Morales-Nebreda L., Kim S. J., Yeldandi A., Williams D. B., et al. *"Asbestos-induced pulmonary fibrosis is augmented in 8-oxoguanine DNA glycosylase knockout mice"*. Am J Respir Cell Mol Biol. **2015**; 52(1):25-36.

Clark D. P., Badea C. T. *"Micro-CT of rodents: state-of-the-art and future perspectives"*. Phys Med. **2014**;30(6):619-34.

Claussen C. A., Long E. C. *"Nucleic Acid recognition by metal complexes of bleomycin"*. Chem Rev. **1999**; 99(9):2797-816.

Collard H. R., Moore B. B., Flaherty K. R., Brown K. K., et al. *"Acute Exacerbations of Idiopathic Pulmonary Fibrosis"*. Am J Respir Crit Care Med. **2007**; 176(7):636-43.

Collard H. R., Yow E., Richeldi L., Anstrom K. J., Glazer C., IPFnet investigators. *"Suspected acute exacerbation of idiopathic pulmonary fibrosis as an outcome measure in clinical trials"*. Respir Res. **2013**;14(1):73.

Collard H. R., Ryerson C. J., Corte T. J., Jenkins G., Kondoh Y., Lederer J. D., et al. *"Acute Exacerbation of Idiopathic Pulmonary Fibrosis. An International Working Group Report"*. Am J Respir Crit Care Med. **2016**; 194(3):265-75.

Conte E., Gili E., Fagone E., Fruciano M., Iemmolo M., Vancheri C. *"Effect of pirfenidone on proliferation, TGF-β-induced myofibroblast differentiation and fibrogenic activity of primary human lung fibroblasts"*. Eur J Pharm Sci. **2014**; 58:13-9.

Costabel U., Inoue Y., Richeldi L., Collard H. R., Tschoepe I., Stowasser S., Azuma A. *"Efficacy of Nintedanib in Idiopathic Pulmonary Fibrosis across Prespecified Subgroups in INPULSIS"*. Am J Respir Crit Care Med. **2016**; 193(2):178-85.

Cowley P. M., Roberts C. R., Baker A. J. *"Monitoring the Health Status of Mice with Bleomycin-induced Lung Injury by Using Body Condition Scoring"*. Comp Med. **2019**; 69(2):95-102.

Cronkhite J. T., Xing C., Raghu G., Chin K. M., Torres F., Rosenblatt R. L., Garcia C. K. *"Telomere shortening in familial and sporadic pulmonary fibrosis"*. Am J Respir Crit Care Med. **2008**; 178(7):729-37.

Cui Y., Osorio J. C., Risquez C., Wang H., Shi Y., et al. *"Transforming growth factor-β1 downregulates vascular endothelial growth factor-D expression in human lung fibroblasts via the Jun NH2-terminal kinase signaling pathway"*. Mol Med. **2014**; 20(1):120-34.

Daniels C. E., Lasky J. A., Limper A. H., Mieras K., Gabor E., Schroeder D. R., Imatinib-IPF Study Investigators. *"Imatinib treatment for idiopathic pulmonary fibrosis: Randomized placebo-controlled trial results"*. Am J Respir Crit Care Med. **2010**; 181(6):604-10.

Darby I., Skalli O., Gabbiani G. *"Alpha-smooth muscle actin is transiently expressed by myofibroblasts during experimental wound healing"*. Lab Invest. **1990**; 63(1):21-9.

Datta A., Scotton C. J., Chambers R. C. *"Novel Therapeutic Approaches for Pulmonary Fibrosis"*. Br J Pharmacol. **2011**; 163(1):141-172.

De Langhe E., Vande Velde G., Hostens J., Himmelreich U., Nemery B., Luyten F. P., Vanoirbeek J., Lories R. J. *"Quantification of lung fibrosis and emphysema in mice using automated micro-computed tomography"*. PLoS One. **2012**; 7(8):e43123.

Degryse A. L., Lawson W. E. *"Progress toward improving animal models for IPF"*. Am J Med Sci. **2011**; 341(6): 444-449.

Degryse A. L., Tanjore H., Xu X. C., Polosukhin V. V., Jones B. R., et al. *"Repetitive intratracheal bleomycin models several features of idiopathic pulmonary fibrosis"*. Am J Physiol Lung Cell Mol Physiol. **2010**; 299(4):L442-52.

Dekoster K., Decaesteker T., Berghen N., Van den Broucke S., Jonckheere A. C., Wouters J., et al. *"Longitudinal micro-computed tomography-derived biomarkers quantify non-resolving lung fibrosis in a silicosis mouse model"*. Sci Rep. **2020**; 10(1):16181.

Demedts M., Behr J., Buhl R., Costabel U., Dekhuijzen R., Jansen H. M., et al. *"High-dose acetylcysteine in idiopathic pulmonary fibrosis"*. N Engl J Med. **2005**; 353(21):2229-42.

Desmoulière A., Geinoz A., Gabbiani F., Gabbiani G. *"Transforming growth factor-beta 1 induces alpha-smooth muscle actin expression in granulation tissue myofibroblasts and in quiescent and growing cultured fibroblasts"*. J Cell Biol. **1993**; 122(1):103-11.

Devos F. C., Maaske A., Robichaud A., Pollaris L., Seys S., Lopez C. A. *"Forced expiration measurements in mouse models of obstructive and restrictive lung diseases"*. Respir Res. **2017**; 18(1):123.

Dhanasekaran D. N., Reddy E. P. *"JNK signaling in apoptosis"*. Oncogene. **2008**; 27(48):6245-51.

Dillingh M. R., van den Blink B., Moerland M., van Dongen M. G. J., Levi M., et al. *"Recombinant human serum amyloid P in healthy volunteers and patients with pulmonary fibrosis"*. Pulm Pharmacol Ther. **2013**; 26(6):672-6.

Douglas W. W., Ryu J. H., Schroeder D. R. *"Idiopathic pulmonary fibrosis: Impact of oxygen and colchicine, prednisone, or no therapy on survival"*. Am J Respir Crit Care Med. **2000**; 161(4 Pt 1):1172-8.

Du Bois R. M., Weycker D., Albera C., Bradford W. Z., Costabel U., et al. *"Forced vital capacity in patients with idiopathic pulmonary fibrosis: test properties and minimal clinically important difference"*. Am J Respir Crit Care Med. **2011**; 184(12):1382-9.

Dymek B., Sklepkiewicz P., Mlacki M., Zagozdzon A., et al. *"CHIT1 is a novel therapeutic target in idiopathic pulmonary fibrosis (IPF): anti-fibrotic efficacy of OATD-01, a potent and selective chitinase inhibitor in the mouse model of pulmonary fibrosis"*. Eur Respir J **2018**; 52: OA5361.

Dyjas R., Lipner J., Dymek B., Malcki M., et al. *"Clinical Development of OATD-01-a Novel, Chitinase Inhibitor for Treatment of Interstitial Lung Diseases"*. Am J Respir Crit Care Med. **2019**; 199:A5626.

Egger C., Cannet C., Gérard C., Dunbar A., Tigani B., Beckmann N. *"Hyaluronidase modulates bleomycin-induced lung injury detected noninvasively in small rodents by radial proton MRI"*. J Magn Reson Imaging. **2015**; 41(3):755-64.

Engler A. J., Sen S., Sweeney H. L., Discher D. E. *"Matrix elasticity directs stem cell lineage specification"*. Cell. **2006**; 126(4):677-89.

Evans C. M., Fingerlin T. E., Schwarz M. I., Lynch D., Kurche J., Warg L., Yang I. V., Schwartz D. A. *"Idiopathic Pulmonary Fibrosis: A Genetic Disease That Involves Mucociliary Dysfunction of the Peripheral Airways"*. Physiol Rev. **2016**; 96(4):1567-91.

Fahim A., Crooks M., Hart S. P. *"Gastroesophageal Reflux and Idiopathic Pulmonary Fibrosis: A Review"*. Pulm Med. **2011**; 2011:634613.

Fang Y., Eglen R. M. *"Three-Dimensional Cell Cultures in Drug Discovery and Development"*. LAS Discov. **2017**; 22(5):456-472.

Fernandez I. E., Amarie O. V., Mutze K., Königshoff M., Yildirim A. O., Eickelberg O. *"Systematic phenotyping and correlation of biomarkers with lung function and histology in lung fibrosis"*. Am J Physiol Lung Cell Mol Physiol. **2016**; 310(10):L919-27.

Fidler L., Sitzer N., Shapera S., Shah P. S. *"Treatment of Gastroesophageal Reflux in Patients With Idiopathic Pulmonary Fibrosis: A Systematic Review and Meta-Analysis"*. Chest. **2018**; 153(6):1405-1415.

Fingerlin T. E., Murphy E., Zhang W., Peljto A. L., Brown K. K., Steele M. P., Loyd J. E., et al. *"Genome-wide association study identifies multiple susceptibility loci for pulmonary fibrosis"*. Nat Genet. **2013**; 45(6):613-20.

Flaherty K. R., Fell C. D., Huggins J. T., Nunes H., Sussman R., et al. *"Safety of nintedanib added to pirfenidone treatment for idiopathic pulmonary fibrosis"*. Eur Respir J. **2018**; 52(2):1800230.

Flecknell P. *"Replacement, reduction and refinement"*. ALTEX. **2002**; 19(2):73-8.

Foskett A. M., Bazhanov N., Ti X., Tiblow A., Bartosh T. J., Prockop D. J. *"Phase-directed therapy: TSG-6 targeted to early inflammation improves bleomycin-injured lungs"*. Am J Physiol Lung Cell Mol Physiol. **2014**; 306(2):L120-31.

Gabbiani G. *"The myofibroblast in wound healing and fibrocontractive diseases"*. J Pathol. **2003**; 200(4):500-3.

Gagnon L., Leduc M., Thibodeau J. F., Zhang M. Z., Grouix B.,et al. *"A Newly Discovered Antifibrotic Pathway Regulated by Two Fatty Acid Receptors: GPR40 and GPR84"*. Am J Pathol . **2018**;188(5):1132-1148.

Galli J. A., Pandya A., Vega-Olivo M., Dass C., Zhao H., Criner G. J. *"Pirfenidone and nintedanib for pulmonary fibrosis in clinical practice: Tolerability and adverse drug reactions"*. Respirology. **2017**; 22(6):1171-1178.

Gelfand E. W. *"Mice are a good model of human airway disease"*. Am J Respir Crit Care Med. **2002**; 166(1):5-6; discussion 7-8.

Getsy J. A., Harper D., Levy M., Burggraaf J., Moerland M., et al. *"The Effects Of Recombinant Human Pentraxin-2, (prm-151), On Circulating Fibrocytes In Idiopathic Pulmonary Fibrosis (IPF)"*. Colorado Convention Center. INTERSTITIAL LUNG DISEASE: NOVEL MANAGEMENT AND OUTCOME STRATEGIES. **2011**. Poster Discussion Session /

Giri S. N., Leonard S., Shi X., Margolin S. B., Vallyathan V. *"Effects of pirfenidone on the generation of reactive oxygen species in vitro"*. J Environ Pathol Toxicol Oncol. **1999**; 18(3):169-77.

Gorina E., Richeldi L., Raghu G., Fernandez Perez E., Costabel U., et al. *"PRAISE, a randomized, placebo-controlled, double-blind Phase 2 clinical trial of pamrevlumab (FG-3019) in IPF patients"*. Eur Respir J. **2017**; 50: OA3400.

Gross T. J., Hunninghake G. W. *"Idiopathic Pulmonary Fibrosis"*. N Engl J Med. **2001**; 345:517-525.

Gruden J. F., Panse P. M., Leslie K. O., Tazelaar H. D., Colby T. V. *"UIP diagnosed at surgical lung biopsy, 2000-2009: HRCT patterns and proposed classification system"*. AJR Am J Roentgenol. **2013**; 200(5):W458-67.

Guo F., Sun Y. B., Su L., Li S., Liu Z. F., Li J., Hu X. T., Li J. *"Losartan attenuates paraquat-induced pulmonary fibrosis in rats"*. Hum Exp Toxicol. **2015**; 34(5):497-505.

Gustafson T., Dahlman-Höglund A., Nilsson K., Ström K., Tornling G., Torén K. *"Occupational exposure and severe pulmonary fibrosis"*. Respir Med. **2007**; 101(10):2207-12.

Han M. K., Zhou Y., Murray S., Tayob N., Noth I., Lama V. N., Moore B. B., et al. *"Lung microbiome and disease progression in idiopathic pulmonary fibrosis: an analysis of the COMET study"*. Lancet Respir Med. **2014**; 2(7):548-56.

Hashimoto N., Jin H., Liu T., Chensue S. W., Phan S. H. *"Bone marrow-derived progenitor cells in pulmonary fibrosis"*. J Clin Invest. **2004**; 113(2):243-52.

Higashiyama H., Yoshimoto D., Kaise T., Matsubara S., et al. *"Inhibition of activin receptor-like kinase 5 attenuates bleomycin-induced pulmonary fibrosis"*. Exp Mol Pathol. **2007**; 83(1):39-46.

Hilberg F., Roth G. J., Krssak M., Kautschitsch S., Sommergruber W., Tontsch-Grunt U., et al. *"BIBF 1120: triple angiokinase inhibitor with sustained receptor blockade and good antitumor efficacy"*. Cancer Res. **2008**; 68(12):4774-82.

Hirani N., Mackinnon A., Nicol L., Walker J., Ford P., et al. "*TD139, A Novel Inhaled Galectin-3 Inhibitor for the Treatment of Idiopathic Pulmonary Fibrosis (IPF). Results from the First in (IPF) Patients Study"*. Am J Respir Crit Care Med. **2017**; 195:A7560.

Homma S., Bando M., Azuma A., Sakamoto S., Sugino K., Ishii Y., et al. *"Japanese guideline for the treatment of idiopathic pulmonary fibrosis"*. Respir Investig. **2018**; 56(4):268-291.

Hostettler K. E., Zhong J., Papakonstantinou E., Karakiulakis G., Tamm M., et al. *"Anti-fibrotic effects of nintedanib in lung fibroblasts derived from patients with idiopathic pulmonary fibrosis"*. Respir Res. **2014**; 15(1):157.

Horan G. S., Wood S., Ona V., Li D. J., Lukashev M. E., Weinreb P. H., et al. *"Partial inhibition of integrin alpha(v)beta6 prevents pulmonary fibrosis without exacerbating inflammation"*. Am J Respir Crit Care Med. **2008**;177(1):56-65.

Hübner R.H., Gitter W., El Mokhtari NE, Mathiak M., Both M., Bolte H., Freitag-Wolf S., Bewig B. *"Standardized quantification of pulmonary fibrosis in histological samples"*. Biotechniques. **2008**; 44(4):507-511, 514-517.

Hutchinson J., Fogarty A., Hubbard R., McKeever T. *"Global incidence and mortality of idiopathic pulmonary fibrosis: a systematic review"*. Eur Respir J. **2015**; 46(3):795-806.

Ikeda K., Shiratori M., Chiba H., Nishikiori H., Yokoo K., Saito A., et al. *"Serum surfactant protein D predicts the outcome of patients with idiopathic pulmonary fibrosis treated with pirfenidone"*. Respir Med. **2017**; 131:184-191.

Inchingolo R., Varone F., Sgalla G., Richeldi L. *"Existing and emerging biomarkers for disease progression in idiopathic pulmonary fibrosis"*. Expert Rev Respir Med. **2019**; 13(1):39-51.

Inoue Y., Kaner R. J., Guiot J., Maher T. M., Tomassetti S., et al. *"Diagnostic and Prognostic Biomarkers for Chronic Fibrosing Interstitial Lung Diseases With a Progressive Phenotype"*. Chest. **2020**; 158(2):646-659.

Ishii G., Sangai T., Sugiyama K., Ito T., Hasebe T., et al. *"In vivo characterization of bone marrow-derived fibroblasts recruited into fibrotic lesions"*. Stem Cells. **2005**; 23(5):699-706.

Ishikawa N., Hattori N., Yokoyama A., Kohno N. *"Utility of KL-6/MUC1 in the clinical management of interstitial lung diseases"*. Respir Investig. **2012**; 50(1):3-13.

Izbicki G., Segel M. J., Christensen T. G., Conner M.W., Breuer R. *"Time course of bleomycin-induced lung fibrosis"*. Int J Exp Pathol. **2002**; 83(3):111-9.

Izumi S., Iikura M., Hirano S. *"Prednisone, Azathioprine, and N-Acetylcysteine for Pulmonary Fibrosis"*. N Engl J Med. **2012**; 367(9):870-871.

Izumo T., Kondo M., Nagara N., Iritani E., et al. *"Effects of a Leukotriene B4 Receptor Antagonist, an Anti-Inflammatory and Anti-Fibrotic Agent, on Bleomycin-Induced Pulmonary Fibrosis"*. Am J Respir Crit Care Med. **2009**; A3441

Jee A. S., Sahhar J., Youssef P., Bleasel J., Adelstein S., Nguyen M., Corte T. J. *"Review: Serum biomarkers in idiopathic pulmonary fibrosis and systemic sclerosis associated interstitial lung disease - frontiers and horizons"*. Pharmacol Ther. **2019**; 202:40-52.

Jenkins R. G., Noth I., Selman M., Cottin V., Nishioka Y., et al. *"Effects of nintedanib on markers of epithelial damage in subjects with IPF: data from the INMARK trial"*. Eu Respir J. **2020**; 56:5187.

Jenkins R. G., Simpson J. K., Saini G., Bentley J. H., Russell A. M., Braybrooke R., et al. *"Longitudinal change in collagen degradation biomarkers in idiopathic pulmonary fibrosis: an analysis from the prospective, multicentre PROFILE study"*. Lancet Respir Med. **2015**; 3(6):462-72.

Jenkins R. G., Moore B.B., Chambers R.C., Eickelberg O., Königshoff M., Kolb M., Laurent GJ., Nanthakumar C.B., Olman M.A., Pardo A., Selman M., et al. *"An Official American Thoracic Society Workshop Report: Use of Animal Models for the Preclinical Assessment of Potential Therapies for Pulmonary Fibrosis"*. Am J Respir Cell Mol Biol. **2017**; 56(5):667-679.

Kakugawa T., Mukae H., Hayashi T., Ishii H., Abe K., et al. *"Pirfenidone attenuates expression of HSP47 in murine bleomycin-induced pulmonary fibrosis"*. Eur Respir J. **2004**; 24(1):57-65.

Kasper M., Barth K. *"Potential contribution of alveolar epithelial type I cells to pulmonary fibrosis"*. Biosci Rep. **2017**; 37(6):BSR20171301.

Kaur A., Mathai S. M., Schwartz D. A. *"Genetics in Idiopathic Pulmonary Fibrosis Pathogenesis, Prognosis, and Treatment"*. Front Med (Lausanne). **2017**; 4:154.

Kendall R. T., Feghali-Bostwick C. A. *"Fibroblasts in fibrosis: novel roles and mediators"*. Front Pharmacol. **2014**; 5:123.

Khalil N., Manganas H., Ryerson C. J., Shapera S., Cantin A. M., el at. *"Phase 2 clinical trial of PBI-4050 in patients with idiopathic pulmonary fibrosis"*. Eur Respir J. **2019**; 53(3):1800663.

Kim D. S. *"Acute Exacerbation of Idiopathic Pulmonary Fibrosis"*. Clin Chest Med. **2012**; 33(1):59-68.

Kim D. S., Park J. H., Park B. K., Lee J. S., Nicholson A. G., Colby T. *"Acute exacerbation of idiopathic pulmonary fibrosis: frequency and clinical features"*. Eur Respir J. **2006**;27(1):143-50.

Kim J. S., Podolanczuk A. J., Borker P., Kawut S. M., Raghu G., Kaufman J. D., et al. *"Obstructive Sleep Apnea and Subclinical Interstitial Lung Disease in the Multi-Ethnic Study of Atherosclerosis (MESA)"*. Ann Am Thorac Soc. **2017**; 14(12):1786-1795.

Kim S. N., Lee J., YangH. S., Cho J. W., Kwon S., et al. "*Dose-response Effects of Bleomycin on Inflammation and Pulmonary Fibrosis in Mice*". Toxicol Res. **2010**; 26(3):217-22.

King Jr T. E., Tooze J. A., Schwarz M. I., Brown K. R., Cherniack R. M. *"Predicting survival in idiopathic pulmonary fibrosis: scoring system and survival model"*. Am J Respir Crit Care Med. **2001**; 164(7):1171-81.

King Jr T. E., Bradford W. Z., Castro-Bernardini S., Fagan E. A., Glaspole I., et al. *"A phase 3 trial of pirfenidone in patients with idiopathic pulmonary fibrosis"*. N Engl J Med. **2014**; 370(22):2083-92.

Knipe R. S., Tager A. M., Liao J. K. *"The Rho kinases: critical mediators of multiple profibrotic processes and rational targets for new therapies for pulmonary fibrosis"*. Pharmacol Rev. **2015**; 67(1):103-17.

Knudsen L., Ruppert C., Ochs M. *"Tissue remodelling in pulmonary fibrosis"*. Cell Tissue Res. **2017**;367(3):607-626.

Koh R. Y., Lim C. L. L., Uhal B. D., Abdullah M., et al. *"Inhibition of transforming growth factor-β via the activin receptor-like kinase-5 inhibitor attenuates pulmonary fibrosis"*. Mol Med Rep. **2015**; 11(5):3808-13.

Kolb M., Margetts P. J., Anthony D. C., Pitossi F., Gauldie J. *"Transient expression of IL-1beta induces acute lung injury and chronic repair leading to pulmonary fibrosis"*. J Clin Invest. **2001**; 107(12):1529-36.

Kolb M., Raghu G., Wells A. U., Behr J., Richeldi L., et al. *"Nintedanib plus Sildenafil in Patients with Idiopathic Pulmonary Fibrosis"*. N Engl J Med. **2018**; 379(18):1722-1731.

Kolb P., Upagupta C., Vierhout M., Ayaub E., Bellaye P. S., et al. *"The importance of interventional timing in the bleomycin model of pulmonary fibrosis"*. Eur Respir J. **2020**; 55(6):1901105.

Koli K., Sutinen E., Rönty M., Rantakari P., Fortino V., et al. *"Gremlin-1 Overexpression in Mouse Lung Reduces Silica-Induced Lymphocyte Recruitment - A Link to Idiopathic Pulmonary Fibrosis through Negative Correlation with CXCL10 Chemokine"*. PLoS One. **2016**; 11(7):e0159010.

Kono M., Nakamura Y., Suda T., Kato M., Kaida Y., Hashimoto D., et al. *"Plasma CCN2 (connective tissue growth factor; CTGF) is a potential biomarker in idiopathic pulmonary fibrosis (IPF)"*. Clin Chim Acta. **2011**; 412(23-24):2211-5.

Koralewski R., Dymek B., Mazur M., Sklepkiewicz P., Olejniczak S., et al. *"Discovery of OATD-01, a First-in-Class Chitinase Inhibitor as Potential New Therapeutics for Idiopathic Pulmonary Fibrosis"*. J Med Chem. **2020**; 63(24):15527-15540.

Kreuter M., Bonella F., Wijsenbeek M., Maher T. M., Spagnolo P. *"Pharmacological Treatment of Idiopathic Pulmonary Fibrosis: Current Approaches, Unsolved Issues, and Future Perspectives"*. Biomed Res Int. **2015**; 2015:329481.

Kusmirek J. E, Martin M. D., Kanne J. P. *"Imaging of Idiopathic Pulmonary Fibrosis"*. Radiol Clin. **2016**; 54(6):997-1014.

Kuwano K., Maeyama T., Inoshima I., Ninomiya K., et al. *"Increased circulating levels of soluble Fas ligand are correlated with disease activity in patients with fibrosing lung diseases"*. Respirology. **2002**;7(1):15-21.

Lakatos H. F., Burgess H. A., Thatcher T. H., Redonnet M. R., Hernady E., Williams J. P., Sime P. J. *"Oropharyngeal aspiration of a silica suspension produces a superior model of silicosis in the mouse when compared to intratracheal instillation"*. Exp Lung Res. **2006**; 32(5):181-99.

Lama V. N., Phan S. H. *"The extrapulmonary origin of fibroblasts: stem/progenitor cells and beyond"*. Proc Am Thorac Soc. **2006**; 3(4):373-6.

Lancaster L., Bonella F., Inoue Y., Cottin C., Siddall J., Small M., Langley J. *"Idiopathic pulmonary fibrosis: Physician and patient perspectives on the pathway to care from symptom recognition to diagnosis and disease burden"*. Respirology. **2021** Oct 5.

Lawson W. E., Grant S. W., Ambrosini V., Womble K. E., Dawson E. P., Lane K. B., et al. *"Genetic mutations in surfactant protein C are a rare cause of sporadic cases of IPF"*. Thorax. **2004**; 59(11):977-80.

Lederer D. J., Jelic S., Basner R. C., Ishizaka A., Bhattacharya J. *"Circulating KL-6, a biomarker of lung injury, in obstructive sleep apnoea"*. Eur Respir J. **2009**; 33(4):793-6.

Leduc M.; Tremblay M.; Grouix B.; Sarra-Bournet F.; Felton A., et al. *"Pbi-4050, A Novel First-In-Class Anti-Fibrotic Compound, Inhibits CTgf And Collagen I Production In Human Alveolar Epithelial Cells And Fibroblasts, And Reduces Lung Fibrosis In The Bleomycin-Induced Lung Fibrosis Model"*. Am J Respir Crit Care Med. **2014**; 189: 1.

Lee H. L., Ryu J. H., Wittmer M. H., Hartman T. E., Lymp J. F., Tazelaar H. D., Limper A. H. *"Familial idiopathic pulmonary fibrosis: clinical features and outcome"*. Chest. **2005**; 127(6):2034-41.

Lee J. S., Collard H. R., Raghu G., Sweet M. P., Hays S. R., et al. *"Does chronic microaspiration cause idiopathic pulmonary fibrosis?"*. Am J Med. **2010**; 123(4):304-11.

Ley B., Brown K. K., Collard H. R. *"Molecular biomarkers in idiopathic pulmonary fibrosis"*. Am J Physiol Lung Cell Mol Physiol. **2014**; 307(9):L681-91.

Ley B., Collard H. R., King Jr T. E. *"Clinical course and prediction of survival in idiopathic pulmonary fibrosis"*. Am J Respir Crit Care Med. **2011**; 183(4):431-40.

Lipson K. E., Wong C., Teng Y., Spong S. *"CTGF is a central mediator of tissue remodeling and fibrosis and its inhibition can reverse the process of fibrosis"*. Fibrogenesis Tissue Repair. **2012**; 5(Suppl 1): S24.

Liu M. H., Lin A. H., Ko H. K., Perng D. W., Lee T. S., Kou Y. R. *"Prevention of Bleomycin-Induced Pulmonary Inflammation and Fibrosis in Mice by Paeonol"*. Front Physiol. **2017**; 8:193.

Liu T., De Los Santos F. C., Phan S. H. *"The Bleomycin Model of Pulmonary Fibrosis"*. Methods Mol Biol. **2017**; 1627:27-42.

Lynch D. A., Sverzellati N., Travis W. D., Brown K. K., Colby T. V., et al. *"Diagnostic criteria for idiopathic pulmonary fibrosis: a Fleischner Society White Paper"*. Lancet Respir Med. **2018**; 6(2):138-153.

Macías-Barragán J., Sandoval-Rodríguez A., Navarro-Partida J., Armendáriz-Borunda J. *"The multifaceted role of pirfenidone and its novel targets"*. Fibrogenesis Tissue Repair. **2010**; 3:16.

Mackinnon A. C., Gibbons M. A., Farnworth S. L., Leffler H., Nilsson U. J., et al. *"Regulation of transforming growth factor-β1-driven lung fibrosis by galectin-3"*. Am J Respir Crit Care Med. **2012**; 185(5):537-46.

Mackinnon A. C., Chen W. S., Leffler H., Panjwani N., Schambye H., et al. "Design, Synthesis, and Applications of Galectin Modulators in Human Health". Top Med Chem. **2014**; 12: 95–122

Maher T. M., Kreuter M., Lederer D. J., Brown K. K., Wuyts W., et al. *"Rationale, design and objectives of two phase III, randomised, placebo-controlled studies of GLPG1690, a novel autotaxin inhibitor, in idiopathic pulmonary fibrosis (ISABELA 1 and 2)"*. BMJ Open Respir Res. **2019**; 6(1):e000422.

Maher T. M., Oballa E., Simpson J. K., Porte J., Habgood A., Fahy W. A., et al. *"An epithelial biomarker signature for idiopathic pulmonary fibrosis: an analysis from the multicentre PROFILE cohort study"*. Lancet Respir Med. **2017**; 5(12):946-955.

Maher T. M., van der Aar E. M., Van de Steen O., Allamassey L., Desrivot J., et al. *"Safety, tolerability, pharmacokinetics, and pharmacodynamics of GLPG1690, a novel autotaxin inhibitor, to treat idiopathic pulmonary fibrosis (FLORA): a phase 2a randomised placebo-controlled trial"*. Lancet Respir Med. **2018**; 6(8):627-635.

Martinez F. J., Collard H. R., Pardo A., Raghu G., Richeldi L., et al. *"Idiopathic pulmonary fibrosis"*. Nat Rev Dis Primers. **2017**; 3:17074.

Mattey D. L., Dawes P. T., Nixon N. B., Slater H. *"Transforming growth factor beta 1 and interleukin 4 induced alpha smooth muscle actin expression and myofibroblast-like differentiation in human synovial fibroblasts in vitro: modulation by basic fibroblast growth factor"*. Ann Rheum Dis. **1997**; 56(7):426-31.

Mecozzi L., Mambrini M., Riuscitti F., et al. *"In-vivo lung fibrosis staging in a bleomycin-mouse model: a new micro-CT guided densitometric approach"*. Sci Rep. **2020**; 10:18735.

Misra H. P., Rabideau C. *"Pirfenidone inhibits NADPH-dependent microsomal lipid peroxidation and scavenges hydroxyl radicals"*. Mol Cell Biochem. **2000**; 204(1-2):119-26.

Miyake Y., Sasaki S., Yokoyama T., Chida K., Azuma A., Suda T., Kudoh S., et al. *"Occupational and environmental factors and idiopathic pulmonary fibrosis in Japan"*. Ann Occup Hyg. **2005**; 49(3):259-65.

Moeller A., Ask K., Warburton D., Gauldie J., Kolb M. *"The bleomycin animal model: a useful tool to investigate treatment options for idiopathic pulmonary fibrosis?"*. Int J Biochem Cell. Biol. **2008**; 40(3):362-382.

Molyneaux P. L., Cox M. J., Willis-Owen S. A. G., Mallia P., Russell K. E., Russell A. M., et al. *"The role of bacteria in the pathogenesis and progression of idiopathic pulmonary fibrosis".* Am J Respir Crit Care Med. **2014**; 190(8):906-13.

Molyneaux P. L., Maher T. M. *"The role of infection in the pathogenesis of idiopathic pulmonary fibrosis"*. Eur Respir Rev. **2013**; 22(129):376-81.

Montesi S. B., Mathai S. K., Brenner L. N., Gorshkova I. A., et al. *"Docosatetraenoyl LPA is elevated in exhaled breath condensate in idiopathic pulmonary fibrosis"*. BMC Pulm Med**. 2014**; 14:5.

Moore B. B., Lawson W. E., Oury T. D., Sisson T. H., Raghavendran K., Hogaboam C. M. *"Animal Models of Fibrotic Lung Disease"*. Am J Respir Cell Mol Biol. **2013**; 49, (2): 167-179.

Morais A., Beltrão M., Sokhatska O., Costa D., Melo N., et al. *"Serum metalloproteinases 1 and 7 in the diagnosis of idiopathic pulmonary fibrosis and other interstitial pneumonias"*. Respir Med. **2015**; 109(8):1063-8.

Morgenthau A.S., Padilla M. L. *"Spectrum of fibrosing diffuse parenchymal lung disease"*. Mt Sinai J Med. **2009**;76(1):2-23.

Murray L. A., Rosada R., Moreira A. P., Joshi A., Kramer M. S., et al. *"Serum amyloid P therapeutically attenuates murine bleomycin-induced pulmonary fibrosis via its effects on macrophages"*. PLoS One. **2010**; 5(3):e9683.

Murray L. A., Zhang H., Oak S. R., Coelho A. L., Herath A., FlahertyM K. R., et al. *"Targeting interleukin-13 with tralokinumab attenuates lung fibrosis and epithelial damage in a humanized SCID idiopathic pulmonary fibrosis model"*. Am J Respir Cell Mol Biol. **2014**; 50(5):985-94.

Myers J. L. *"Histopathology of IPF and related disorders"*. K.C. Meyer and S.D. Nathan (eds.), Idiopathic Pulmonary Fibrosis: A Comprehensive Clinical Guide, Respiratory Medicine 9. **2014**; Ch.3: 35-54.

Naikawadi R. P., Disayabutr S., Mallavia B., Donne M. L., Green G., et al. *"Telomere dysfunction in alveolar epithelial cells causes lung remodeling and fibrosis"*. JCI Insight. **2016**; 1(14):e86704.

Nakayama S., Mukae H., Sakamoto N., Kakugawa T., Yoshioka S., et al. *"Pirfenidone inhibits the expression of HSP47 in TGF-beta1-stimulated human lung fibroblasts"*. Life Sci. **2008**; 82(3-4):210-7.

Navaratnam V., Fleming K. M., West J., Smith C. J., Jenkins R. G., Fogarty A., Hubbard R. B. *"The rising incidence of idiopathic pulmonary fibrosis in the UK"*. Thorax. **2011**; 66:462-467.

Neighbors M., Cabanski C. R., Ramalingam T. R., Sheng X. R., Tew G. W., et al. *"Prognostic and predictive biomarkers for patients with idiopathic pulmonary fibrosis treated with pirfenidone: post-hoc assessment of the CAPACITY and ASCEND trials"*. Lancet Respir Med. **2018**; 6(8):615-626.

Noble P. W., Albera C., Bradford W. Z., Costabel U., du Bois R. M., Fagan E. A., et al. *"Pirfenidone for idiopathic pulmonary fibrosis: analysis of pooled data from three multinational phase 3 trials"*. Eur Respir J. **2016**; 47(1):243-53.

Noble P. W., Albera C., Bradford W. Z., Costabel U., Glassberg M. K., Kardatzke D., et al. *"Pirfenidone in patients with idiopathic pulmonary fibrosis (CAPACITY): two randomised trials"*. Lancet. **2011**; 377(9779):1760-9.

Noth I., Zhang Y., Ma S. F., C., Barber M., Huang Y., et al. *"Genetic variants associated with idiopathic pulmonary fibrosis susceptibility and mortality: a genome-wide association study"*. Lancet Respir Med. **2013**; 1(4):309-317.

Ogura T., Taniguchi H., Azuma A., Inoue Y., Kondoh Y., et al. *"Safety and pharmacokinetics of nintedanib and pirfenidone in idiopathic pulmonary fibrosis"*. Eur Respir J. **2015**; 45(5):1382-92.

Oikonomou N., Mouratis M. A., Tzouvelekis A., Kaffe E., Valavanis C., et al. *"Pulmonary autotaxin expression contributes to the pathogenesis of pulmonary fibrosis"*. Am J Respir Cell Mol Biol. **2012**; 47(5):566-74.

Oku H., Shimizu T., Kawabata T., Nagira M., Hikita I., et a. *"Antifibrotic action of pirfenidone and prednisolone: different effects on pulmonary cytokines and growth factors in bleomycin-induced murine pulmonary fibrosis"*. Eur J Pharmacol. **2008**; 590(1-3):400-8.

Okuda R., Hagiwara E., Baba T., Kitamura H., Kato T., Ogura T. *"Safety and efficacy of pirfenidone in idiopathic pulmonary fibrosis in clinical practice"*. Respir Med. **2013**;107(9):1431-7.

Oldham J. M., Ma S. F., Martinez F. J., Anstrom K. J., Raghu G., et al. *"TOLLIP, MUC5B, and the Response to N-Acetylcysteine among Individuals with Idiopathic Pulmonary Fibrosis"*. Am J Respir Crit Care Med. **2015**; 192(12):1475-82.

Olson A. L., Swigris J. J. *"Idiopathic pulmonary fibrosis: diagnosis and epidemiology"*. Clin Chest Med. **2012**; 33(1):41-50.

Olson A. L., Swigris J. J., Lezotte D. C., Norris J. M., Wilson C. G., Brown K. K. *"Mortality from pulmonary fibrosis increased in the United States from 1992 to 2003"*. Am J Respir Crit Care Med. **2007**; 176(3):277-84.

Olson M. F. *"Applications for ROCK kinase inhibition"*. Curr Opin Cell Biol. **2008**; 20(2):242-8.

Ongenaert M., Dupont S., Blanqué R., Brys R., van der Aar E. M., Heckmann B. *"Strong reversal of the lung fibrosis disease signature by autotaxin inhibitor GLPG1690 in a mouse model for IPF"*. Eu Resp J. **2016**; 48: OA4540.

Palmer S. M., Snyder L., Todd J. L., Soule B., Christian R., et al. *"Randomized, Double-Blind, Placebo-Controlled, Phase 2 Trial of BMS-986020, a Lysophosphatidic Acid Receptor Antagonist for the Treatment of Idiopathic Pulmonary Fibrosis"*. Chest. **2018**; 154(5):1061-1069.

Pardo A., Cabrera S., Maldonado M., Selman M. *"Role of matrix metalloproteinases in the pathogenesis of idiopathic pulmonary fibrosis"*. Respir Res. **2016**; 17:23.

Pardo A., Selman M. *"Idiopathic pulmonary fibrosis: new insights in its pathogenesis"*. Int J Biochem Cell Biol. **2002**; 34(12):1534-8.

Park J. K., Coffey N. J., Bodine S. P., Zawatsky C. N., Jay L., Gahl W. A., et al. *"Bleomycin Induces Drug Efflux in Lungs. A Pitfall for Pharmacological Studies of Pulmonary Fibrosis"*. Am J Respir Cell Mol Biol. **2020**; 62(2):178-190.

Paun A., Kunwar A., Haston C. K. *"Acute adaptive immune response correlates with late radiation-induced pulmonary fibrosis in mice"*. Radiat Oncol. **2015**; 10:45.

Peljto A. L., Zhang Y., Fingerlin T. E., Ma S. F., Garcia J. G. N., Richards T. J., et al. *"Association between the MUC5B promoter polymorphism and survival in patients with idiopathic pulmonary fibrosis"*. JAMA. **2013**; 309(21):2232-9.

Peters-Golden M., Henderson W. R. *"Leukotrienes"*. N Engl J Med **2007**; 357:1841-1854.

Phan S. H. *"The Myofibroblast in Pulmonary Fibrosis"*. Chest J. **2002**. 122(6):286S-289S.
Phan S. H., Kunkel S. L. *"Lung cytokine production in bleomycin-induced pulmonary fibrosis"*. Exp Lung Res. **1992**; 18(1): 29–43.

Pilling D., Roife D., Wang M., Ronkainen S. D., Crawford J. R., Travis E. L., Gomer R. H. *"Reduction of bleomycin-induced pulmonary fibrosis by serum amyloid P"*. J Immunol. **2007**; 179(6):4035-44.

Pontis S., Bignami F., Miglietta D., et al. *"Automated Histological Image Analysis for the Assessment of Bleomycin-Induced Pulmonary Fibrosis in Rodents"*. Eu Resp J. **2019**; 54: PA2420.

Raghu G., Brown K. K., Bradford W. Z., Starko K., Noble P. W., Schwartz D. A., King Jr T. E. *"A placebo-controlled trial of interferon gamma-1b in patients with idiopathic pulmonary fibrosis"*. N Engl J Med. **2004**; 350(2):125-33.

Raghu G., Chen S. Y., Yeh W. S., Maroni B., Li Q., Lee Y. C., Collard H. R. *"Idiopathic pulmonary fibrosis in US Medicare beneficiaries aged 65 years and older: incidence, prevalence, and survival, 2001-11"*. Lancet Respir Med. **2014**; 2(7):566-72.

Raghu G., Collard H. R., Egan J. J., Martinez F. J., Behr J., Brown K. K., et al. *"An official ATS/ERS/JRS/ALAT statement: idiopathic pulmonary fibrosis: evidence-based guidelines for diagnosis and management"*. Am J Respir Crit Care Med. **2011**; 183:788-824.

Raghu G., Collard H. R., Egan J. J., Martinez F. J., Behr J., Brown K. K., et al. *"An official ATS/ERS/JRS/ALAT statement: idiopathic pulmonary fibrosis: evidence-based guidelines for diagnosis and management"*. Am J Respir Crit Care Med. **2011**; 183: 788-824.

Raghu G., Freudenberger T. D., Yang S., Curtis J. R., Spada S., Hayes J., Sillery J. K., Pope C. E., Pellegrini C. A. *"High prevalence of abnormal acid gastro-oesophageal reflux in idiopathic pulmonary fibrosis"*. Eur Respir J. **2006**; 27(1):136-42.

Raghu G., Pellegrini C. A., Yow E., Flaherty K. R., Meyer K., Noth I., et al. *"Laparoscopic anti-reflux surgery for the treatment of idiopathic pulmonary fibrosis (WRAP-IPF): a multicentre, randomised, controlled phase 2 trial"*. Lancet Respir Med. **2018**; 6(9):707-714.

Raghu G., Remy-Jardin M., Myers J. L., Richeldi L., Ryerson C. J., Lederer D. J., Behr J., Cottin V., et al. *"Diagnosis of Idiopathic Pulmonary Fibrosis. An Official ATS/ERS/JRS/ALAT Clinical Practice Guideline"*. Am J Respir Crit Care Med. **2018**; 198(5):e44-e68.

Raghu G., Selman M. *"Nintedanib and pirfenidone. New antifibrotic treatments indicated for idiopathic pulmonary fibrosis offer hopes and raises questions"*. Am J Respir Crit Care Med. **2015**; 191(3):252-4.

Raghu G., van den Blink B., Hamblin M. J., Brown A. W., Golden J. A., et al. *"Effect of Recombinant Human Pentraxin 2 vs Placebo on Change in Forced Vital Capacity in Patients With Idiopathic Pulmonary Fibrosis: A Randomized Clinical Trial"*. JAMA. **2018**; 319(22):2299-2307.

Raghu G., Wells A. U., Nicholson A. G., Richeldi L., Flaherty K. R., et al. *"Effect of Nintedanib in Subgroups of Idiopathic Pulmonary Fibrosis by Diagnostic Criteria"*. Am J Respir Crit Care Med. **2017**; 195(1):78-85.

Rangarajan S., Bone N. B., Zmijewska A. A., Jiang S., Park D. W., Bernard K., et al. *"Metformin reverses established lung fibrosis in a bleomycin model"*. Nat Med. **2018**; 24(8):1121-1127.

Redente E. F., Jacobsen K. M., Solomon J. J., Lara A. R., et al. *"Age and sex dimorphisms contribute to the severity of bleomycin-induced lung injury and fibrosis"*. Am J Physiol Lung Cell Mol Physiol. **2011;** 301(4):L510-8.

Richeldi L., Costabel U., Selman M., Kim D. S., Hansell D. M., Nicholson A. G., et al. *"Efficacy of a tyrosine kinase inhibitor in idiopathic pulmonary fibrosis"*. N Engl J Med. **2011**; 365(12):1079-87.

Richeldi L., Cottin V., du Bois R. M., Selman M., Kimura T., et al. *"Nintedanib in patients with idiopathic pulmonary fibrosis: Combined evidence from the TOMORROW and INPULSIS(®) trials"*. Respir Med. **2016**; 113:74-9.

Richeldi L., du Bois R. M., Raghu G., Azuma A., Brown K. K., Costabel U., Cottin V., et al. *"Efficacy and safety of nintedanib in idiopathic pulmonary fibrosis"*. N Engl J Med. **2014**; 370(22):2071-82.

Richeldi L., Fernández Pérez E. R., Costabel U., Albera C., Lederer D. J., et al. *"Pamrevlumab, an anti-connective tissue growth factor therapy, for idiopathic pulmonary fibrosis (PRAISE): a phase 2, randomised, double-blind, placebo-controlled trial"*. Lancet Respir Med. **2020**; 8(1):25-33.

Richeldi L., Fletcher S., Adamali H., Chaudhuri N., et al. *"No relevant pharmacokinetic drug-drug interaction between nintedanib and pirfenidone"*. Eur Respir J. **2019**; 53(1):1801060.

Richeldi L., Varone F., Bergna M., de Andrade J., Falk J., Hallowell R., et al. *"Pharmacological management of progressive-fibrosing interstitial lung diseases: a review of the current evidence"*. Eur Respir Re **2018**; 27(150):180074.

Rochwerg B., Neupane B., Zhang Y., Garcia C. C., Raghu G., et al. *"Treatment of idiopathic pulmonary fibrosis: a network meta-analysis"*. BMC Med. **2016**; 14:18.

Rosas I. O., Richards T. J., Konishi K., Zhang Y., Gibson K., Lokshin A. E., et al. *"MMP1 and MMP7 as potential peripheral blood biomarkers in idiopathic pulmonary fibrosis"*. PLoS Med. **2008**; 5(4):e93.

Rosen G., Sivaraman L., Cheng P., Murphy B., Chadwick K., et al. *"LPA1 antagonists BMS-986020 and BMS-986234 for idiopathic pulmonary fibrosis: Preclinical evaluation of hepatobiliary homeostasis"*. Eu Resp J. **2017**; 50: PA1038.

Roy S. G., Nozaki Y., Phan S. H. *"Regulation of alpha-smooth muscle actin gene expression in myofibroblast differentiation from rat lung fibroblasts"*. Int J Biochem Cell Biol. **2001**;33(7):723-34.

Ruscitti F., Ravanetti F., Bertani V., Ragionieri L., Mecozzi L., et al. *"Quantification of Lung Fibrosis in IPF-Like Mouse Model and Pharmacological Response to Treatment by Micro-Computed Tomography"*. Front Pharmacol. **2020**; 11:1117.

Saini G., Jenkins G., Mckeever T., Simpson J., Hubbard R., Johnson S., Braybrooke R., et al. *"The Profile Study: A Prospective Study Of Fibrosis In Lung Endpoints To Discover And Qualify Biomarkers For Use In Clinical Trials"*. Am J Respir Crit Care Med. **2012**; 185:A5169.

Sandbo N. *"Mechanisms of Fibrosis in IPF"*. Idiopathic Pulmonary Fibrosis. Chapter 8. **2013**; pp 161-205.

Sato N., Takasaka N., Yoshida M., Tsubouchi K., Minagawa S., Araya J., Saito N., et al. *"Metformin attenuates lung fibrosis development via NOX4 suppression"*. Respir Res. **2016**; 17(1):107.

Schmidt W. T. *"Driving research and awareness of pulmonary fibrosis: Pulmonary Fibrosis Foundation is leading the path to a cure"*. Am J Physiol Lung Cell Mol Physiol. **2020**; 319: L550-L553.

Scotton C. J., Chambers R. C. *"Bleomycin revisited: towards a more representative model of IPF?"*. Am J Physiol Lung Cell Mol Physiol. **2010**; 299(4):L439-41.

Scotton C. J., Hayes B., Alexander R., Datta A., Forty E. J., Mercer P. F., Blanchard A., Chambers R. C. *"Ex vivo micro-computed tomography analysis of bleomycin-induced lung fibrosis for preclinical drug evaluation"*. Eur Respir J. **2013**;42(6): 1633-1645.

Seger S., Stritt M., Vezzali E., Nayler O., Hess P., Groenen P. M. A., Stalder A. K. *"A fully automated image analysis method to quantify lung fibrosis in the bleomycin-induced rat model"*. PLoS One. **2018**; 13(3):e0193057.

Seibold J. R., Denton C. P., Furst D. E., Guillevin L., Rubin L. J., Wells A., et al. *"Randomized, prospective, placebo-controlled trial of bosentan in interstitial lung disease secondary to systemic sclerosis"*. Arthritis Rheum. **2010**; 62(7):2101-8.

Seibold M. A., Wise A. L., Speer M. C., Steele M. P., Brown K. K., Loyd J. E., Fingerlin T. E., et al. *"A common MUC5B promoter polymorphism and pulmonary fibrosis"*. N Engl J Med. **2011**; 364(16):1503-12.

Selman M., Carrillo G., Estrada A., Mejia M., Becerril C., Cisneros J., Gaxiola M., et al. *"Accelerated variant of idiopathic pulmonary fibrosis: clinical behavior and gene expression pattern"*. PLoS One. **2007**; 2(5):e482.

Selman M., Pardo A. *"Idiopathic pulmonary fibrosis: an epithelial/fibroblastic cross-talk disorder"*. Respir Res. **2002**; 3(1):3.

Selman M., Pardo A. *"Revealing the pathogenic and aging-related mechanisms of the enigmatic idiopathic pulmonary fibrosis. an integral model"*. Am J Respir Crit Care Med. **2014**; 189(10):1161-72.

Selman M., Pardo A. *"Role of epithelial cells in idiopathic pulmonary fibrosis: from innocent targets to serial killers"*. Proc Am Thorac Soc. **2006**; 3: 364-72.

Shao X., Li M., Luo C., Wang Y., Lu Y. Y., Feng S., et al. *"Effects of rapamycin against paraquat-induced pulmonary fibrosis in mice"*. J Zhejiang Univ Sci B. **2015**; 16(1):52-61.

Shulgina L., Cahn A. P., Chilvers E. R., Parfrey H., Clark A. B., Wilson E. C. F., et al. *"Treating idiopathic pulmonary fibrosis with the addition of co-trimoxazole: a randomised controlled trial"*. Thorax. **2013**; 68(2):155-62.

Smithmyer M. E., Sawicki L. A., Kloxin A. M. *"Hydrogel scaffolds as in vitro models to study fibroblast activation in wound healing and disease"*. Biomater Sci. **2014**; 2(5):634-650.

Song J. W., Hong S. B., Lim C. M., Koh Y., Kim D. S. *"Acute exacerbation of idiopathic pulmonary fibrosis: incidence, risk factors and outcome"*. Eur Respir J. **2011**; 37(2):356-63.

Stellari F.F., Ruscitti F., Ravanetti F., Cacchioli A., Villetti G., Civelli M. *"Pharmacological validation of a new IPF bleomycin-induced mouse model"*. Eu Respir J. **2017**; 50:PA1053.

Strieter R. M. *"What differentiates normal lung repair and fibrosis? Inflammation, resolution of repair, and fibrosis"*. Proc Am Thorac Soc. **2008**;5(3):305-10.

Strongman H., Kausar I., Maher T. *"Incidence, prevalence, and survival of patients with idiopathic pulmonary fibrosis in the UK"*. Adv Ther. **2018**; 35 (5), 724-736.

Stuart B. D., Lee J. S., Kozlitina J., Noth I., Devine M. S., Glazer C. S., Torres F., et al. *"Effect of telomere length on survival in patients with idiopathic pulmonary fibrosis: an observational cohort study with independent validation"*. Lancet Respir Med. **2014**; 2(7):557-65.

Sundarakrishnan A., Chen Y., Black L. D., Aldridge B. B., Kaplan D. L. *"Engineered Cell and Tissue Models of Pulmonary Fibrosis"*. Adv Drug Deliv Rev. **2018**; 129, 78-94.

Surber M. W., Beck S., Pham S., Marsden A. T., Gandi S. K., Baily J., McElroy M. C. *"Inhaled nintedanib is well-tolerated and delivers key pharmacokinetic parameters required to treat bleomycin-induced pulmonary fibrosis"*. Pulm Pharmacol Ther. **2020**; 63:101938.

Tager A. M. *"Autotaxin emerges as a therapeutic target for idiopathic pulmonary fibrosis: limiting fibrosis by limiting lysophosphatidic acid synthesis"*. Am J Respir Cell Mol Biol. **2012**; 47(5):563-5.

Tager A. M., Lacamera P., Shea B. S., Campanella G. S., Selman M., Zhao Z., Polosukhin V., et al. *"The lysophosphatidic acid receptor LPA1 links pulmonary fibrosis to lung injury by mediating fibroblast recruitment and vascular leak"*. Nat Med **2008**; 14: 45-54.

Takei R., Yamano Y., Kataoka K., Yokoyama T., Matsuda T., et al. *"Pulse oximetry saturation can predict prognosis of idiopathic pulmonary fibrosis"*. Respir Investig. **2020**; 58(3):190-195.

Talbot S. R., Biernot S., Bleich A., van Dijk R. M., Ernst L., Häger C., et al. *"Defining body-weight reduction as a humane endpoint: a critical appraisal"*. Lab Anim. **2020**; 54(1):99-110.

Tanjore H., Blackwell T. S., Lawson W. E. *"Emerging evidence for endoplasmic reticulum stress in the pathogenesis of idiopathic pulmonary fibrosis"*. Am J Physiol Lung Cell Mol Physiol. **2012**; 302(8): L721-9.

Tannenbaum J., Bennett B. T. *"Russell and Burch's 3Rs then and now: the need for clarity in definition and purpose"*. J Am Assoc Lab Anim Sci. **2015**;54(2):120-32.

Tashiro J., Rubio G. A., Limper A. H., Williams K., Elliot S. J., Ninou I., Aidinis V., Tzouvelekis A., Glassberg M. K. *"Exploring Animal Models That Resemble Idiopathic Pulmonary Fibrosis"*. Front Med. **2017**; 4:118.

Taskar V. S., Coultas D. B. *"Is Idiopathic Pulmonary Fibrosis an Environmental Disease?"*. Proc Am Thorac Soc. **2006**; 3(4):293-8.

Tatler A. L., Jenkins G. *"TGF-β activation and lung fibrosis"*. Proc Am Thorac Soc. **2012**; 9(3):130-6.

Tcherakian C., Cottin V., Brillet P. Y., Freynet O., Naggara N., et al. *"Progression of idiopathic pulmonary fibrosis: lessons from asymmetrical disease"*. Thorax. **2011**; 66(3):226-31.

Travis W. D., Costabel U., Hansell D. M., King T. E., Lynch D. A., Nicholson A. G., Ryerson C. J., Ryu J. H., Selman M., Wells A. U., et al. *"An Official American Thoracic Society/European Respiratory Society Statement: Update of the international multidisciplinary classification of the idiopathic interstitial pneumonias"*. Am J Respir Crit Care Med. **2013**; 188 (6), 733-748.

Uhl F. E., Vierkotten S., Wagner D. E., Burgstaller G., Costa R., et al. *"Preclinical validation and imaging of Wnt-induced repair in human 3D lung tissue cultures"*. Eur Respir J. **2015**; 46(4):1150-66.

Umezawa H., Maeda K., Takeuchi T., Okami Y. *"New antibiotics, bleomycin A and B"*. J Antibiot (Tokyo). **1966**; 19(5): 200-209.

van den Blink B., Dillingh M. R., Ginns L. C., Morrison L. D., Moerland M., et al. *"Recombinant human pentraxin-2 therapy in patients with idiopathic pulmonary fibrosis: safety, pharmacokinetics and exploratory efficacy"*. Eur Respir J. **2016**; 47(3):889-97.

van der Aar E. M., Heckmann B., Blanque, R., et al. *"Pharmacological profile and efficacy of GLPG1690, a novel autotaxin inhibitor for the treatment of idiopathic pulmonary fibrosis"*. Am J Respir Crit Care Med. **2016**; 193: A4523.

Vancheri C., Failla M., Crimi N., Raghu G. *"Idiopathic pulmonary fibrosis: a disease with similarities and links to cancer biology"*. Eur Respir J. **2010**; 35(3):496-504.

Vancheri C., Kreuter M., Richeldi L., Ryerson C. J., Valeyre D., et al. *"Nintedanib with Add-on Pirfenidone in Idiopathic Pulmonary Fibrosis. Results of the INJOURNEY Trial"*. Am J Respir Crit Care Med. **2018**; 197(3):356-363.

Vande Velde G., Poelmans J., De Langhe E., Hillen A., Vanoirbeek J., Himmelreich U., Lories R. J. *"Longitudinal micro-CT provides biomarkers of lung disease that can be used to assess the effect of therapy in preclinical mouse models, and reveal compensatory changes in lung volume"*. Dis Model Mech. **2016**;9(1):91-8.

Vanoirbeek J. A. J., Rinaldi M., De Vooght V., Haenen S., Bobic S., et al. *"Noninvasive and invasive pulmonary function in mouse models of obstructive and restrictive respiratory diseases"*. Am J Respir Cell Mol Biol. **2010**; 42(1):96-104.

Wang D., Ma Y., Tong X., Zhang Y., Fan H. *"Diabetes Mellitus Contributes to Idiopathic Pulmonary Fibrosis: A Review From Clinical Appearance to Possible Pathogenesis"*. Front Public Health. **2020**; 8:196.

Wang Q., Usinger W., Nichols B., Gray J., Xu L., Seeley T. W., Brenner M., Guo G., Zhang W., Oliver N., Lin A., Yeowell D. *"Cooperative interaction of CTGF and TGF-β in animal models of fibrotic disease"*. Fibrogenesis Tissue Repair. **2011**; 4(1): 4.

Wilborn J., Bailie M., Coffey M., Burdick M., Strieter R., Peters-Golden M. *"Constitutive activation of 5-lipoxygenase in the lungs of patients with idiopathic pulmonary fibrosis"*. J Clin Invest. **1996**; 97(8):1827-36.

Wollin L., Maillet I., Quesniaux V., Holweg A., Ryffel B. *"Antifibrotic and anti-inflammatory activity of the tyrosine kinase inhibitor nintedanib in experimental models of lung fibrosis"*. J Pharmacol Exp Ther. **2014**; 349(2):209-20.

Wollin L., Trinh-Minh T., Zhang Y., Distler J.H.W. *"The effect of nintedanib versus mycophenolate mofetil in the Fra2 mouse model of systemic sclerosis-associated interstitial lung disease"*. Clin Exp Rheumatol. **2021**; 39 Suppl 131(4):134-141.

Wollin L., Wex E., Pautsch A., Schnapp G., Hostettler K. E., Stowasser S., Kolb M. *"Mode of action of nintedanib in the treatment of idiopathic pulmonary fibrosis"*. Eur Respir J. **2015**; 45(5):1434-45.

Wolters P. J., Collard H. R., Jones K. D. *"Pathogenesis of idiopathic pulmonary fibrosis"*. Annu Rev Pathol. **2014**; 9:157-79.

Wygrecka M., Zakrzewicz D., Taborski B., Didiasova M., et al. *"TGF-β1 induces tissue factor expression in human lung fibroblasts in a PI3K/JNK/Akt-dependent and AP-1-dependent manner"*. Am J Respir Cell Mol Biol. **2012**; 47(5):614-27.

Yanagihara T., Chong S. G., Vierhout M., Hirota J. A., Ask K., Kolb M. *"Current Models of Pulmonary Fibrosis for Future Drug Discovery Efforts"*. Expert Opin Drug Discov. **2020**; 15 (8), 931-941.

Yang I. V., Fingerlin T. E., Evans C. M., Schwarz M. I., Schwartz D. A. *"MUC5B and Idiopathic Pulmonary Fibrosis"*. Ann Am Thorac Soc. **2015**;12 Suppl 2(Suppl 2):S193-9.

Yang J., Xue Q., Miao L., Cai L. *"Pulmonary fibrosis: a possible diabetic complication"*. Diabetes Metab Res Rev. **2011**;27(4):311-7.

Zaman T., Lee J. *"Risk factors for the development of idiopathic pulmonary fibrosis: A review"*. Curr Pulmonol Rep. **2018**; 7 (4), 118-125.

Zhou Y., Huang X., Hecker L., Kurundkar D., Kurundkar A., et al. *"Inhibition of mechanosensitive signaling in myofibroblasts ameliorates experimental pulmonary fibrosis"*. J Clin Invest. **2013**; 123(3):1096-108.

Zibrak J. D., Price D. *"Interstitial lung disease: raising the index of suspicion in primary care"*. NPJ Prim Care Respir Med. **2014**; 24:14054.

3rd Annual IPF Summit; August 27-29, **2019**; San Diego, CA.

6.1   POSTERS AND PRESENTATIONS

Fragni D., Murgo A., Federico G., Ruscitti F., Mambrini M., Bignami F., Stellari F., Lucattelli M., Civelli M., Villetti G., Miglietta D. *"Multiple readouts to assess antifibrotic efficacy of Nintedanib in a bleomycin-induced pulmonary fibrosis mouse model"*.
- Poster presentation at the 19th Fraunhofer Seminar "Models of Lung Disease". Feb 6-7, **2020**.

Fragni D., Murgo A., Federico G., Bignami F., Lucattelli M., Villetti G., Miglietta D. *"Time-course analysis of multiple readouts in the bleomycin-induced pulmonary fibrosis mouse model"*. EU-IPFF SUMMIT 2021, Virtual Summit 23-25 Apr **2021**.